Martino, Chiara (2013) *Droplet-based microfluidic platforms for protein investigations.* PhD thesis.

# Droplet-based microfluidic platforms for protein investigations

**Chiara Martino**

A thesis submitted to

The School of Engineering

College of Science and Engineering

The University of Glasgow

In fulfilment of the requirements for

The Degree of Doctor of Philosophy

28th February 2013

# Abstract

In the last two decades, the integration of life science and micro-engineering has developed systems which are able to perform laboratory functions on devices only 10-100 μm in size. These microfluidic systems, called lab-on-chip (LOC), show promising capabilities in reducing both the time and the cost of a wide range of chemical and biological processes.

More recently, the creation of microfluidic systems which are able to form and control sub-nanolitre droplets, comprising two phase emulsions, have been developed to deliver new experimental platforms. Such systems, also known microdroplets or segmented flow platforms, consist of stable liquid droplets, suspended in a second immiscible phase, with volumes on the nanolitre to the femtolitre scale. The potential of these systems within chemical and biological sciences has already been clearly demonstrated in the literature and commercial platforms are now becoming available. Some of the appealing features that these systems allow are the compartmentalization, the ultra-high throughput experimentation, the imitation of cellular conditions in terms of volumes and chemical composition.

The aim of this research project is to exploit the droplet-based LOC systems using the two phase segmented flow to create platforms where proteins can be investigated and even expressed within the droplet chassis.

Initial work used a single emulsion strategy (i.e. droplet of water in oil) to selectively capture cellular proteins from a cell suspension, which was directly processed on chip. It was observed that proteins remain active in these systems. In addition, a complexity of conventional laboratory procedures for protein quantification assays was reduced, both in terms of investigation times and amounts of valuable biological samples used. The obtained results demonstrated that this system has the potential to provide the same level of quantitative information obtained using standard biological techniques (i.e. Western blot) at a lower cost.

The research has been moving over the development of artificial cell models, nanolitre sized watery droplets comprising a membrane separating the inner from the external environment. Within these systems, realised using a double

emulsion strategy (i.e. droplet of water with a droplet of oil or other immiscible phase surrounded by another watery phase), proteins have been expressed using cell-free protein expression systems. The technology adopted lies broadly within the field of synthetic biology involving the transformation of microorganism's DNA for the production of the desired proteins. Fluorescent proteins were designed and expressed within the artificial cell and fluorescence assays, implemented within the microfluidic format, confirmed not only the functionality of the expressed protein which behaved like *in vivo*, but also the possibility of its controlled release. Protein release was possible through the use of polymers, within the double emulsion format, which represent a good class of material for the production of nanometre thickness shells.

Future developments in this research will aim to *(i)* expand the capabilities of the single emulsion system for the capture of multiple proteins from a cell lysate and *(ii)* use different class of polymers to enrich the artificial cell membrane with membrane proteins aiming towards the natural cell mimicking. Emulsions capable to mimic some aspects of the living cell, like the protein synthesis, represent a great opportunity to be used as tools for protein investigations.

# List of Publications, Conferences and Awards

**Publications**

C. Martino, S-H Kim, L. Horsfall, A. Abbaspourrad, S. Rosser, J. M. Cooper, D. A. Weitz, Protein Expression, Aggregation, and Triggered Release from Polymersomes as Artificial Cell-like Structures, *Angewandte Chemie*, 124, 26, 6522–6526, 2012.

C. Martino, L. Horsfall, Y. Chen, M. Chanasakulniyom, D. Paterson, A. Brunet, S. Rosser, Y-J Yuan, J. Cooper, Cytoskeletal Protein Expression and its Association within the Hydrophobic Membrane of Artificial Cell Models, *ChemBioChem*, 13, 792–795, 2012.

C. Martino, M. Zagnoni, M. E. Sandison, M. Chanasakulniyom, A. R. Pitt, J. M. Cooper, Intracellular protein determination using droplet-based immunoassays, *Analytical Chemistry*, 83, 5361–5368, 2011.

M. Chanasakulniyom, C. Martino, D. Paterson, L. Horsfall, S. Rosser, J. M. Cooper, Expression of membrane-associated proteins within single emulsion cell facsimiles, *Analyst*, 137, 2939–2943, 2012. Front cover.

C. D. Syme, C. Martino, R. Yusvana, N. M. S. Sirimuthu, J. M. Cooper, Quantitative Characterization of Individual Microdroplets using Surface-Enhanced Resonance Raman Scattering Spectroscopy, *Analytical Chemistry*, 84, 1491–1495, 2011.

**Conferences**

Poster presentation entitled: "Droplet-based Microfluidics for Protein Investigation". *EMBL Microfluidics 2012*, Heidelberg (DE), July 2012.

Oral presentation entitled: "Droplet-based microfluidic system for intracellular protein quantification". *PGBioMed2011*, Glasgow (UK), August 2011.

Poster presentation entitled: "Cellular protein in microdroplets: capture and quantification". *Physics and Chemistry of Microfluidics*, Waterville Valley, New Hampshire (USA), June 2011.

**Awards**

William Wilson Scott Award 2011 - Support Women in Engineering.

Mac Robertson Scholarship Award 2011 – International Collaborations.

Chinese Government Scholarship Award 2010 – International Collaborations.

James Watt Scholarship 2009

# Table of Contents

# List of Tables

# List of Figures

The MreB-RFP molecules deposit to the hydrophobic membrane. B) Detail of droplets at the membrane does not show any aggregation due to polymerisation.

# Acknowledgements

I would like to thank Professor Jonathan Cooper for his trust in my capabilities and his support in any aspects of this work, including my international collaborations with Professor Ying-Jin Yuan (Tianjin University, China) and Professor David Weitz (Harvard University, USA).

My acknowledgements also go to all the people who helped me in any technical aspects of this work, namely: Dr. Andrew Glidle, Dr. Michele Zagnoni, Dr. Mairi Sandison, Miss Mayuree Chanasakulniyom, Miss Yan Chen, Dr. Susan Rosser, Dr. Louise Horsfall, Mr David Paterson, Mr Adrien Brunet, Prof. Shin-Hyun Kim, Miss Kimia Mohammadi, Mr Yannyk Bourquin and all the technicians from the James Watt Nanofabrication Centre.

Special thanks also go to Dr. Steven Neal, Dr. Alasdair Clark and Dr. Craig Auchinvole who kindly contributed to the proofreading of this thesis.

An essential contribution was given by The University of Glasgow that founded this research through the James Watt Scholarship.

Final thanks go to Dr. Manlio Tassieri for his precious advices, and to all the colleagues, friends and flatmates I met in these years who made my staying in Glasgow an enjoyable and unique adventure.

# Author declaration

"I declare that, except where explicit reference is made to the contribution of others, this dissertation is the result of my own work and has not been submitted for any other degree at the University of Glasgow or any other institution".

Chiara Martino

# Abbreviations

| | |
|---|---|
| ATP | Adenosine-triphosphate |
| BSA | Bovine serum albumin |
| CMC | Critical micelle concentration |
| CV | Coefficient of variation |
| DEP | Dielectrophoresis |
| DI water | Deionised water |
| EGFP | Enhanced green fluorescent protein |
| ELISA | Enzyme-linked immunosorbent assays |
| FITC | Fluorescein isothiocyanate |
| FRAP | Fluorescence recovery after photobleaching |
| FSA | Fluorescent secondary antibody |
| GFP | Green fluorescent protein |
| HLB | Hydrophilic-lipophilic balance |
| H-Ras | Human Ras |
| IBF | Intrinsic bead fluorescence |
| IDT | Interdigitated trasducer |
| IVC | In vitro compartmentalization |
| LOC | Lab-on-a-chip |
| PCR | Polymerase chain reaction |
| PDMS | Poly(dimethylsiloxane) |
| PEG | Poly(ethylene glycol) |
| PG | Peptidoglycan |
| PLA | Poly(lactic acid) |
| PTFE | Poly(tetrafluoroethylene) |
| PVA | Poly(vinyl alcohol) |
| RFP | Red fluorescent protein |
| SDS | Sodium dodecyl sulphate |
| TRITC | Tetramethyl rhodamine iso-thiocyanate |
| W/O droplet | Water in oil droplet |
| W/O/W droplet | Water in oil droplet re-dispersed in water |

# 1  Introduction and review of the literature

This Chapter aims to discuss the research problems addressed in this PhD thesis. The reader is first introduced to droplet-based microfluidics and its uses, then to the three main applications developed in this study, widely detailed in the following Sections and published in international scientific journals. An outline of the thesis is also presented at the end of this Chapter.

## 1.1 Background

During the past three decades, the realization of miniaturised devices, able to handle and process small volumes of fluids at the micron scale, has been used in a broad range of fields. Particularly in (bio-)chemistry and cell biology, miniaturised devices have been employed to address a wide variety of problems often with greatly reduced samples volumes, waste production and costs, enabling faster and more sensitive analysis (1-4).

The miniaturization of these devices, also known as microfluidic devices, has boosted the design and fabrication of portable and semi-portable systems useful for point of care diagnostics, which can integrate many operations such as sample pre-treatment, labelling reactions, separation, downstream reactions and detection (5). These operations have been demonstrated in proof-of-concept devices. Robust approaches to fabrication, integration and packaging remain great areas of research (3).

According to their liquid propulsion principle, microfluidic devices can be classified in five major groups, namely: pressure driven, capillary, centrifugal, electrokinetic and acoustic systems (6). In this research, only pressure driven systems are taken in consideration. Within these systems the liquid transport mechanism is due to pressure gradients produced by syringes, pumps or

pneumatic displacement of membranes. The liquids are injected into the chip either in batch or in a continuous way.

A particular class of pressure driven microfluidic devices are those known as *droplet-based microfluidic devices* which are able to generate and utilize uniform streams of plugs and/or droplets (µl to fl volume range) dispersed within an immiscible continuous phase (gas or liquid) and confined within microfluidic channels or chambers.

Over the last ten years, droplet-based microfluidic systems have augmented the existing portfolio of microfluidic devices finding various applications in different fields of science. An important advantage of the droplet-based technology is that it offers confined compartments, of a comparable geometry to that of a cell (nl-fl in volume) with short diffusion distances and created at rates between 10-10000 Hz, depending upon the fluid flow rates. By using such two-phase-flow systems that create well characterised emulsions comprising droplets of water-in-oil (or vice-versa), it is possible to perform thousands of reactions each second in parallel at low volumes (from µl to fl), offering the potential for multiplexed and high-throughput analysis (7).

The research presented here aims to give a contribution to protein based investigations by the development of new droplet-based microfluidic platforms and the exploitation of existing ones. Using an interdisciplinary approach, based on knowledge of *bioengineering* and *microfluidics*, three major investigations were carried out. Firstly, the thesis presents an approach for protein trapping and quantification from a cell lysate; secondly, the construction of a biological platform used in validation of protein behaviour; and thirdly, the realization of polymeric vesicles capable to release proteins in a controlled manner.

## 1.2 Droplet-based microfluidics and its applications

As previously anticipated, droplet-based microfluidic systems can form highly monodisperse emulsions with droplet diameters ranging from hundreds of nanometers to hundreds of micrometers (7). This characteristic represents an advantage over the continuous flow microfluidic systems when the ability to run parallel experiments at the same moment is a required feature (8). Each water

in oil (W/O) droplet can constitute an isolated microcompartment, suitable for carrying out quantitative assays and cell-based studies or even suitable as a chassis for therapeutic agent delivery with the advantage to guarantee a more uniform delivery compared to polydisperse microcapsules. Figure 1-1 shows a comparison between an emulsion obtained by stirring oil and water phases for few minutes (Figure 1-1 A) and one obtained using a microfluidic chip (Figure 1-1 B).
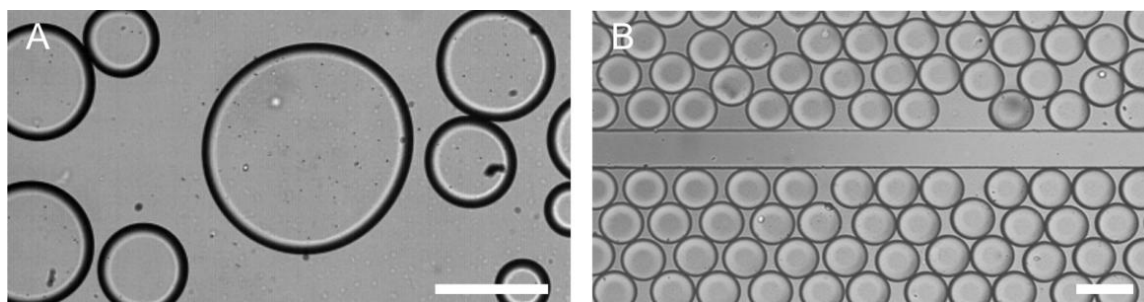


Figure 1-1 Emulsion of water droplets in organic phase. A) Emulsion obtained by mixing the two phases in a vial through simple stirring for 5 minutes and B) by using a microfluidic chip. The two methods result in the production of polydisperse (broad size distributions) and monodisperse emulsions with standard deviations equal to 0.60 and 0.03 respectively. Scale bar equal to 100 $\mu$m.

Beyond compartmentalization and throughput analysis, droplet-based microfluidics has also shown the ability to perform operations on droplets including mixing, splitting, fusion and sorting (8). These operations are conducted either actively or passively. In the former case, they rely on the use of external power (9). In the latter, droplets are manipulated by the flow variation operated by channel geometries or surface wetting characteristics (9). For example, mixing of solution within a droplet can be achieved either by using electrodes which produce an electric field and move the polar solution through the electric field (10) or by using winding channels which promote the chaotic mixing within the droplet (11).

Among the active methods, in addition to the electrical force, optical and acoustic forces have also been exploited to split/fuse (12) and separate droplets (13). Passive methods use narrow channels and pillars where the droplet is forced to pass through to be fused (14), sorted (15) or split (16). Figure 1-2 shows the above mentioned approaches adopted by some research groups working on droplet-based microfluidics.

Droplet microfluidics has been successfully used for a wide range of applications that include analytical applications (chemical and biological assays) and chemical synthesis (6, 17). The reaction rate within the droplet depends on droplet volume and external temperature, and it has already been demonstrated that in hydrolysis reaction the rate and the efficiency of reaction are enhanced in a microreactor rather than conventional flask (18). Droplet-based microfluidics has also been demonstrated to be a successful instrument for a variety of other techniques including: protein crystallization, which aims to determine the three-dimensional structures and functions of molecules and complexes (19) (Figure 1-3); enzymatic assay on single cell selectively encapsulated within a droplet (20) (Figure 1-4); more rapid and efficient DNA amplification (21) (Figure 1-5) and the synthesis of monodisperse polymeric particles with different shapes (microspheres, rods, disks, ellipsoids) (22) (Figure 1-6). Using droplet-based microfluidics complex core-shell structures of various sizes, patterns and composition have also been obtained (23-26). This is the case of double emulsions, which consist of a droplet containing another droplet within itself as to emulate the Matryoshka doll concept (23) (24), or multiple emulsion which is made of droplets containing many droplets within their interiors (27) (Figure 1-7).

Droplet-based microfluidics is also having a significant impact in the emerging field of *synthetic biology*, an interdisciplinary science which aims to engineer and create biological systems that can be modelled, understood, or have enhanced capabilities able to produce drugs, green fuels and high valuable biomaterials (18, 28). It has been shown that it is possible to express proteins within microdroplets using the basic components of a living cell and modified DNA templates carrying the genetic information needed to be expressed (29, 30). This represents a useful format in those cases where the expression of protein is toxic for the host expressing organism.

**ACTIVE**        **PASSIVE**

## Mixing

A

E

REORIENT

stretch AND fold

## Fusion

B

Flow

F

| | |
|---|---|
| **Small drop** | 0 ms    5 ms |
| **3 drops** | 0 ms    10 ms |
| **2 drops** | 0 ms    10 ms |
| **Big drop** | 0 ms    10 ms |

## Sorting

C

IDT

OFF

(a)

IDT

ON

(b)

G

236msec

96msec

0msec

100μm

71msec

100μm

0msec

## Splitting

D

(a) Laser off

Flow

L1

L2

(b) Laser on

H

$\ell_1$

$\ell_2$
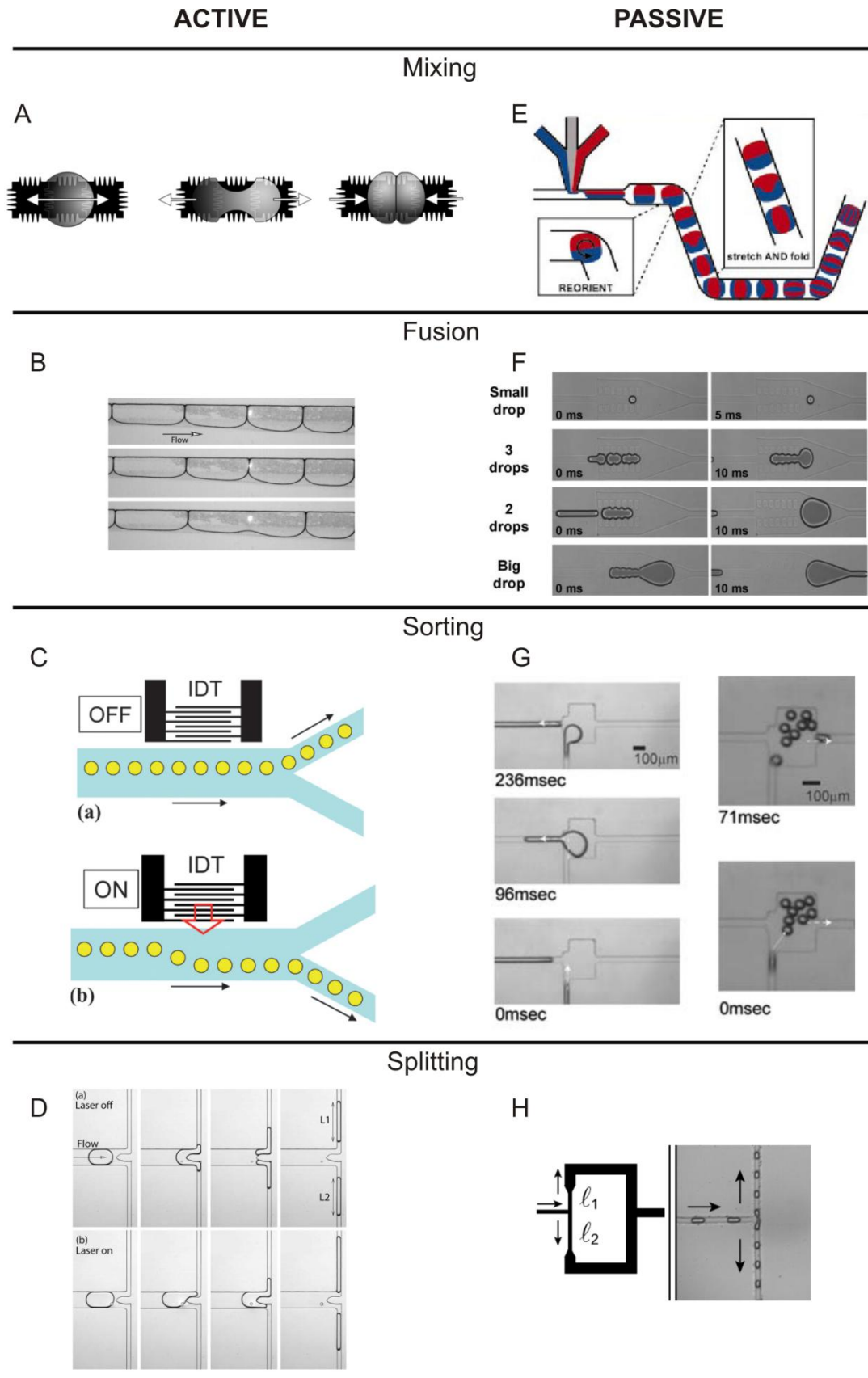
Figure 1-2 Active and passive methods for droplet manipulation. A) Active droplet mixing obtained by a splitting and merging approach controlled by three electrodes operated at 16 Hz. Image from (10). B) Fusion of a train of droplets flowing from left to right and merged as the interface crosses the laser (white spot). Image from (12). C) Droplet separation operated when an interdigidated electrode (IDT) is turned on and causes an acoustic streaming within the major channel which drives the droplets in the

lower channel of the branch. Image from (13). D) Droplet splitting operated by a laser source whose power was demonstrated to influence the symmetry of droplet division. Image from (12). E) Passive mixing within the droplet operated by winding channel where the droplet passes through. Image from (11). F) Merging chamber working for small, medium and large droplets. Image taken from (14). G) Droplet sorting achieved by controlling the flow rate ratio of the daughter channels and the bifurcating junction geometry. Larger droplets move to the left of the device while smaller droplets move to the right. Image taken from (15). H) Splitting of a droplet in two daughter droplets is operated by the different flow resistance of the two channels at the T-junction. Image taken from (16).



Figure 1-3 Protein crystallization within a microdroplet. Microphotograph of well formed protein crystals after chaotic mixing within the droplet. Fast mixing resulted to be favourable for the formation of well crystallized proteins. Image taken from (19).
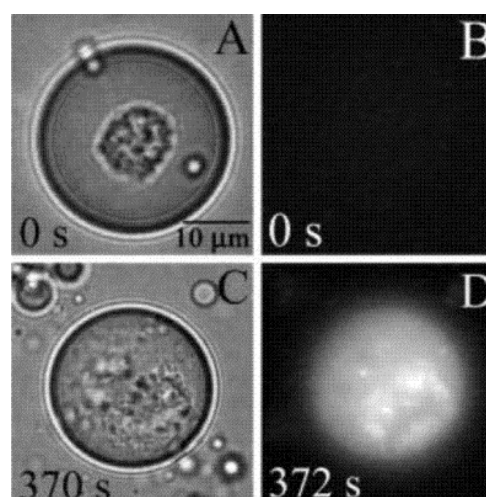


Figure 1-4 Single cell enzymatic assay performed in a droplet. After photolysis the intracellular enzyme is released within the droplet and it catalyses the formation of fluorescent product. Image taken from (20).
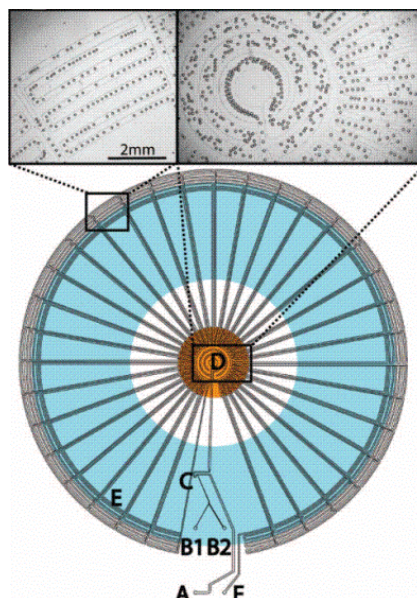
Figure 1-5 Continuous flow PCR in W/O droplets. The oil carrier (injected from inlet A) and the biological solutions, entering from inlets B, allow the formation of droplet at the point C. The droplets flow through alternating temperature zones so that DNA denaturation (in part D), primer annealing and template extension (in part E) occur. The droplets exit the chip from outlet F after 34 cycles. Image taken from (21).
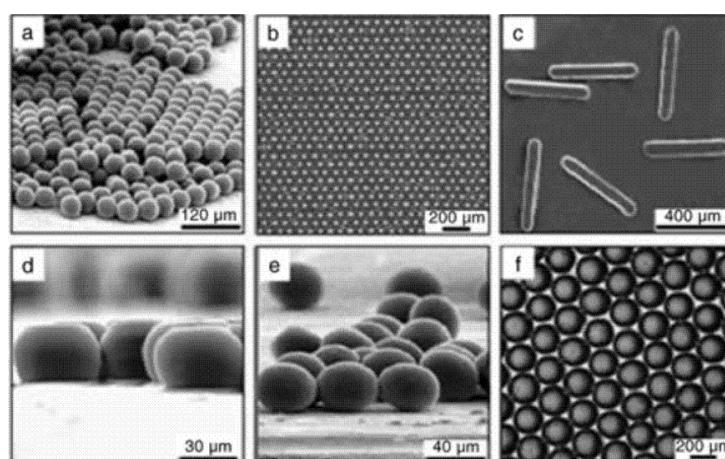


Figure 1-6 Microscopy images of polyTPGDA particles taking the shapes of microspheres, crystal of microspheres, rods, disks, ellipsoids (a-d) and agarose disks (f). Image taken from (22).
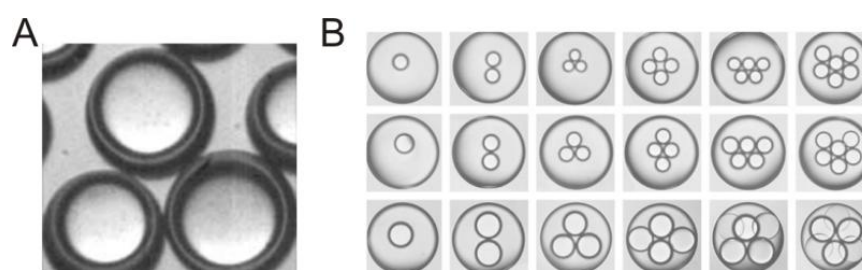


Figure 1-7 Double and multiple emulsions. A) Core-shell structures, also known as double emulsion, generated by a microcapillary device. Figure taken from (24). B) Multiple emulsions produced using scalable microcapillary devices that simultaneously controls the droplet monodispersity as well as the number and size of the inner droplets. Scale bar 200 $\mu$m. Image taken from (27).

## 1.3 Droplet-based microfluidics for protein trapping and quantification

The production of proteins in a cell comes about due to the expression of specific genes at a certain moment, thus identification and quantification of its expression can give an idea of what is happening to a cell in a particular phase of its existence. Conventional laboratory methods such as Western blot methods (31) and enzyme-linked immunosorbent assays (ELISA) (32) allow sensitive detection and quantification of a specific protein within a cell population but they are often labor-intensive, time consuming and in many cases they can require large sample volumes on the order of millilitres. Droplet-based microfluidic systems for protein analysis have already been reported in the literature, including a system for performing immunoassays using encapsulated single cells in W/O droplets, where the cells were lysed by laser photolysis (20). Although suitable for performing enzymatic activity assays at the single-cell level, this approach is not suitable for high-throughput applications.

Cells have also been trapped within droplets, for the detection of surface protein biomarkers using enzymatic amplification (33) (Figure 1-8 A), and in a segmented gas-liquid flow microsystem capable to perform stimulation of mammalian cells followed by chemical cell lysis (34) (Figure 1-8 B). However, fully integrated analysis was not demonstrated in either case, with antibody staining and flow cytometry measurements having been performed off-chip.

The first aim of this project strives to develop a new microfluidic architecture that enables rapid and quantitative intracellular protein detection from cell suspensions. The system used low cell numbers, reduced sample volumes and a fully integrated on-chip procedure. By combining the compartmentalisation and high-throughput characteristics of droplet-based microfluidics with on-chip electrical lysis, epifluorescence protein detection is performed on numerous microdroplets, inside which cell lysate and antibody-conjugated beads are encapsulated.

Due to the simplicity of integration, together with the lack of interference arising from the addition of detergents (as is the case with chemical lysis) and its high efficiency, on-chip electrical lysis is an attractive technique which was adopted in this chip architecture. Thus a suspension containing less than a

thousand cells was injected into the device and cell lysis was performed using microelectrodes, prior to droplet formation, without any need for further sample preparation. In order to test the system two different proteins were detected respectively, HRas-mCitrine, expressed within HEK-293 cells, and actin-EGFP, expressed within MCF-7 cells. Description of the proposed approach, chip fabrication and obtained results are described in Chapter 4.
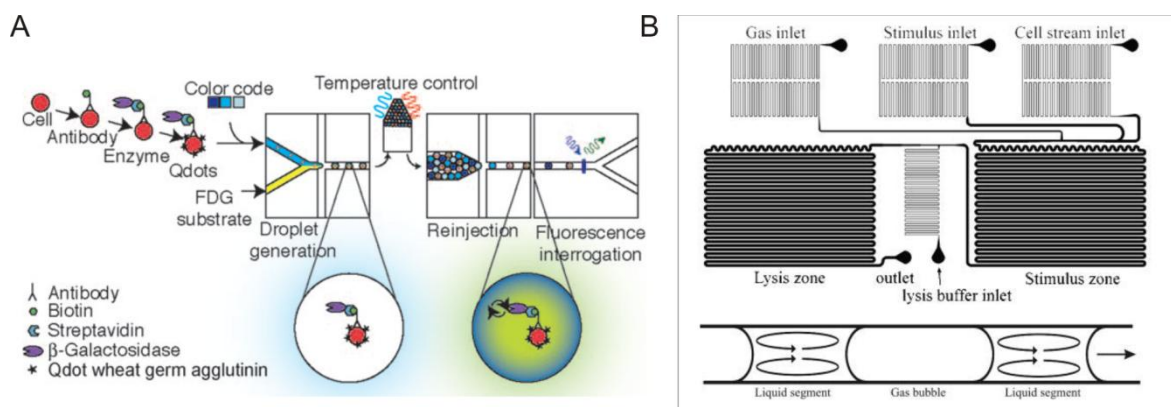


Figure 1-8 Applications of droplet-based microfluidics involving the use of cells. A) Schematic representation of a system used to count cells that exhibit specific proteins on their surface. Cells are first mixed with enzyme-linked antibodies (capable to bind only to the specific protein on the cell surface) outside the chip and then injected and mixed with FDG, a substrate that produces a fluorescent product after the reaction with the ß-Galactosidase enzyme. Cells, stained through the use of quantum dots to make them visible, are collected outside the chip and afterwards reinjected for being detected. Picture taken from (33).  B) Schematic of a microfluidic device with segmented gas-liquid flow used to perform cell stimulation and chemical cell lysis on-chip. Droplets of air are used to separate the liquid segments where the reactions occur. Image taken from (34).

## 1.4 Droplet-based microfluidics for artificial cell model construction

Bearing in mind the diversity of cell types (tens of millions), the diversity of cellular functions and molecular pathways associated to them, the full understanding of a cell and its biological processes seems an impossible task or at least one of the biggest challenges of the 21$^{st}$ century.

In the last few years it has been shown how molecular and conceptual similarities between prokaryotic and eukaryotic cell biology make bacteria powerful model systems for addressing fundamental biological questions (35). Nevertheless bacteria also represent complex systems in which not all biological

mechanisms have been completely understood. Taking in account this problem, there is a growing need of new tools capable to help experimentalists in the difficult task of understanding the components of life.

In order to demonstrate the understanding of biological processes, often scientists strive to synthetically recreate them (36) believing in the Richard Feynman's quote *"What I cannot create, I do not understand"*. This appealing and challenging approach aims for the construction of artificial cell systems which could help us try to understand life and its components by mimicking them.

In the last century, the term "artificial cell" has been widely used to refer to man-made systems capable of replacing or substituting cell functions leading to applications including blood cells substitutes (37), gene therapy (38) and targeted drug delivery systems (39).

In the late 1990s scientists successfully compartmentalized genes in small aqueous droplets of water in oil emulsion for directed evolution of proteins and RNAs (40) giving rise to the technique known as *in vitro* compartmentalization (IVC) (41) (Figure 1-9). This appeared as a simple example of artificial cell production, where gene expression function was occurring within a close compartment resembling the cell. This work not only broadened the applicative field of artificial cell systems but also showed the compatibility of expression systems with polydisperse and later on with monodisperse emulsions achieved using droplet-based microfluidics. Due to the micron dimensions of microdroplets produced through droplet-based systems, it has suddenly become clear that this technology will be useful in experimental biology (42), cell mimic and directed evolution.

Taking inspiration from this last work, the second major investigation of this research focused on the development of artificial cell platforms where biological investigation of proteins can be carried out. This results in the construction of monodisperse artificial-cell models where proteins can be directly produced within the chassis, opportunely analysed with conventional techniques of investigation like optical microscopy, and even released under osmotic shock.
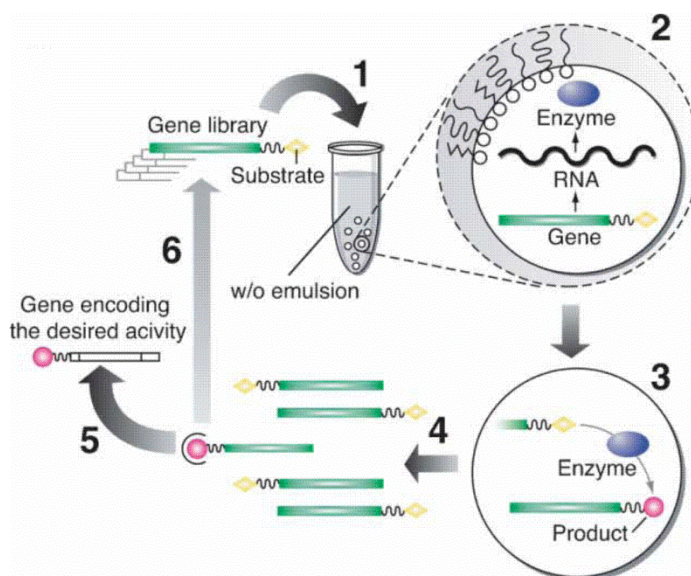
Figure 1-9 In vitro compartmentalization (IVC). (1) Formation of an emulsion of droplets of water in oil. Droplets contain genes with substrate molecule(s) attached and all the ingredients necessary for cell-free gene expression. The genes are expressed (2) and they produce enzymes able to convert substrates into products (3). The genes are recovered from the emulsion (4) and those of interest are isolated (5). Image taken from (40).

## 1.4.1 Protein expression within microdroplets

The expression of proteins using the basic biologic constituents of cells encapsulated within microdroplets has already appeared in literature. For example, customised DNA templates and commercially available cell-free expression systems have been combined and encapsulated into microdroplets, in which water-soluble proteins such as Green Fluorescent Protein (GFP), rsGFP (red-shifted GFP) and organophosphorus hydrolase enzyme (OpdA) are expressed and freely diffuses in the droplet's "cytosol" (29, 30) (43).

Droplets of water in oil (W/O), synthesised in microflow systems, are attractive in their simplicity and ease of production but provide only a limited cellular model, being, by their nature, surrounded by a continuous phase that is hydrophobic. One of the main properties of cellular organisations, that enables highly complex biochemical tasks and responses, lies with their ability to compartmentalise biological molecules through the use of membranes. For example, the cell membrane provides a non-polar environment which separates the aqueous extracellular environment from the cell's aqueous internal compartment. Hydrophobic interactions generated within this membrane space provide one of the driving forces which account for the distribution of different

proteins in the cell. Thus, in order to create a system which mimics more closely some aspects of a natural cell, more complex microfluidic systems comprising water in oil droplets re-dispersed in water (W/O/W), where a thin hydrophobic environment (O) separates the continuous external aqueous environment (W) and the segmented internal environment (W) could be used.

In much the same way as water-soluble proteins have been expressed in cell free systems in W/O microdroplets, the same water-soluble proteins have also been expressed in these double emulsion systems (44).

The W/O/W droplet is particularly attractive as a simple model of a biological cell as it provides a non-polar, hydrophobic membrane environment, as an interface between a predominantly aqueous internal (segmented) and external (continuous) environment. Although such structures have generally been formed as phospholipidic vesicles, which have been produced in both bulk reactors (45-48), and using microfluidics (47, 49), such systems are not robust and generally present the user with significant complications in their storage, transfer and use due to the fragility of the thin bilayer membrane. In fact the low molecular weight of lipids (total molecular weight of less than 1 kDa) imparts biomembranes with lateral fluidity (50), moreover lipids are subjected to ready oxidation and mechanical stresses (51). Nevertheless the phospholipidic vesicle represents a useful method for the production of cell mimics since they are the natural component of cell membranes (52).

The investigation carried out in this research aims to develop structures with robust and stable hydrophobic membranes where any kind of protein would be suitable to be expressed. In this study, the protein taken into consideration was an actin-like prokaryotic protein, called MreB. This protein would naturally assemble in the bacterial membrane environment amongst cytoplasmic filaments lying just beneath the membrane (Figure 1-10).

To gain understanding of the role of MreB, scientists have used many different methods of investigation, including site directed mutageneis, immunocytochemical fluorescence staining with fluorescence microscopy, drug treatment and biophysical simulation (53), (54) but a complete understanding of all its functions in bacteria is still missing. The availability of platforms which resemble in some aspects the living cell would certainly allow experimentalists

to prove their hypothesis on some not well understood aspects of this protein behaviour.

Most recently, it has been hypothesized that the origin of *E. coli* MreB membrane binding activity relies on the presence of an N-terminal amphipathic helix (53). Here in this study it has been also proved that MreB protein has some preference towards hydrophobic membranes. Results achieved in this study proved that, even if thickness and chemical compositions of the membranes are far from the biological ones they are still able to provide sufficient stimuli and demonstrate that this protein exhibits a notable preference towards the hydrophobic membranes. Description of the proposed approach and obtained results can be found in Chapter 5.
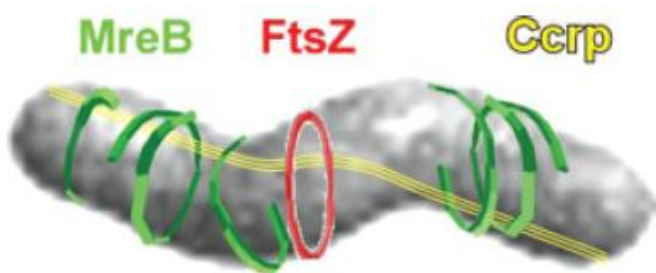


Figure 1-10 Cytoskeletal elements in rod-shaped bacteria like *E. coli*. MreB (green) is a protein that shows preference towards the cell membrane and it polymerises as helical filaments within the cell. FtsZ (red) is a protein forming a ring at the mid of cell in the point where cell division is initiated. Ccrp (yellow) is a protein that affects the membrane curvature and crosses all the entire length of the cell. Image taken from (55).

## 1.4.2 Polymersomes as artificial cells

Although a double emulsion consists of robust shells that mimic the cell membranes with an aqueous interior and exterior, and allow the synthesis of biological molecules (including the production of proteins), they present several limits. Due to the presence of the oil phase, the membrane thicknesses cannot reach the nanometre magnitude order limiting any application that would include a complex protein within the membrane. Membrane proteins are in fact usually related to signal transduction, cell response and cell communication and they are useful for expanding the functionality of a cell model system. Moreover the oil phase affects the biocompatibility of these systems, which represents an

ideal characteristic for applications of these systems in tissue engineering, drug delivery and cosmetics (56).

An interesting alternative to double emulsion and phospholipidic vesicles is represented by polymeric vesicles, also known as polymersomes, whose membranes are made of amphiphilic synthetic block copolymers (57). Depending on the relative length of hydrophobic and hydrophilic chains, in aqueous environment these systems are able to assemble in various structures such as vesicles, wormlike and spherical micelles (58) (Figure 1-11). Moreover, the thicknesses of the membrane, which ranges from a few nanometre to a few micrometres and is strictly dependent on the molecular weight of the polymers, as well as elasticity, permeability and mechanical stability can be tuned according to the chemical composition of the chosen polymers (59).
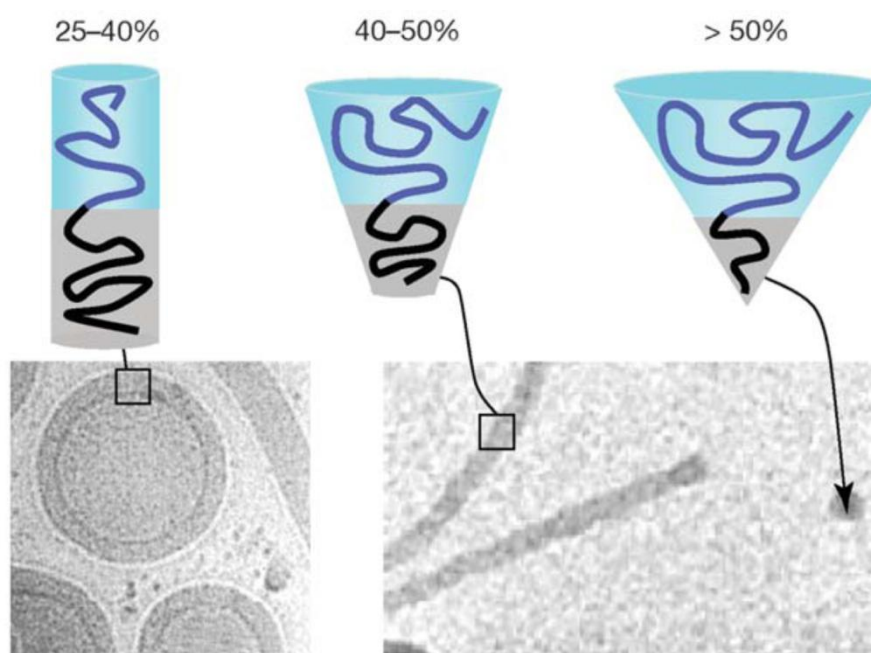


Figure 1-11 Polymersome's morphology. The morphology of polymersomes is ruled by the hydrophilic fraction *f* present in the polymer and expressed as percentage of the total mass of the block polymer used. Experimental rule establish that for f~35% polymeric vesicles are formed, whereas 40%<f<50% and f>50% worm like structure and spherical micelles. For f<25% inverted structures are formed. Image taken from (50).

For the construction of artificial cell models, polymersomes represent a valid alternative to W/O/W double emulsion droplets and indeed they have already been used in several applications (56) including mimicking of leukocytes adhesive properties (60) (Figure 1-12 A) and production of membranes responsive to stimuli such as illumination (61) (Figure 1-12 B) and pH (62).
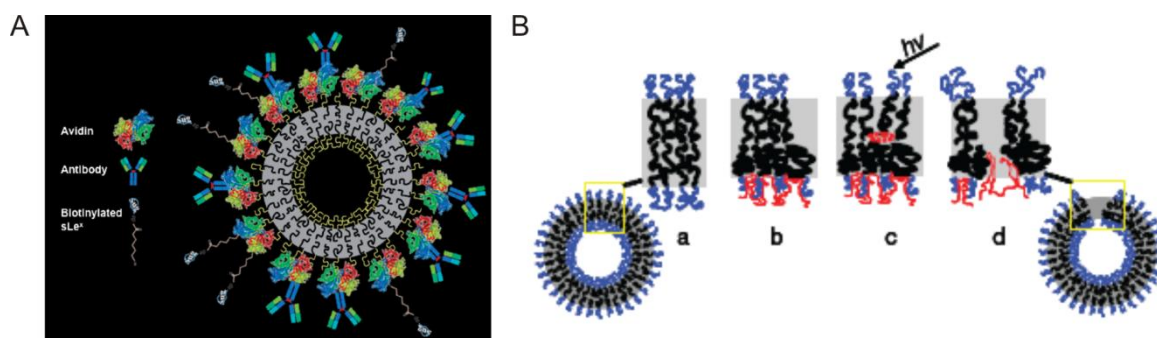
Figure 1-12 Polymersomes applications. A) Leukopolymersome realised through insertions of selectin ligand SLe$^x$ and antibody. Image taken from (60). B) Light sensitive membrane which integrated porphyrin protein within the polyethylene oxide-polybutadiene diblock copolymer membrane. When the light reaches the porphyrin, the receptor modify its structure and acts as channel opening the polymersome. Image taken from (61).

However, conventional approaches to polymerosome production, including for example electroformation, produce polymersomes with poor control of size and a low efficiency of encapsulation, which has restricted their use as artificial cells. The limitations associated with the introduction of material within the polymerosome chassis and the uniformity of their size can both be overcome through the use of microfluidic techniques for the production of polymersomes (63, 64). Moreover the possibility to choose polymers with different block ratios and to incorporate different homopolymers within the shell expands the application of this class of systems.

The third goal of this research aimed to combine the experience gained by expressing protein within a double emulsion with the use of polymeric shells to produce a novel system for protein release, which has never appeared in the literature. Using biocompatible and biodegradable shells, osmotic shock was performed on these systems demonstrating a synchronised ability to release cell-free expressed proteins. Description of the proposed approach and obtained results are described in Chapter 6.

## 1.5 Thesis outline

The thesis is organised in seven chapters which are structured as follows.

Chapter 2 gives the reader a theoretical background of fluid mechanics at the nanolitre scale where microdroplet formation is detailed. The chapter also introduces physical ingredients to describe the motion of fluids and shows different approaches to produce microdroplets homogenous in size. A few essential concepts such as stability and surface chemistry control are also described.

Chapter 3 deals with the materials and the methods used in the entire research. This comprises microfabrication and biotechnology techniques. The former are techniques developed for microelectronics and are used for fabrication of microfluidic devices, the latter belong to the biology field and are used for the development of immunoassays and the formation of artificial cell models.

Chapter 4 describes the development of an immunoassay in microdroplets and the results obtained.

Chapter 5 presents the characterization of a commercially available system for double emulsion production, the results obtained in cell-free MreB-RFP expression and observations of the protein's behaviour.

Chapter 6 describes the formation of polymersomes and MreB-RFP release after its previous cell-free expression within the polymeric chassis.

Chapter 7 summarizes the findings obtained during the entire research and indicates some of the avenues that future works could focus on.

# 2 Theoretical background

The term microfluidics refers to the science and technology of systems that manipulate small amounts of fluids, generally on the nanolitre scale and below (65). It is a multidisciplinary research field aimed at the precise control and manipulation of fluids that are geometrically constrained to small, typically sub-millimetre, length scales (65). The dimensions of microfluidic systems exploit the counter intuitive characteristics of fluids at these scales. The fluid motion in a microfluidic channel can be represented by *laminar flow*.

Through control and understanding of fluid dynamics and chemical composition, it has been shown that microfluidic devices are able to produce emulsions; systems of two immiscible fluids mixed together where one fluid is dispersed in the form of small droplets inside the other fluid (oil droplets in a water flow, for example). This Chapter introduces an understanding of fluid behaviour at the micron scale, microdroplet formation within microfluidic channels and some parameters that characterise and control emulsion stability over the time.

## 2.1 Single and double phase fluid physics at nanolitre scale

Fluids flowing in micrometre-scale conduits, or microchannels, are dominated by the viscous properties of the fluid at the expense of the inertial forces generated by the fluid. This flow regime, called laminar flow, allows the movement of momentum, heat, and chemical species inside a microfluidic device to be calculated with great accuracy (66).

In laminar fluid motion conditions, a fluid flowing in a channel is considered as a composition of parallel layers which slide over one another, with no disruption between the layers. The innermost layer flows the fastest, and the layer touching the wall does not move at all (Figure 2-1). In this flow regime the

friction between the layers, also known as *shear stress*, depends almost only on the dynamic viscosity and is independent of fluid density. The shear stress $\tau(y)$ at a surface element, at any point $y$ on the radial direction of the channel, is given by Equation 2-1

$$\tau(y) = -\mu \frac{\partial v}{\partial y}$$

2-1

where $\mu$ is the dynamic viscosity of the fluid, $v$ is the velocity of the fluid along the boundary and $y$ is the height above the boundary. Fluids which respect the Equation 2-1, for a constant $\mu$, are called Newtonian.
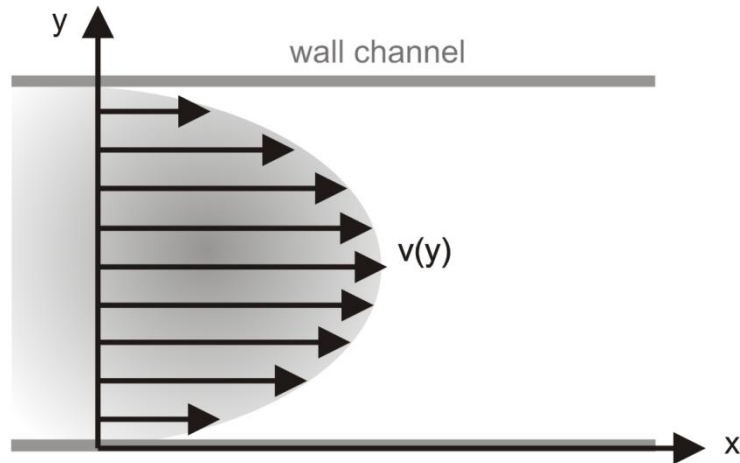


Figure 2-1 Velocity field of a Newtonian fluid flowing in a microchannel. Velocity has a parabolic profile, it is maximum in the centre of the channel and is null at the wall.

The Newtonian fluid behaviour is described by the *Navier-Stokes* equation (Equation 2-2) that, together with the *equation of mass conservation* (Equation 2-3) and well formulated boundary conditions, accurately models fluid motion. For an incompressible fluid, where the density is considered uniform in every part of the fluid, it is possible to write the two aforementioned equations as follows:

$$\rho \left( \frac{\partial v}{\partial t} + v \cdot \nabla v \right) = -\nabla \cdot p + \mu \nabla^2 v + f$$

2-2

$$\frac{\partial \rho}{\partial t} + \nabla \cdot (\rho v) = 0$$

2-3

where $\rho$ is the density (Kg m$^{-3}$), *v* the velocity (m s$^{-1}$), *p* the pressure (N m$^{-2}$), $\mu$ the dynamic viscosity (Pa s) and *f* the external applied body forces (N). As previously stated, in microfluidic devices inertial forces are small compared to viscous ones and thus the nonlinear term can be neglected, leading to Equation 2-4:

$$\rho \frac{\partial v}{\partial t} = -\nabla \cdot p + \mu \nabla^2 v + f \qquad \text{2-4}$$

Considering a constant density the Equation 2-3 becomes

$$\nabla \cdot v = 0 \qquad \text{2-5}$$

In fluid dynamics, the relative importance between inertial and viscous forces is expressed with the dimensionless *Reynolds number (Re)* (Equation 2-6) defined as

$$\text{Re} \equiv \frac{\rho U_0 D_h}{\mu} = \frac{f_i}{f_v} \qquad \text{2-6}$$

with $f_i$ and $f_v$ being inertial and viscous stress respectively, $\rho$ the density, $U_0$ velocity of the fluid and $D_h$ the hydraulic diameter (given by 4 times the ratio between the cross sectional area and the wetted perimeter of the cross-section). For common microfluidic devices, considering water as the working fluid, typical velocities in the range of 1 μm s$^{-1}$ - 1 cm s$^{-1}$ and channel radii of 1–100 μm, Reynolds numbers range between 10$^{-6}$ and 10. Having these low Reynolds numbers allow microfluidic systems to exploit linear regular deterministic flows. However, in the presence of particular physical processes, such as capillary effects at free surfaces, viscoelasticity in polymer solutions and electrokinetic effects, some non-linearities can arise.

Another important physical characteristic in low Reynolds number flows is the absence of turbulent mixing. Laminar flows ensure mixing occurs only by diffusion, thus increasing mixing time. The dimensionless *Peclet number (Pe)* expresses the ratio between convection and diffusion (Equation 2-7)

$$Pe \equiv \frac{U_0 w}{D} \qquad \text{2-7}$$

where *D* is the diffusivity of a substance (m$^2$ s$^{-1}$) and *w* the width of the channel.

Thus low *Reynolds* and *Peclet* numbers characterize a laminar flow regime where two joining fluids will not mix readily via turbulence, thus, finally, the diffusion must cause the two fluids to mix. Thus, gradients of concentration are produced only with diffusion. This phenomenon becomes tangible observing the *convection-diffusion equation* for non compressible fluids (Equation 2-8), which describes the conservative transport of mass of a species *a,* in this case expressed in molar quantities (67)

$$\frac{\partial c_a}{\partial t} = -v \cdot \nabla c_a - (\nabla J_a) + R_a \qquad \text{2-8}$$

where $c_a$ is the molar concentration defined as the number of moles of *a* per unit volume of solution, $J_a$ is the molar flux of species defined as the number of moles of *a* flowing through a unit area per unit time, *v* is the molar average velocity, $R_a$ is the molar rate of production of *a* per unit volume. If the convective term is negligible and no chemical reactions occur (this means all chemical production terms are zero) the equation is governed only by the diffusion term. In these conditions the equation 2.1 becomes equal to

$$\frac{\partial c_a}{\partial t} = D \nabla^2 c_a \qquad \text{2-9}$$

which is called *Fick's second law of diffusion*, or *diffusion equation,* where *D* is the diffusion coefficient of species *a* in the medium where it diffuses.

The introduction of a second immiscible phase within the considered system originates an interface between the two phases and modification to the flow and pressure fields (66). These modifications are introduced by the presence of *interfacial tension* between the immiscible fluids which represents the energy per unit area ($J\ m^{-2}$ or $N\ m^{-1}$) required to minimise the total surface area in order to reduce the free energy of the interface. The minimum area for a given volume is a sphere which is the shape taken by isolated droplets in two phases system (66).

The interfacial tension is also related to the pressure difference between the inside and the outside of the droplet which is also known as *Laplace pressure (ΔP)* and described by the *Young-Laplace equation* (Equation 2-10)

$$\Delta P = \left( \frac{1}{R_1} + \frac{1}{R_2} \right) \gamma \qquad\qquad \text{2-10}$$

where *R1* and *R2* are the principal radii of curvature of the interface into orthogonal directions and *γ* the interfacial tension between the two fluids.

## 2.2 Physics of microdroplet formation in microfluidic devices

As previously described in Chapter 1, microfluidic technology has demonstrated the ability to produce uniform stream of droplets having diameters ranging from a few micrometres to hundreds of micrometres in a uniform, evenly spaced, continuous stream (7). Generally, the uniformity of the produced emulsion is measured through the *coefficient of variation (CV)* between the droplet diameters which represents the ratio between the standard deviation and the mean value of the droplet diameters in the emulsion. This value is usually expressed as a percentage.

Various strategies for droplet production have been implemented in recent years. All of them have in common a carrier phase, usually called a *continuous phase*, and a *dispersed phase* which represents the actual fluid of the droplet. The most common methodology of droplet generation involves the use of immiscible fluids actuated by either constant volumetric flow rate (l s$^{-1}$) of dispersed and continuous phase ($Q_D$ and $Q_C$) or pressure ($P_D$ and $P_C$) (Figure 2-2).

In the understanding of droplet formation within a system that comprises two immiscible phases, a wide range of phenomena need to be taken in account. In broad terms, the droplet formation always originates from a competition between local fluid stresses that act to deform the interface (continuous-dispersed phase) and capillary pressure, which is the difference in pressure across the interface between the two immiscible fluids, acting to resist the deformation (7). In addition, the growing droplet within the junction leads to an increase in the up-stream pressure leading to the droplet pinchoff. The relative magnitude of the viscous stress (viscous shear forces) compared with the

capillary pressure (or interfacial tension between the two fluids) is described by a dimensionless number called *Capillary number (Ca)* given in Equation 2-11

$$Ca \equiv \frac{U_0 \mu_C}{\gamma}$$

2-11

where $U_0$ is the mean velocity of the continuous phase in the channel, $\mu_c$ the viscosity of the outer phase and $\gamma$ the surface tension between the two fluids. In microfluidic droplet formation the capillary number is typically >1 with values that range from $10^{-3}$ to $10^1$. Inertial forces also have a role in the droplet formation, even if in microfluidics inertia is the least important of the three key entities (viscous stress, capillary pressure and inertia) (7).

Two additional dimensionless parameters can be found in the literature for the characterization of microfluidic droplet formation. These are the *ratio of volumetric flow rates φ* ($Q$d/$Q$c) and the *viscosity ratio λ* ($\mu$d/$\mu$c). In the limit as φ tends to 0, the dispersed phase liquid remains stationary (7).

Two-phase flow characteristics in microchannels are determined by flow conditions, fluid properties and channel geometry (68). A complete understanding of droplet formation within microfluidic channels has yet to be achieved, leading to a variety of geometries appearing in the literature (68). The three geometries adopted in this research are reported below.

## 2.2.1 Crossflow stream: T-junction and X-junction

The T-junction geometry was demonstrated for the first time in 2001 by Quake's Group (69) and consists of two channels intersecting to form a T. The emerging droplet can be unconfined in the continuous phase channel or confined in the continuous flow channel. For the first case, the width of the continuous phase channel has to be at least five times larger than the dispersed phase channel, with the droplet size depending solely on the capillary number. In confined droplet formation, the channel widths of both phases are comparable or equal; the emerging droplet disrupts the continuous flow obstructing the junction as it grows, leading to an increase in the upstream pressure which, in turn, drives the "pinch off" of the droplet. Moreover, the plug length decreases by increasing

the ratio of flow rate between the dispersed and the continuous phase (70). A schematic representation of the forces acting at a T-junction is presented in Figure 2-2.

The X-junction was introduced for the first time in 2003 for the formation of microdroplets of tetradecane in water (71). It consists of two perpendicular channels forming a cross (Figure 2-3). Unlike the T-junction geometry, where the plug length depends by the ratio of the two phases, in the X-junction the plug length decreases only by increasing the continuous phase flow rate (70). This can be attributed to the symmetrical flow of the continuous phase that plays a crucial role in the droplet break-up (70).
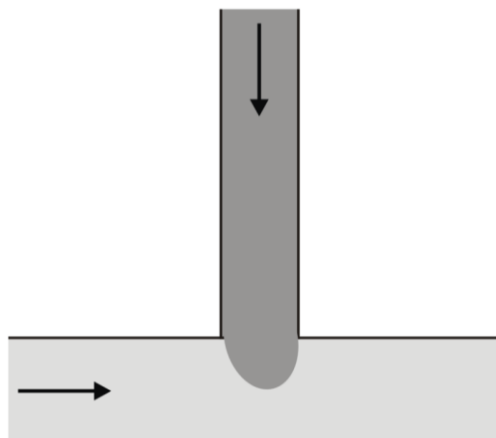
Figure 2-2 Planar T-junction geometry. Droplet formation at the T-junction of two channels where continuous and dispersed phases meet. Arrows describe the direction of the two fluids.
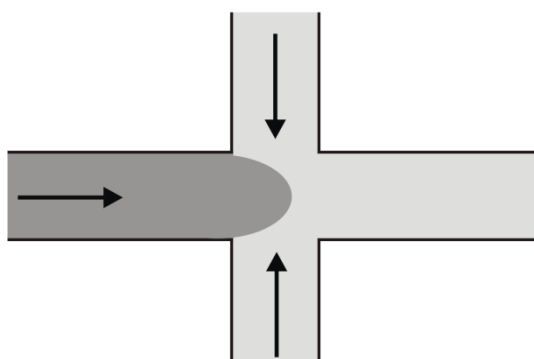
Figure 2-3 Planar X-junction geometry. Droplet formation in this geometry is strongly dominated by continuous phase flow rate. The plug length decreases only by increasing the continuous phase flow rate. Arrows describe the direction of the two fluids.

## 2.2.2 Flow focusing

In this geometry the two immiscible fluids flow into coaxial channels and enter in contact at the tip of the inner channel. At this point the inner fluid forms a droplet at the junction downstream. This geometry was implemented in a microfluidic format for the first time in 2003 by Stone's Group (72) with several variations on this theme having appeared in the years since. A flow focusing geometry was also adapted for the production of double emulsions (24) and used in this study for the production of polymersomes. In a flow focusing configuration the droplet formation is mostly helped by the elongation-dominated velocity field in the continuous phase that deforms the inner dispersed phase into a thin jet that breaks into droplets. A diagram of the geometry is given in Figure 2-4.
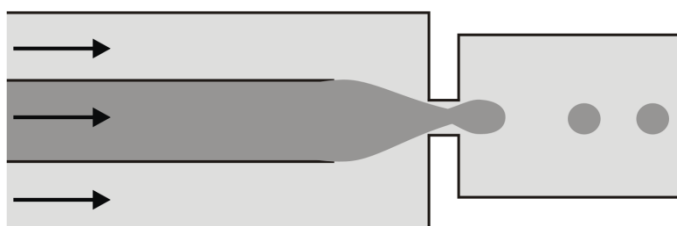


Figure 2-4 Planar flow focusing geometry. Elongational flow generates droplets. The restriction of the continuous phase channel is called orifice. Arrows describe the direction of the two fluids.

## 2.2.3 Wetting and dewetting

The ability of a liquid to maintain contact with a surface is called wetting. The wettability of microchannel surfaces has a direct influence on the formation of droplets, and determines which liquid phase is dispersed (7). For example, in the formation of a water droplet in a continuous oil phase it is expected that if the cohesive forces of the water molecules are higher than the adhesive forces to the channel, the detachment of the water phase will produce droplets more easily. The water flowing into the channel will produce a convex meniscus, further helping the process of droplet formation (Figure 2-5).

hydrophobic        hydrophilic
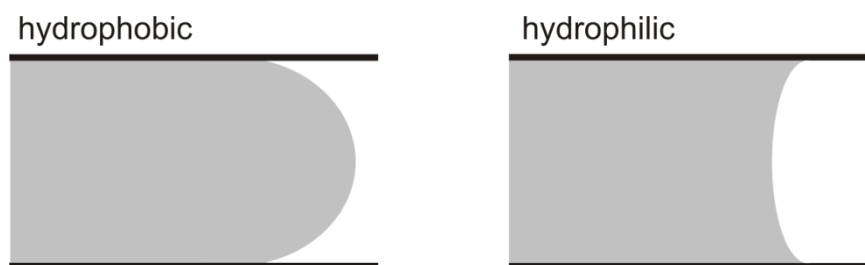
Figure 2-5 Water behaviour in hydrophobic and hydrophilic channels. In the first case (on the left), the cohesion forces of molecules of the fluid are higher than adhesion forces to the surface, in the second case (on the right) is the inverse.

Measurements of wettability are obtained by observing the contact angle *θ* formed at the liquid/substrate interface (Figure 2-6). A contact angle <90˚ (low contact angle) usually indicates favourable high degree of wetting, spreading the fluid over a large area of the surface. Contact angles >90˚ (high contact angle) generally indicate a surface which does not wet well; the fluid minimizes contact with the surface and forms a compact liquid droplet. In the case of water based solutions, surfaces with a low contact angle are referred to as *hydrophilic*, whereas those with high contact angles are referred to as *hydrophobic* surfaces.
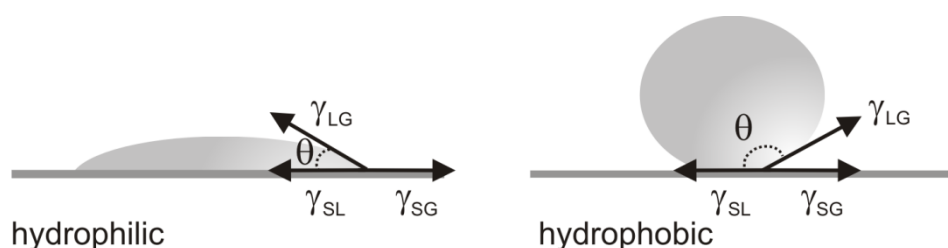


Figure 2-6 Contact angle θ of a water droplet on hydrophilic and hydrophobic surfaces and vectorial representation of surface tension between solid and liquid $\gamma_{SL}$, solid and gas $\gamma_{SG}$ and liquid and gas $\gamma_{LG}$.

The contact of a droplet on a solid surface (Figure 2-6) can be described by *Young's equation* which puts in correlation the contact angle between the droplet and the substrate with the three surface tensions: solid-liquid, liquid-gas and liquid-solid. This equation can be interpreted as a force balance on the three contact lines and it is equal to (Equation 2-13)

$$\gamma_{SG} = \gamma_{SL} + \gamma_{LG} \cos \theta$$

2-12

where $\gamma_{SL}$ is the surface tension between solid and liquid, $\gamma_{SG}$ is the surface tension between solid and gas and $\gamma_{LG}$ the surface tension between liquid and gas.

The way how a liquid, like water, behaves when is in contact with another liquid (like a droplet of oil) can also be described by a parameter called *spreading coefficient (S)*. Taking in consideration the system presented in Figure 2-7 the spreading coefficient is calculated as follows (Equation 2-14):

$$S = \gamma_{WA} - (\gamma_{WO} + \gamma_{OA})$$

<div align="right">2-13</div>

where $\gamma_{WA}$ is the surface tension between water and the gas phase, $\gamma_{WO}$ is the surface tension between water and the oil phase and $\gamma_{OA}$ the surface tension between liquid and gas. Positive values of S imply that spreading (of oil on the water surface) occurs spontaneously, whereas for negative values dewetting between the two phases occurs.



Figure 2-7 The displacement of a droplet of oil on a water surface is described by the spreading coefficient S. A positive value implies that the droplet spreads on the surface forming a layer (wetting), whereas a negative value implies that the droplet will form an oil lenses on the water surface.

The formation of stable core-shell structures such as double emulsion systems (W/O/W and O/W/O droplet) requires that the shell completely wets the inner core. When this is not the case, a dewetting of the shell occurs with consequent disruption of the double emulsion system. Interestingly the dewetting between the inner core and the outer shell of a double emulsion system has been exploited for the production of polymersomes (63). Figure 2-8 presents the mechanism of dewetting between the inner and the middle phase and the formation of a thin bilayer of copolymer dispersed in the middle phase. In this system the S coefficient (Equation 2.15) is equal to:

$$S = \gamma_{IO} - \gamma_{IM} - \gamma_{MO}$$

2.14

where $\gamma_{IO}$, $\gamma_{IM}$ and $\gamma_{MO}$ are respectively the surface tensions between the inner-outer phase, the inner-middle phase and the middle-outer phase.
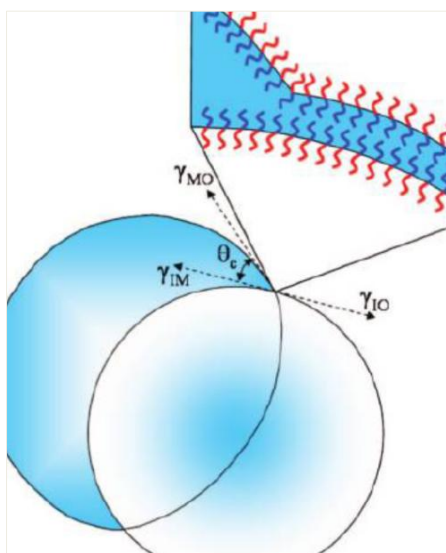


Figure 2-8 Dewetting of the middle organic phase, from the watery core, of a double emulsion system dispersed in a water based solution (W/O/W). Copolymer molecules (containing both hydrophobic and hydrophilic portions) are dispersed in the middle phase. Dewetting event allows the formation of a bilayer of copolymer. $\theta_c$ is the contact angle at the three-phase contact point. Figure taken from (63).

## 2.3 Emulsion stability

A mixture of two immiscible fluids, where one is dispersed in the form of small droplets inside the other, is known as an emulsion. Emulsions may also contain smaller droplets of the continuous phase dispersed within each droplet of the dispersed phase. Such systems are called double emulsions or multiple emulsions (73).

From a fluid dynamic point of view, when the emulsion is strongly diluted droplets are agitated by Brownian motion (73), and the emulsion behaves as a viscous Newtonian fluid. When the emulsion is concentrated (64% of the emulsion is made of monodisperse droplets) the emulsion behaves as a viscoelastic solid (74, 75).

Emulsions are not thermodynamically stable systems, requiring energy for preparation and specific properties to persist. Without any stabilizing agents the two immiscible phases can break down, which may proceed through two mechanisms.

The first is called *Ostwald ripening* (76), also known as *molecular diffusion,* and it originates from the spontaneous tendency of droplets to grow in radius as time evolves. Small droplets in the continuous phase diffuse towards the larger droplets until they merge. This is a thermodynamically-driven spontaneous process occurring both in solid and liquid systems and it occurs because larger particles are more energetically stable than smaller particles due to the lower surface/volume ratio. The second mechanism is called *coalescence* which happens when a thin liquid film formed between two adjacent droplets undergoes to a rupture. The result of this phenomenon is the formation of large droplets originating from smaller adjacent droplets. The interplay of these two phenomena results in the destruction of the emulsion. To contrast and delay these phenomena and consequently increase the lifetime of the emulsion the addition of surface-active species is required.

## 2.3.1 Surfactants

Surface-active substances (also known as *surfactants*) can increase the kinetic stability of emulsions, by decreasing the surface tension, so that the emulsion does not change significantly over time. Surfactants are amphiphilic molecules meaning that they contain both hydrophilic and hydrophobic groups. The former are contained in a portion of the molecule called "head", the latter in the "tail" (Figure 2-9).
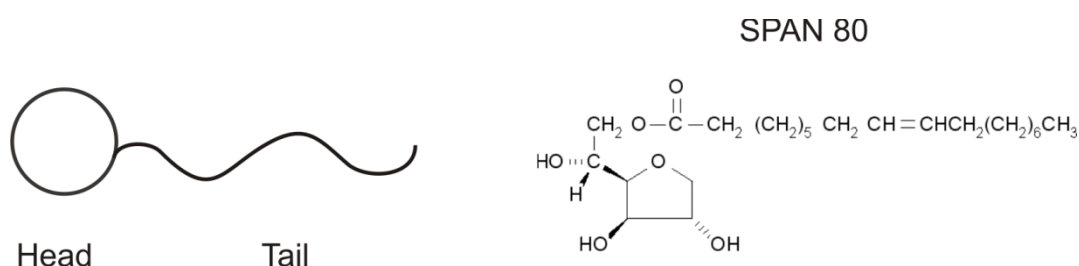


Figure 2-9 Surfactant structure. On the left, the surfactant structure representation made of a hydrophilic head and a hydrophobic tail. On the right, the chemical structure of one of the most common non ionic surfactant (SPAN™ 80) used in droplet-based microfluidics.

Different types of surfactants exist; all of them are classified according to either the composition of the head which is hydrophilic, or the composition of the tail which is hydrophobic. Surfactant molecules assemble at the interface of the two fluids and form an oriented layer causing an expansion of the interface. This phenomenon balances the natural behaviour of the surface of contraction. The measure of how a surfactant is hydrophilic or hydrophobic is established by the *hydrophilic-lipophilic balance (HLB)* and is measured by empirical formulae. A value <10 indicates the surfactant is lipid soluble and ideal for the formation of droplets of water in oil. A value >10 indicates that the surfactant is water soluble and suitable for the formation of droplet of oil in water. In droplet-based microfluidic applications, SPAN 80 is one of the most common surfactant used to stabilize droplets of water in mineral oil. Its HBL is equal to 4.3 and it is usually dispersed in mineral oil, in a weight percentage equal to 2%.

The concentration of surfactants dispersed in solution is a parameter to be considered because every surfactant has its own *critical micelle concentration (CMC)*. For concentrations above the CMC surfactants tend to aggregate into structure called *micelle*, which can be made of single or double layer. Figure 2-10 illustrates the trend of surface tension by the increasing of surfactant concentration. Micelles are formed above the CMC and their inner core is populated with hydrophobic chains while the corona contains polar groups.
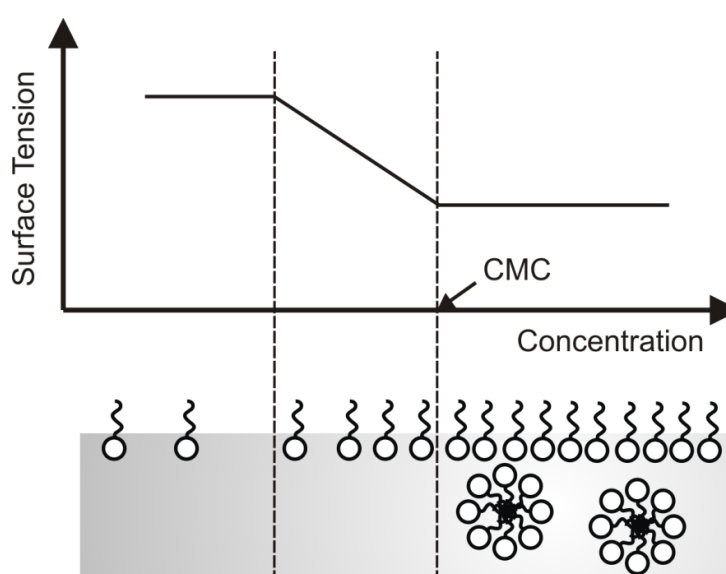


Figure 2-10 Trend of surface tension by the increasing of surfactant concentration. Micelles are formed above the CMC. In a watery solution, the inner core of micelles is populated with hydrophobic chains while the corona contains polar groups.

The morphology of the micelle is ruled by a dimensionless number called *packing parameter* (*p*), expressed by the Equation 2.16

$$p = \frac{V}{a_0 l}$$

2-15

where *V* is the volume of the hydrophobic chain, $a_0$ the optimal headgroup area and *l* the critical length chain which is the longest effective length that the chain can be extended in the fluid (Figure 2-11). According to the value of the packing parameter the micelles can organize themselves in:

- Spherical structures, for $p > 1/3$
- Cylindrical structures, for $1/3 < p < 1/2$
- Bilayer structures, for $p \approx 1$.

Cubic structures have also been observed for $1/2 < p < 2/3$ and $1 < p < 3/2$. The choice of which surfactant needs to be used, as well as the choice of the continuous phase and droplet liquids, depends highly on the nature of the application (17). For example, some experiments with biological material require increased oxygen permeability within the droplet, which can be achieved by choosing fluorinated oil rather than hydrocarbon oil like mineral oil.
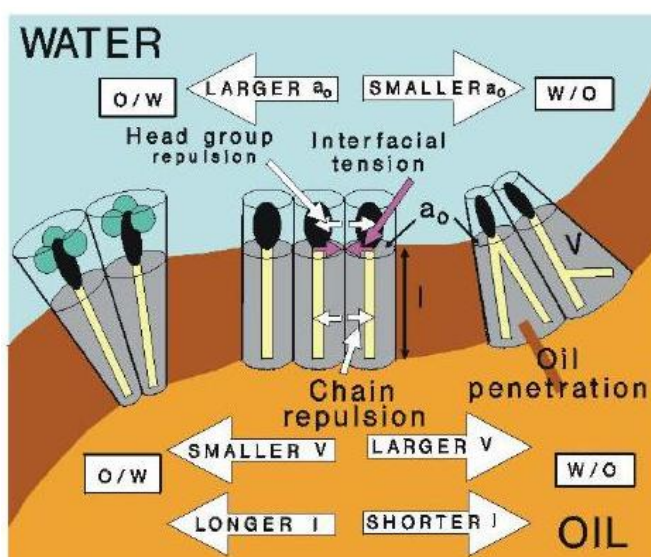


Figure 2-11 The packing parameter. It depends on the volume *V* of the hydrophobic chain, the optimal headgroup area $a_0$ and the critical length chain *l*. During the micelle formation process, the surface area is decreased, the interfacial energy is lowered but the repulsive energy of the headgroup (crowded into a smaller area) is increased. Picture taken from (77).

## 2.3.2 Water transport under osmotic pressure mismatch

When solutions made of the same solvent at different concentrations of solute are separated by a semi permeable membrane (permeable to the passage of solvent but not to the solute), the solvent molecules migrate from the less concentrated solution to the more concentrated solution in order to equalize the two compartments. This causes a rise in the level of fluid column and an increase of pressure against the membrane. This pressure increase is called *osmotic pressure*. A well-known representation of this phenomenon is given in Figure 2-12.
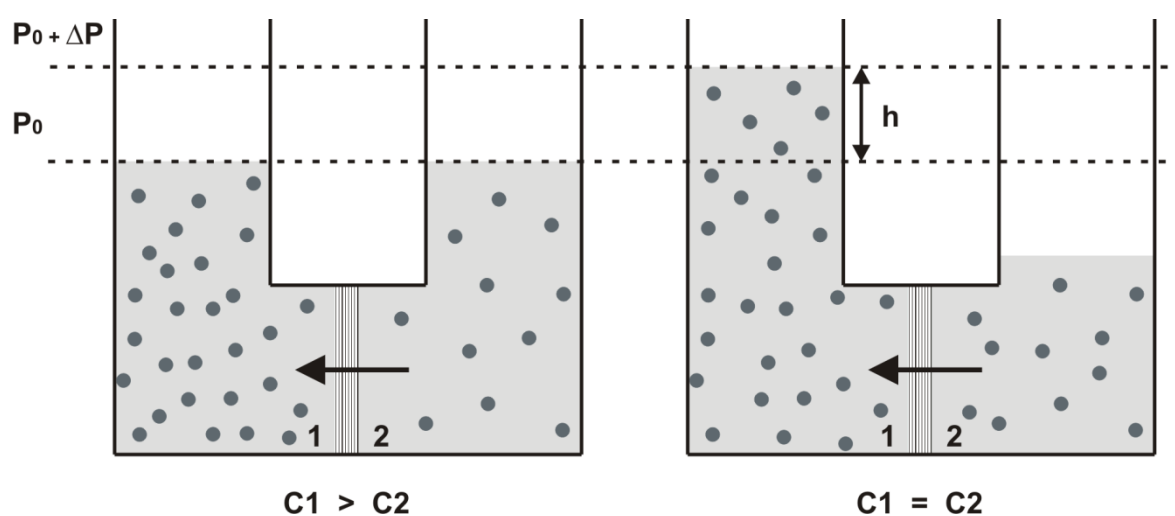


Figure 2-12 Water transport under osmotic pressure mismatch. Compartments 1 and 2 separated by a semi permeable membrane which allows the passage of solvent. At the start point the two compartments has different concentrations (C1>C2) which become equal at the equilibrium. The value of additional pressure ΔP is equal to ρgh.

This process needs to be taken in account in the formation of double emulsions made of thin membranes of oil or polymers. Under osmotic pressure gradients between the two aqueous phases of W/O/W emulsions, water may migrate either from the internal to the external phase (or vice versa) and compromise the stability of the emulsion. This depends on the direction of the osmotic pressure gradient. Figure 2-13 shows two possible scenarios where the droplet is exposed to inward (C1<C2) or outward (C1>C2) flux of solvent. Thus the solute concentration of the inner and outer water solution needs to be monitored and adjusted. This parameter is also known as osmolarity, defined as the number of osmoles of solute per litre of solution (Osm/L).
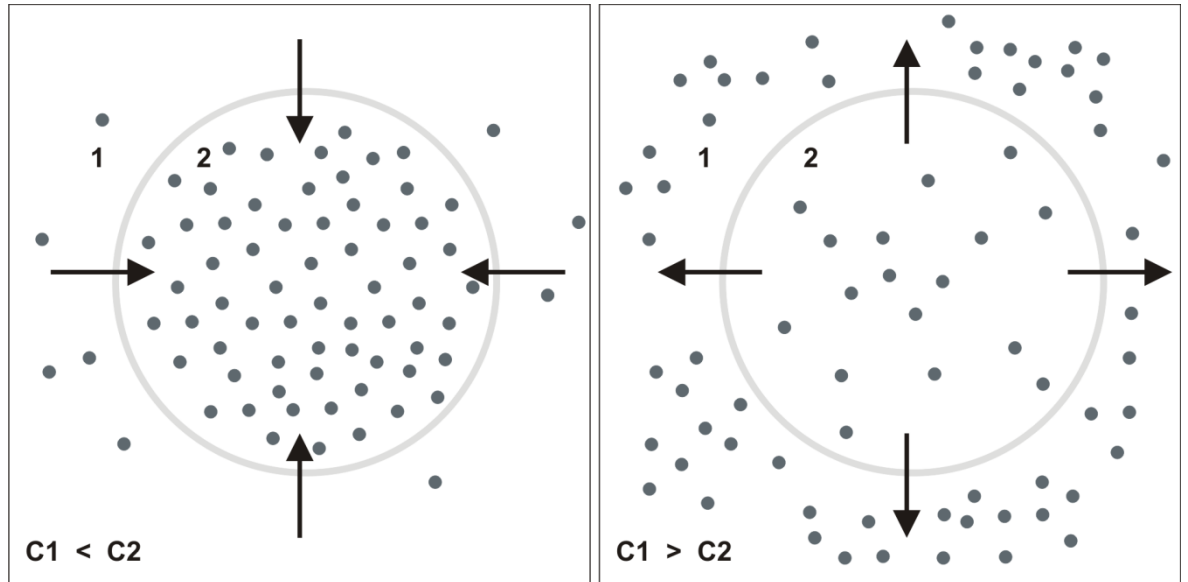
Figure 2-13 Emulsion made of a semi permeable membrane which allows the passage of solvent. On the left, the droplet has inward flux of solvent whereas on the right there is a net flux of solvent migrating out of the droplet.

# 3  Materials and methods

This Chapter is concerned with the general materials and the methods used through the entire thesis. These include microfabrication techniques used for fabrication of the microfluidic device, optical methods for the detection and measurement of protein concentrations and biological procedures used in DNA manipulation. Where necessary, more details of procedures can be found in the specified Section.

## 3.1 Introduction

The formation of single and double emulsions was obtained through the use of microfluidic chips realised with microfabrication techniques. The research used both plastic and glass chips. The former were made of a silicon-based organic polymer called polydimethylsiloxane (PDMS), transparent to visible light and sealed to a microscopy glass slide, the latter were either entirely made of a whole piece of glass or made by the assembly of two circular glass capillaries in a squared glass capillary. PDMS chips and one type of glass microfluidic chip used in this work (purchased from Dolomite Company, UK), were obtained by microfabrication techniques, namely, photolithographic and wet etching processes. These processes are discussed in this Chapter.

Moreover, in every application showed in this work, proteins were often tagged to fluorescent molecules in order to be detected.  The fluorescent molecules used are natural proteins that if excited by a particular wavelength, emit light at another wavelength. In order to link a fluorescent protein to the protein of interest, DNA manipulations were necessary. This Chapter discusses aspects of the optical detection of fluorescent molecules and the conventional laboratory procedures required for DNA cloning.

The Chapter also describes a method, used to achieve immobilization of biomolecules on solid support, which exploits the strong affinity between the avidin and biotin molecules and, finally, it details the method adopted to lyse cells on chip. This relies on the generation and exploitation of an electrical field capable of trapping cells and lysing cell membranes.

## 3.2 Materials

### 3.2.1 Droplets formation

As previously mentioned in Chapter 2, the droplet formation requires the use of two immiscible fluids such as water and oil, flowing in channels with a surface chemistry carefully controlled. In this research, the watery phase of the emulsion was either deionised (DI) water or a biological solution such as: an antibody solution, a cell suspension or a DNA solution in buffer. The oily phase was made of fluorocarbon oil (FC 40, Fluorinert$^{TM}$, 3M, USA) with addition of 2% (w/w) fluorinated surfactants PEG-PFPE (EA, Raindance Technology, USA) in the single emulsion formation and hydrocarbon oil (Mineral oil, M3516, Sigma, UK) with addition of 2% (w/w) of sorbitane monooleate (Span 80, Sigma, UK) in double emulsion formation. For the formation of polymeric vesicles the two immiscible phases were represented by a polymer PEG(5000)-b-PLA(10000) (Polysciences, Inc. USA) dissolved in a mixture of chloroform (25693, Sigma, USA) and Hexane (15671, Sigma, USA) and a biological mixture for protein expression. For imaging purposes fluorescent molecules were dissolved into the solutions; fluorescein isothiacyanate (FITC, Sigma, UK) was dissolved in water while dialkyl-carbocyanine iodide (DiI, Invitrogen, UK) and boron-dipyrromethene (BODIPY, Invitrogen, UK) were dispersed in the oil phase. Additional details on the materials used in this research can be found in the following Sections 4.2, 5.2.1, 6.2.1

## 3.3 Methods: microfabrication techniques

### 3.3.1 Soft lithography

Soft lithography is a microfabrication technique which allows the creation of polymeric microfluidic devices containing fluidic circuits made of chambers,

microchannels and valves, able to constrain and/or control fluids at the micron scale level (65). Soft lithography requires a master mould, created by lithographic and dry etching techniques, and a stamp, which is obtained by casting an elastomer into the master (Figure 3-1).



Master mould

Cast elastomer on master

Peel cured elastomer off the master
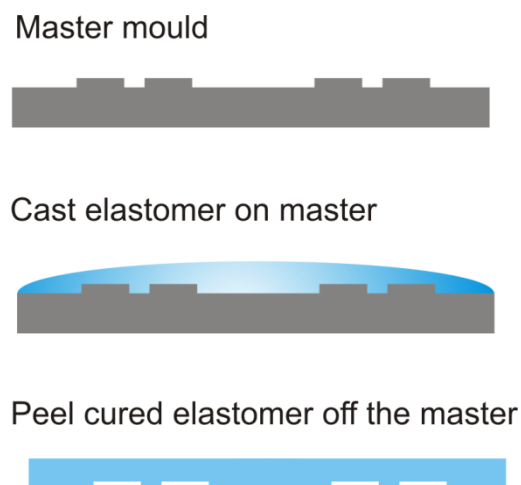
Figure 3-1 Sketch of the basic steps required for making an elastomeric mould used as microchip device. The master mould is usually an engraved silicon wafer on top of which an elastomer is casted and polymerised. After polymerisation the elastomer is peeled off and ready to be bonded to a glass substrate.

The elastomer, most often PDMS, consists of a polymer network that deforms under the influence of a force and regains its shape when the force is released. This elasticity explains the use of the term "soft" lithography. The PDMS is a two-component addition-cure silicone rubber. The monomer and the catalyst once mixed together start the polymerisation reaction. The final product is a material transparent to visible light, which is elastic, easy to manipulate, durable, gas permeable and chemically inert.

After polymerisation and cross-linking, solid PDMS presents an external hydrophobic surface caused by the exposure of methyl groups at the surface. This surface chemistry makes it difficult for polar solvents to wet the PDMS surface. However its interfacial properties can be modified, for example altering the surface chemistry with plasma oxidation. This process uses ionized oxygen atoms that, hitting the surface, make it reactive. With this treatment, frequently required for water-based microfluidics, the PDMS is also able to bond tightly to glass or other PDMS surfaces allowing the formation of sealed

channels. The bonding between glass and PDMS chains is assured by the covalent bonds between silicon oxygen radicals of the PDMS along with silicon radicals of the glass.

Details of protocol used for PDMS chip fabrication can be found in Section 4.3.1.

## 3.3.2 Photolithography

Photolithography is a microfabrication technique that enables the transfer of a desired geometric pattern onto a substrate (silicon wafer or glass slide) using UV light, a mask and a light sensitive chemical agent called photoresist.

The geometric pattern is designed using computer assisted design software which creates a file that gives instructions to a machine to form the pattern either on a glass slide or a transparent film. The mask is usually made of a thin layer of chrome deposited on a glass slide but for resolution down to 6 µm an inexpensive plotted transparent film can be taped to a glass slide.

The photoresists are polymers that, once exposed to a particular radiation, polymerise (78). Two kinds of photoresists exist: positive and negative. In the case of positive resist the radiation breaks the main and side polymer chains making the photoresist more soluble in developing solutions; for the negative photoresist, the radiation strengthens the polymer, which becomes slower in dissolving. Figure 3-2 shows the processes which involve the different types of photoresists.

Details of the protocol used for photolithography can be found in Section 4.3.1.

Spinning resist
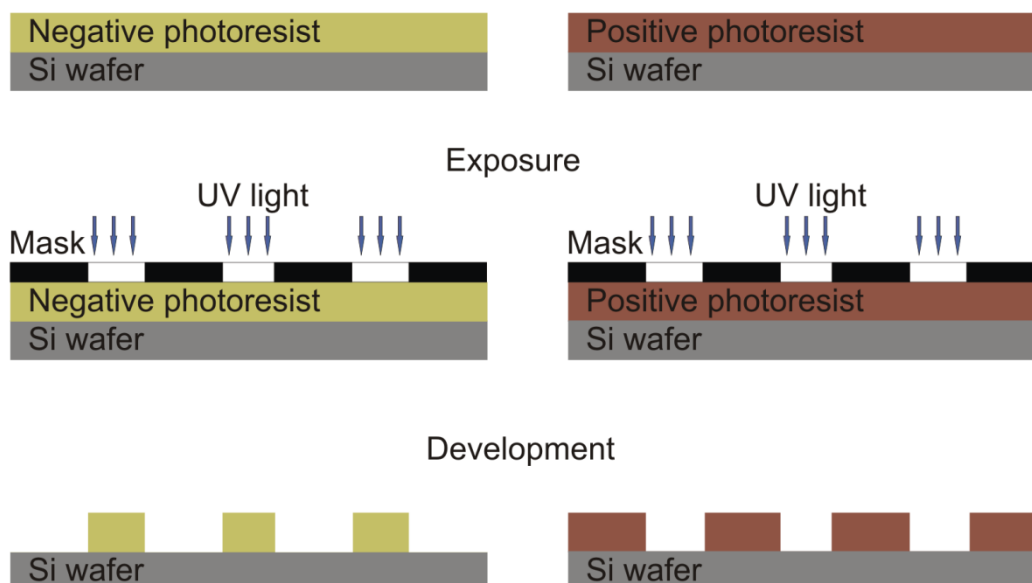


Figure 3-2 Photolithographic process for negative and positive photoresists. Spinning resist: the photoresist is poured on silicon wafer and spun for a set time and velocity which determines the thickness of the layer. Exposure: Exposure to UV light which allows the polymerisation of the photoresist. Development: the exposed wafer is dipped into a development solution eliminating the soluble photoresist. With these steps the pattern transfer onto a Si wafer is achieved.

### 3.3.3 Etching

The etching process is a technique that enables the removal of material from the surface of the substrate which is not protected by a masking material. The etching procedure is divided into two classes: wet etching and dry etching. In the former process a solid reacts with a liquid etchant producing soluble products, while in the latter one the solid reacts with a gaseous etchant (a plasma) producing volatile products. The depth of the etch can be controlled using the etching time and the etching rate.

The masking material can be either a photoresist layer patterned using the photolithographic process, described above, or a deposited hard mask material. For example in silicon etching with KOH, silicon dioxide and silicon nitride are standard mask materials, while for glass etching in HF solution a metal layer (nickel, chromium, amorphous silicon) is generally a suitable masking material. A patterned layer of photoresist is a usual masking material in the dry etching process of silicon with $SF_6$ plasma.

Different etching profiles can be obtained in both classes of etching. When the etching front proceeds as a spherical wave from all points opened by the etchant the lateral extent of the etching is identical to the vertical etched depth. In this case the etching is called isotropic and it undercuts the protecting layer forming cavities with sloping sidewalls. Alternatively, anisotropic etching produces etching in a preferential direction. Anisotropic etching can be controlled by the material crystal plane anisotropy; indeed different crystal planes have different crystal etch rates. For this reason amorphous materials like glass usually undergo to isotropic etching (Figure 3-3) (79). Anisotropic etching can also be achieved by directing the etching particles at the substrate in a particular direction as in parallel plate Reaction Ion Etcher (RIE).

Details of the protocol used in this thesis can be found in Section 4.3.1
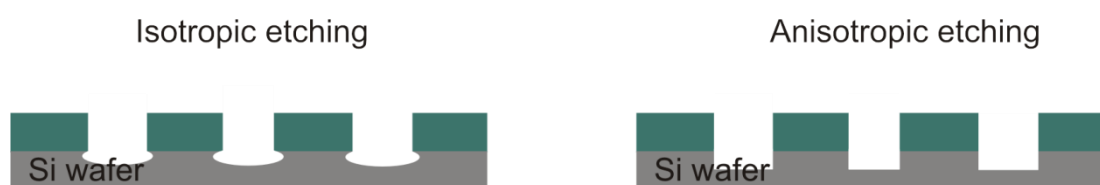


Figure 3-3 Isotropic and anisotropic etching profiles.

## 3.3.4 Lift-off metallization

Lift-off metallization is a technique that allows the deposition of metal onto areas of a substrate which are not masked. This technique is suitable for the fabrication of metal electrodes on a substrate like glass. It is basically a metallization with a sacrificial layer of photoresist.

A negative design of the desired electrodes is patterned onto a layer of photoresist using photolithography. Then a thin metal layer is deposited on top of the substrate. Deposition can be achieved by using thermal or electron beam metal evaporator machines. The photoresist layer is then dissolved in solvent and only the metal attached on the substrate can remain. To promote the metal adhesion to the glass, a 10 nm layer of Ti can be deposited before the metal deposition (Figure 3-4).

Details of the protocol used for electrodes fabrication can be found in Section 4.3.1.

Metal deposition

Resist dissolution and metal lift-off

Final product
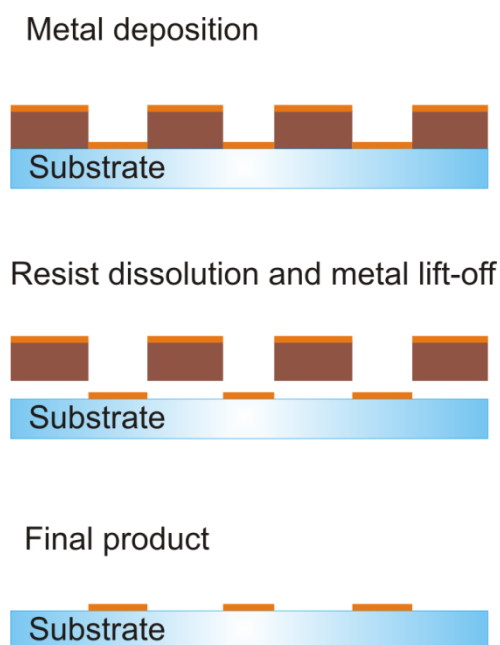
Figure 3-4 Lift-off process. Metal deposition on patterned resist, resist dissolution in a solvent and metal lift-off.

## 3.4 Optical detection methods: optical and fluorescence microscopy

Microscopy represents the observation technique of choice for biological systems where the sample is illuminated by light which can be reflected, refracted and absorbed (80). Quite often in biology a property of some substances called *fluorescence* is exploited. This consists of the ability of these substances to re-emit electromagnetic radiation when excited by the light at a particular wavelength.

An incident radiation, at the excitation wavelength, that excites the molecules of the fluorescent substance, excites its electrons from the ground state into higher electronic energy states. If the absorbed photon contains more energy than is necessary for a simple electronic transition, the excess energy is usually converted into vibrational and rotational energy. In few nanoseconds the energy can be released as light as the molecule decays to its ground state. Immediately after the absorption of a photon, loss of energy without light emission can also occur. This process is called internal conversion or vibrational relaxation and the energy is converted into heat, absorbed by the neighbouring molecules of the

fluorophore. It can also happen that the excited molecules collide with other molecules transferring energy in non radiative processes that can be either quenching or intersystem crossing. The latter phenomenon can led to a transition back to the excited state that produces a delayed fluorescence or to the emission of a photon through a process called phosphorescence (81).

The Jablonski energy diagram, in Figure 3-5, shows the mentioned possible paths that an excited molecule can take to return to its ground energy state (81). Thicker lines represent energy levels, while thinner lines represent the different vibrational energy states. If the transition is associated with absorption or emission of a photon, the transitions between the states are illustrated as straight arrows. Transitions that results from a molecular internal conversion or non-radiative relaxation process are illustrated as wavy arrows (81).
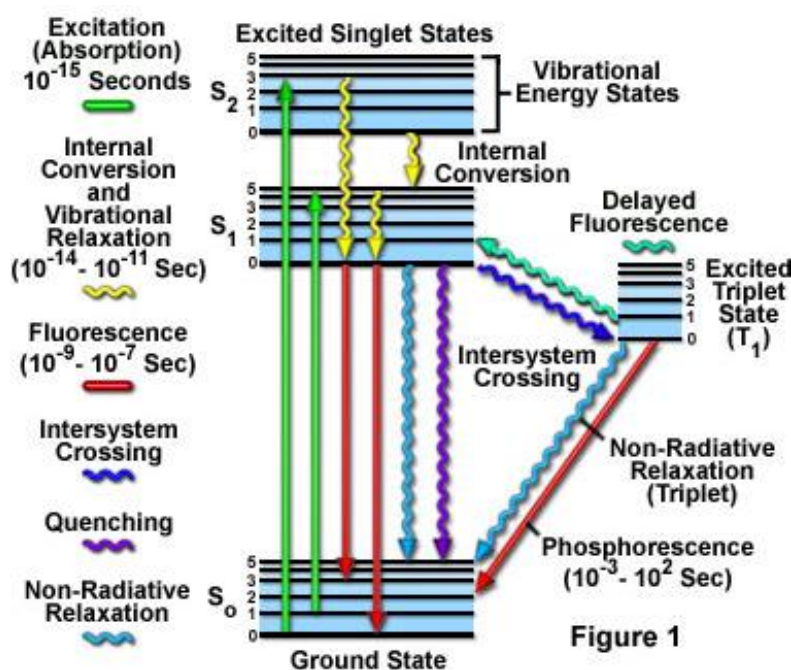


Figure 3-5 Jablonski energy diagram. Graphic description of the paths that excited electrons, after excitation at a particular wave length, take to go back to their previous ground state ($S_0$). Absorption of light occurs in $10^{-15}$ seconds. In the case of fluorescent light emission, the process is rapid and it takes $10^{-9}$ seconds whereas the phosphorescent emission is slower taking $10^{-3}$ - $10^{-2}$ seconds. Image taken from (81).

Molecules capable of fluorescing (known as fluorophore or fluorocrome) are characterised by an excitation and emission spectra which represent the relative intensity of fluorescence signal versus, respectively, the wavelength of excitation and emission. Many factors and characteristics can affect the

fluorescence performance of the fluorophores. Some of the main fluorophore characteristics are reported as follows: molar extinction coefficient, fluorescence quantum yield, photobleaching and the environment of the fluorophore.

The molar extinction coefficient ($M^{-1} cm^{-1}$), also known as molar absorptivity, is a measure of the fluorophore's ability to absorb light. It is calculated as the ratio between the absorbance $log_{10}(I_{in}/I_{out})$ and the product of the light pathlength and the fluorophore concentration. This property determines the amount of light that a molecule can generate through fluorescent emission.

The fluorescent quantum yield (%) represents the ratio between the number of photons emitted and photons absorbed.

Fluorophores may undergo to a phenomenon called *photobleaching* which represents the irreversible destruction of the fluorophore due to either prolonged exposure to the excitation source or exposure to high-intensity excitation light. The excitation and emission cycle can be repeated for many hundreds to thousands of times before the phluorophore is photobleached.

The fluorescence of molecules is influenced by some factors like pH of the solution, viscosity, temperature and fluorophore concentration. These factors have to be defined and controlled in order to obtain reproducible measurements.

The electronic configuration of the fluorophore, determined by the pH of the solution, can change the property of the fluorophore. For example, coumarin substrates like the 7-hydroxy-4-methylcoumarin develops maximum fluorescence at a pH value of 10 whereas the 4-trifluoromethyl-7-hydroxycoumarins are more acidic and thus fluoresce at much lower pH values.

Temperature also has an effect on the viscosity of the solution and could favour (or not) the collision of the fluorophore with neighbouring particles changing the electronic configuration of the molecule. Tryptophan, quinine and indoleacetic are among the compounds whose fluorescence varies greatly with temperature.

Moreover, the fluorescent emission increases linearly with the fluorophore concentration at low amounts but then it reaches a saturation point after some concentration. Often it can be opportune to build a calibration curve that

creates a relationship between the fluorescence intensity with the fluorophore concentration.

Interaction between a fluorophore and other substances present in the system could also lead to a reduction of its fluorescence. This mechanism is generally denoted as quenching and the oxygen for example is one of the most notorious quenchers.

In biology, the fluorescence of some molecules has been exploited to examine the spatial distribution of cellular components, for example using fluorescently-labeled antibodies for protein localization, dyes such as DAPI or Hoechst 33258 to specifically label DNA, pH or $Ca_2^+$ dependent fluorophores to allow details in cellular organization and function (80). In this study fluorescence detection was used to observe protein distribution and protein dynamics. Fluorescent proteins such as mCitrine, enhanced green fluorescent protein (EGFP) and red fluorescent protein (RFP1) were linked to the proteins of interest: H-Ras, Actin and MreB.

Microscopy investigation was performed by using an inverted optical microscope (AXIO Observer A1, Zeiss) and a laser scanning confocal microscope system (LSM 510 META, Zeiss) with an inverted microscope (Aviovert 200 M, Zeiss) equipped with a range of laser sources and excitation filters.

Additional details can be found in Sections 4.3.2, 4.3.6, 5.2.5 and 6.2.1.

## 3.5 Methods involving biological material treatment

### 3.5.1 DNA cloning

Deoxyribonucleic acid, well known as DNA, is a biopolymer which contains the genetic instructions for the development and functioning of living organisms. It consists of two polymers made of units called nucleotides, each composed of a nitrogenous base (Adenine, Thymine, Cytosine, Guanine) linked to a five carbon sugar (deoxyribose) linked to a phosphate group. The two polymers are bound together by hydrogen bonds occurring between two nitrogenous bases, specifically, three hydrogen bonds between cytosine (C) and guanine (G) and two hydrogen bonds between thymine (T) and adenine (A).

The information carried by DNA is held in the sequence of pieces of DNA called genes which in a cell can be either copied in a process called DNA replication or to be used for translating into protein. The protein synthesis requires first the transcription of DNA genes into mRNA molecules which are then translated by ribosomes into proteins.

Using molecular genetic approaches, it is possible to express only the genes of interest opportunely inserted in structures called cloning vectors. Cloning vectors can be used for protein expression both *in vivo* using a host (bacteria, yeasts, phages) and *in vitro* using cell-free protein expression systems. These commercially available systems contain all the biological machinery required for the protein synthesis that includes amino acids, specific enzymes, ribosomes and adenosine-triphosphate (ATP).

Figure 3-6 A shows a schematic representation of the reconstruction of a cloning vector where a foreign DNA fragment can be inserted. The insertion of the DNA fragment is carried out by treating the vector (commercially available) and the foreign DNA with a restriction enzyme that creates the same overhang and then ligating the fragments together with ligase enzymes. The gene of interest is first extracted from the foreign DNA and amplified using a polymerase chain reaction (PCR) technique. This is then inserted into the vector using restriction and ligation enzymes that cut and sew the DNA.

Figure 3-6 B shows the transformation of a host with the cloning vector carrying the gene of interest. Bacterial cells are cultured in order to multiply and produce a lot of copies of the plasmid.

Figure 3-6 C shows the technique adopted for cell-free protein expression. Purified vector is mixed with *E. coli* cell lysate containing the biological machinery required for protein synthesis.
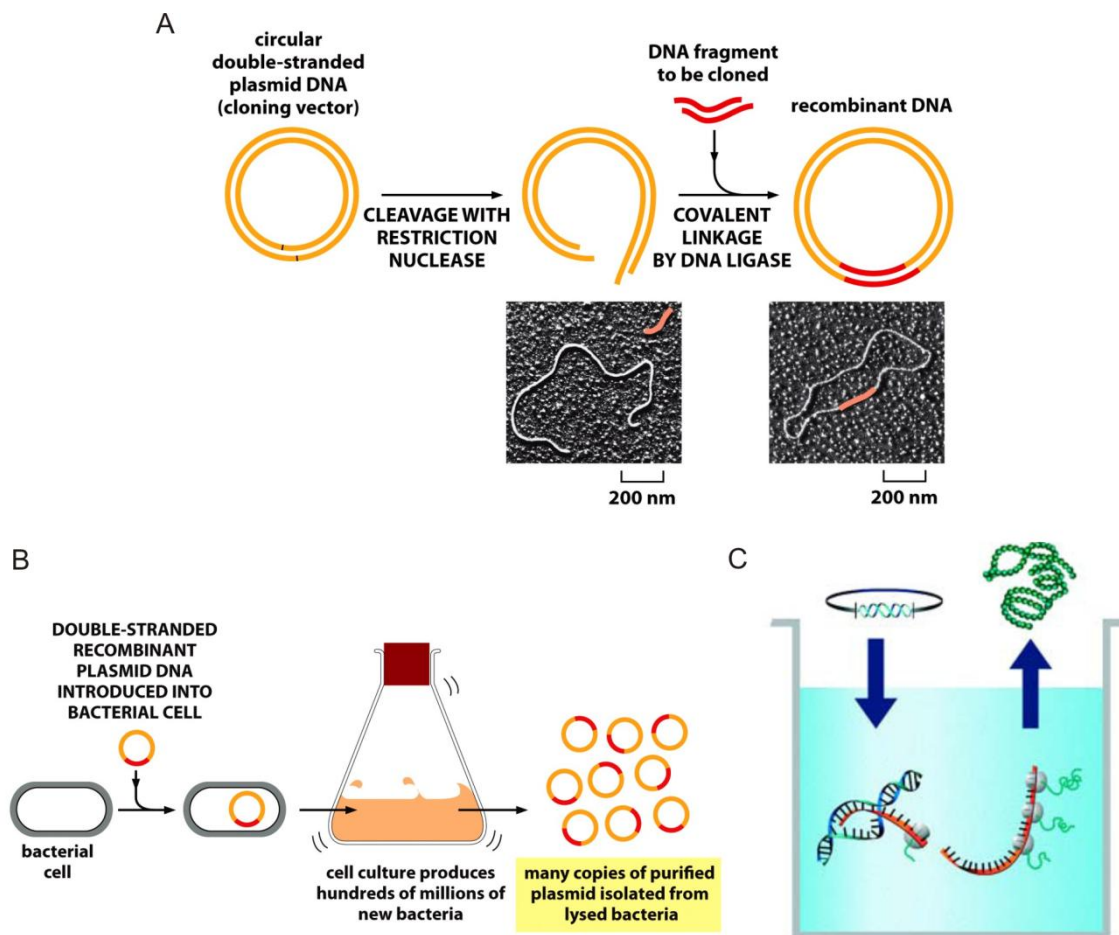
Figure 3-6 Schematic representation of the operations used in bacteria transformation and cell-free protein expression. A) A cloning vector commercially available or naturally present in bacteria (in that case it is called plasmid) is cleaved and afterwards sealed with opportune enzymes to host a DNA fragment. Image taken from Figure 10-9 Essential Cell Biology 3/e (Garland Science 2010). B) The vector/plasmid is then introduced into bacteria cells which are cultured for plasmid amplification and opportune test of its functionality. The plasmids are then harvested from bacteria through lysis. Image taken from Figure 10-10 Essential Cell Biology 3/e (Garland Science 2010). C) The plasmid/vector is then used with commercially available E. coli cell lysate containing the biological machinery required for protein synthesis. Picture taken from Cat. No. 03 186 148 001, Roche.

### 3.5.1.1 Vector design

A vector, generally made of a few thousand base pairs, usually includes a few common parts within its structure, these are:

- A promoter, a DNA sequence that recruits the transcriptional machinery and leads to the transcription of the downstream DNA sequence;

- A ribosome binding site (RBS), an RNA sequence found in mRNA to which ribosomes can bind and initiate the translation;

- – A terminator, an RNA sequence that usually occurs at the end of the gene and cause the transcription to stop;
- – Resistance gene, that provides resistance to a specific kind of antibiotic;
- – Origin of replication, a sequence that controls the replication of the plasmid in the host (bacteria, yeasts, phages).
- – Restriction sites, locations on the DNA containing specific sequences (4-8 base pairs in length) which are recognized by restriction enzymes. These are generally palindromic sequences and a particular restriction enzyme may cut the sequence between two nucleotides within its recognition site, or somewhere nearby. For example, the restriction enzyme EcoRI recognizes the sequence GAATTC and cuts between the G and the A on both the top and bottom strands, leaving an overhang (a portion of a DNA without any attached complement) AATT called "sticky end". This overhang is used to ligate in a piece of DNA with a complementary overhang (TTAA).

Designing of the vectors can be done using opportune software such as VectorNTI or CLC. Structures of the designed vector can be found in Section 5.2.3 and Appendix II.

### 3.5.1.2 Polymerase chain reaction (PCR)

The method relies on thermal cycling, consisting of cycles of repeated heating and cooling of the reaction for DNA melting and enzymatic replication of the DNA. Primers (short DNA fragments) containing sequences complementary to the target region along with a DNA polymerase (after which the method is named) are key components to enable selective and repeated amplification. As PCR progresses, the DNA generated is itself used as a template for replication, setting in motion a chain reaction in which the DNA template is exponentially amplified. The fundamental steps that characterize this technique namely: denaturation, annealing and elongation are illustrated in Figure 3-7.

In the denaturation step the DNA is heated to 94-98 °C for 20-30 seconds. The heat breaks the hydrogen bonds that keep the two helixes of DNA attached. This step is followed by annealing which lowers down the temperature to 50-65 °C for 20-40 seconds and allows the annealing of the primers to the single strands of

DNA. Afterwards the temperature is raised again to 75-80 ºC in the step called elongation during which the DNA polymerase enzyme elongates the single strand DNA. This process is repeated for n cycles and gives rise to $2^n$ new filaments of DNA. Details of the protocol used can be found in found in Section 5.2.3 and Appendix II.
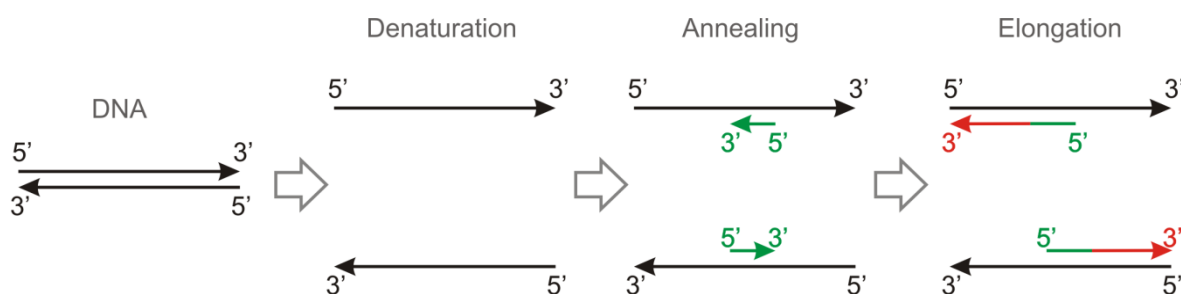


Figure 3-7 PCR cycle. It consists of 3 steps: denaturation, annealing and elongation. In the first step the hydrogen bonds that hold together the two strands of DNA are broken. Primers anneal to the unpaired strands during the annealing step which is then followed by the elongation where 2 filaments of DNA are formed. For n cycles the total amount of DNA molecules formed are $2^n$.

### 3.5.1.3 E.coli transformation

The vector is then inserted into *E. coli* bacteria cultured in broth or on petri dishes. The culture is then treated with the same drug for which the vector is carrying its resistance gene. The transformant colony survival demonstrates that the vector is working and ready to be extracted from the cells through thermal shock. Details of protocols used can be found in Section 5.2.3 and Appendix II.

## 3.5.2 Protein concentration determination methods

The methods used in this study to determine protein and DNA concentration are detailed in this section, namely:

- Bradford protein Assay
- Bicinchoninic acid (BCA) protein assay
- Western blot.

The first two techniques are both spectroscopic analytical procedures based on the change in the absorbance of light of the solution when it contains proteins.

In the first method the solution containing an un-quantified amount of protein is mixed with the Coomassie blue dye which changes its colour when bound to protein. The dye donates electrons to the ionisable groups of the protein which first denatures and then exposes its hydrophobic pocket to non polar regions of the dye. Between the hydrophobic region of the protein and the non polar regions Wan der Walls interactions are established which form the bound state of the dye. The absorption spectrum maximum of this dye in the bound state is at 595 nm. The increase of absorbance is proportional to the amount of bound dye, and thus to the concentration of protein within the sample.

In the BCA method, a solution containing bicinchoninic acid, sodium carbonate, sodium bicarbonate, sodium tartrate and cupric sulfate pentahydrate reacts with the sample protein. Peptide bonds within the protein reduce $Cu^{2+}$ ions from the cupric sulfate to $Cu^{+}$ which are chelated forming a product that absorbs light at 562 nm. Also in this case, the amount of $Cu^{2+}$ is proportional to the amount of protein present in the solution.

In both cases the absorption is measured by using a spectrophotometer. The concentration of protein present in the solution can be compared with known concentration standards of protein solutions like Bovine Serum Albumin (BSA).

The Western Blot analysis is the most commonly used technique capable of: 1) separating the proteins present in the solution upon their molecular weight and 2) determining the presence of a specific protein present in the suspension. The technique starts by performing a gel electrophoresis which consists of separating the proteins of the sample upon their molecular weight. The sample is loaded in a well within a polyacrylamide gel containing sodium dodecyl sulphate (SDS) a detergent that denatures the protein and provides the protein with negative charges that is proportional to the protein mass. When an electric field is applied to the gel, the protein migrates through the acrylamide mesh to the positive pole at a different speed according to their relative molecular weight. After a certain time, proteins with different molecular weights are separated in bands along the same lane.

In DNA analysis, electrophoresis is usually run to determine the molecular weight and the amount of amplified DNA after PCR process. In this case, the gel matrix

is made of non denaturing material like agar. This allows the DNA to run through its pores and afterwards to be collected.

When the separation is completed the protein is transferred from the gel onto a membrane (either nitrocellulose or polyvinylidene) through a technique called eletroblotting. The gel is sandwiched between filter paper and the membrane and placed between two electrodes. When the electric field is applied, the proteins are pulled to the membrane maintaining the same organization they had in the gel.

The membrane is then treated with BSA or protein milk. This operation is required in order to allow the antibody (that is added in the next step) to attach only to the specific protein they recognise. The membrane is then incubated with a primary antibody specific for the protein of interest. Afterwards the membrane is rinsed and incubated with a secondary antibody which will bind to the primary antibody. The secondary antibody is responsible for the generation of a chemiluminescent signal which is proportional to the amount of protein. Details of the protocol used can be found in Section 4.3.5.

### 3.5.3 Immobilization of biomolecules using avidin-biotin system

Nature has developed a protein called avidin that expresses high affinity towards a small molecule called biotin, also known as vitamin H. On one molecule of avidin there are four sites at which biotin may bind. Dissociation constant value of this system, that represents the concentration at which half of the binding sites of a protein are occupied, is one of the smallest values in nature for non covalent bonding ($K_D \sim 10^{-15}$ M).

These interesting properties have been wisely exploited in biotechnology for immobilization of molecules on surfaces and/or isolation of biological material. In fact, biotinilated molecules can act as a carrier because they are capable of binding to surfaces covered by avidin molecules (Figure 3-8).

The greatest source of avidin is found in the white part of the egg but it has also shown non-specific binding properties. This problem was not found in that avidin produced by *Streptomyces* bacteria, also known as streptavidin, which on the other hand has a less accessible biotin-binding site. In order to use streptavidin

and minimize the non binding absorption, the biotin molecule is usually modified by adding a spacer arm molecule (i.e. *N*-Hydroxysuccinimide and its water-soluble analogue Sulfo-NHS). Different protocols have been developed to artificially incorporate the biotin molecule to proteins, antibodies and nucleic acids as well as cover surfaces with avidin molecules (82). In this research streptavidin covered beads were bought and used to bind biotinilated antibodies capable of linking to a specific molecule. Details of the protocol used can be found in section 4.3.3 and Appendix I.
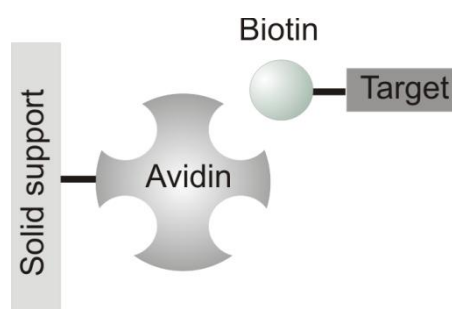


Figure 3-8 Avidin-biotin interaction. It provides a useful strategy to capture target molecules which are linked to biotin molecule. Avidin has four binding sites for biotin molecule and exhibits great affinity towards it.

## 3.5.4 Electrical cell lysis and cell trapping

Cell lysis is defined as disrupting cells achieved by physical and chemical means in order to get the cellular content (83). Apart from chemical lysis, which can require the use of detergents molecules to destroy the membrane lipid bilayer, all the mechanical techniques, namely sonication, freeze/than cycles, manual grinding, can be difficultly integrated on a microfluidic device.

A common technique used to move and lyse cells on chip adopts the means of electrical field capable to trap the cells and destroy their membranes. This technique, commonly referred as electrical lyisis, makes use of electrodes to generate an electric field which has the effect to polarize the cells until the point where the reached membrane voltage is able to destroy the membrane itself. This is due to the compression pressure generated by the attraction of opposite charges at the sides of the membrane of cell that acts as a dielectric (Figure 3-9).
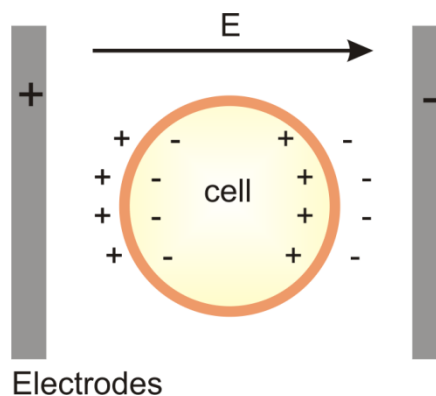
Figure 3-9 Polarization of the membrane of a cell immersed in an electric field E generated by two charged electrodes. The membrane lipid bilayer breakdown is induced by linear rising voltage.

It has been calculated that electric fields generating transmembrane potentials of the order of 0.2–1.5 V cause rupture of the lipid bilayer forming pores, and with sufficient magnitudes of electric field strengths and time of exposure lead to cell lysis (84). Moreover, the passage of ions across the membrane raises the temperature of the system by the Joule-heating effect. A jump faster than the thermal expansion of the system can create a large pressure, which dissipates as shock waves (85). In addition, movement of ions across the membrane induces a flow of water in/out of the cell causing shrinkage/swelling of the cell itself (85).

In a non-uniform electric field, depending on the relative polarizability of the cell with respect to the surrounding medium, the cell will be induced to move either towards the high-electric-field region or towards the electrode where the field is weaker (86). This phenomenon is well known as *dielectrophoresis (DEP)* and it is defined positive DEP and negative DEP whether the force generated towards the electric field source is attractive or repulsive. For a moving cell in a microchannel, cell trapping occurs when the dielectrophoretic force experienced by the cell is able to overcome the Stokes' drag force acting on the cell (Figure 3-10). These two forces are respectively expressed as in Equation 3-1 and Equation 3-2:

$$F_{DEP} = 2\pi\varepsilon_m r^3 \, \text{Re}[\, CMF \,]\nabla\left|\vec{E}\right|^2$$

3-1

$$F_{Drag} = 6\pi\mu r v$$

3-2

where $\varepsilon_m$ is the dielectric permittivity of the medium[1] (F m$^{-1}$), $r$ is the cell radius, *CMF* is the Clausius-Mossotti factor (86), *E* is the electric field, $\mu$ is the dynamic viscosity of the medium and $v$ is the difference between the fluid dynamic velocity of the particle and that of the medium. The expression of Clausius-Mossotti factor (CMF) determines the sign of the forces and it is calculated as follow:

$$CMF(\omega) = \frac{\varepsilon_p^* - \varepsilon_m^*}{\varepsilon_p^* + \varepsilon_m^*}$$

3-3

where

$$\varepsilon^* = \varepsilon + \frac{\sigma}{j\omega}$$

3-4

where $\varepsilon_m$ and $\varepsilon_p$ are the dielectric permittivity of the medium and particle and $\sigma$ is the conductivity[2] (S m$^{-1}$). Details of how cell lysis was achieved on-chip can be found in Section 4.4.6.
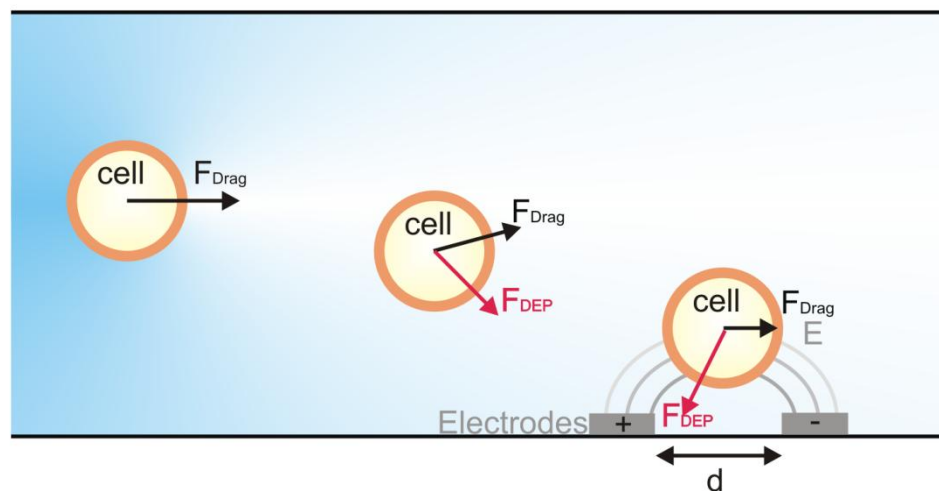


Figure 3-10 Dielectrophoresis and cell trapping. In a system containing electrodes and dielectric materials such as a cell suspension, when electrodes are active they generate an electric field *E* which is responsible of a dielectrophoretic force (*F*$_{DEP}$) able to compete with the drag force (*F*$_{Drag}$) acting on the moving cell. The intensity of this force is dependent by the electric field, the radius of the dielectric and the permittivity of the medium. 2 V transmembrane potential is responsible of cell membrane disruption.

---

[1] Dielectric permittivity of a material is a characteristic describing how the material affects any electric field set up in it.

[2] Conducibility measures the ability of a material to conduct an electric current.

## 3.6 Conclusions

In this Chapter the main generic materials and the methods mostly used during the thesis were taken in consideration. Each following Chapter will include a specific section of materials and methods which details more deeply any aspects and protocols not discussed in this section.

# 4 Analytical system for intracellular protein determination

Chapter 4 describes the development of a droplet-based microfluidic device used for determining the concentration of a specific intracellular protein expressed by a small population of cells. Living cells are introduced into the device and lysed by electrodes. In this chapter, a novel analytical approach able to reduce the time and cost of protein detection-quantification compared to conventional laboratory techniques (i.e. Western-blot technique) is presented. The work described in this Chapter has been published in Analytical Chemistry (2011), Volume 13, Pages 5361–5368, and presented at the GRC Research conference "Microfluidics" (Waterville, USA, July 2011) and at PGBiomed 2011 IEEE Conference (Glasgow, UK, August 2011).

## 4.1 Introduction and proposed approach

Described below is the development of a new method to perform an immunoassay for the selective capture of cellular proteins from a small population of cells directly lysed within a microfluidic device. Two proteins of interest were captured in two separate sets of experiments, namely the Human Ras protein (H-Ras) (roughly 21 kDa) and Actin (roughly 42 kDa).

Ras proteins belong to the family of small GTPases and are involved in intracellular signalling pathways that regulate numerous cellular processes, including proliferation, differentiation, adhesion, migration and apoptosis (87). It was observed that over-expression of H-Ras in cells is indicative of their malignant transformation (88).

On the other hand actin is a globular, cytoskeletal protein found in high concentration in eukaryotic cells (can be >100 μM) and it is involved in key cellular processes, including muscle contraction, cell motility, cell division and

the establishment and maintenance of cell junctions (89). Actin monomers polymerise to form microfilaments within the cell, one of the three major filaments that makes up the cellular cytoskeleton.

Using droplet-based microfluidics it is possible to create discrete compartments containing the biological sample under investigation, and do so many thousands of times on a single chip. The research explores the use of binding reagents, such as antibodies, and their ability to selectively bind a protein of interest using the molecular recognition mechanism of the antigen-antibody reaction. This Chapter covers the following methods:

1. Realization of a support that used antibodies, bound to the surface of a bead, to bind specifically the protein of interest;
2. Realization of a platform to generate and store stable droplets in a microfluidic system;
3. Creation of dose-response curve (calibration curve) in order to find a relationship between the concentration of fluorescent proteins bound to an antibody coated bead and fluorescence value measured;
4. Estimation of non specific protein absorption to the antibody coated support;
5. Protein capture within a droplet containing a cell lysate produced both on and off-chip.

The device was conceived to have three inlets, one for the injection of the continuous phase and two for the dispersed phase. A schematic of the device structure is given in Figure 4-1.

An oil solution, a watery solution containing functionalised beads able to bind a specific protein and an aqueous solution containing a cell suspension were injected respectively from inlets A, B and C. The aqueous fluid streams met at a Y junction (D) and flow parallel within the emerging channel until they met a T-junction (E), where water droplets in oil (W/O) are generated. When cells were injected from inlet C, an electric field was applied to the interdigitated microelectrodes (position marked in Figure 4-1) in order to trap and permanently electroporate the cells that flow over the electrode array. Cell trapping due to positive dielectrophoresis occurs when the dielectrophoretic force experienced by the cells is able to overcome the Stokes' drag force on the cells.

Downstream, the two aqueous solution were mixed only after droplet formation because of convective phenomena that originate at the interface of a W/O drop moving inside the channel. The protein molecules within the droplet were able to diffuse and adsorb onto the antibody coated bead.
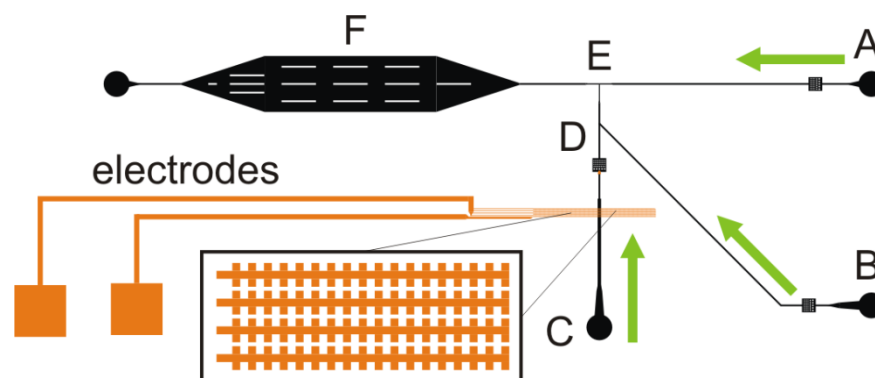


Figure 4-1 Device architecture. Inlet A was used to inject oil-surfactant solution, inlet B to inject a suspension of functionalised beads and inlet C to inject either a calibration solution, a lysate or a cell suspension. The two aqueous phases merged at a Y junction (D) and further downstream W/O droplets were generated at a T-junction (E). Droplets were stored after the junction in a microfluidic chamber (F). Interdigitated square-shaped microelectrodes were aligned to the channel between inlet C and the Y junction to electrically lyse flowing cells.

## 4.2 Materials

Unless otherwise noted all reagents were purchased from Sigma-Aldrich (Dorset, UK). The fabrication of T-junction microfluidic devices used moulds made of an etched silicon <100> wafers (12 inches in diameter). PDMS (Sylgard 184 Silicone Elastomer, Dow Corning, USA), AZ4562 (Microchemicals, DE), AZ400K (Microchemicals, DE), 1H,1H,2H,2H-perfluorooctyl-trichlorosilane (Fluka, UK), Aquapel (PPG Industries, PA, USA) and glass microscope slides (22x50 mm, 0.13-0.17 mm thick, Menzel, DE) were used for the fabrication of the devices. Electrodes were fabricated using S1818 (Shipley, USA), Microposit developer (Shipley, USA) and hydrogen silsesquioxane (HSQ) (Fox 16, Dow Corning, USA). Fluorocarbon oil (Fluorinert FC40, 3M, USA) containing 2% wt PEG-PFPE blockcopolymer (Raindance Technologies, USA), for stabilising the on-chip emulsions, was used as the continuous phase.

The dispersed aqueous phase consisted of either phosphate buffer saline (PBS, 137 mM sodium chloride, 2.7 mM potassium chloride, 10 mM sodium phosphate

and 2 mM potassium phosphate, pH 7.4) containing an appropriate antibody concentration and 1% v/v bovine serum albumin (BSA), a cell lysate solution or a suspension of cells in 0.6 M D-Sorbitol. Anti-H-Ras (MAB3291, Millipore, UK) and anti-GFP (AB6658, Abcam, UK) were used for on-chip cell lysis experiments. Fluorescein isotiocyanate(FITC)-conjugated anti-mouse (F5262, Sigma), FITC-conjugated anti-rabbit (F0382, Sigma) and tetramethylrhodamine isothiocyanate (TRITC)-conjugated anti-mouse (T5393, Sigma) were used for off-chip and on-chip calibration and quantification of non specific absorption.

Antibodies were biotinylated using Vector Laboratories Biotin (long arm) *N*-Hydroxysuccinimide (NHS) reagent and dialysed using a mini-dialysis unit (69576, Thermo Scientific Pierce, UK). Protein concentrations were measured by Bradford assay using a protein assay kit (BIO-RAD, USA) and a plate reader (GENios, Tecan, USA). Biotinylated antibodies were conjugated to 10.14 µm Superavidin™ microbeads (CP01N/8978, BangsLab, USA). The functionalised beads were suspended either in PBS or in G-actin buffer (containing 5 mM Tris pH 8.0, 0.2 mM calcium chloride, 0.2 mM ATP and 0.5 mM DL-Dithiothreitol) for promoting depolymerisation of actin filaments.

In addition, anti-GST (13-6700, Invitrogen, UK), anti-mouse-peroxidase (Sigma) and anti-goat-peroxidase (Sigma) were used for Western blot analysis.

## 4.3 Methods

### 4.3.1 Device design and fabrication

Microfluidic devices were fabricated using the soft lithography techniques discussed in Chapter 3. Masks were designed using CorelDRAW X3 (Corel, CA) software. Details of the designs are shown in Figure 4-2.

The chip was composed of three 100 µm wide channels, each of which contained a matrix of squared pillars, acting as a filter to prevent dust clogging the T-junction. The channels decreased to 60 and 70 µm as they approached the T-junction, so that the water phase entered the oil channel through a narrow space of 40 µm. A hexagonal chamber few centimetres wide was designed for storage of droplets and fluorescence analysis. Four pairs of interdigitated electrodes were designed according to Zagnoni et al. design (90).

## Chip



5 mm

## Filter



500 µm

## T-junction



100 µm

## Electrodes



5 mm

300 µm

100 µm
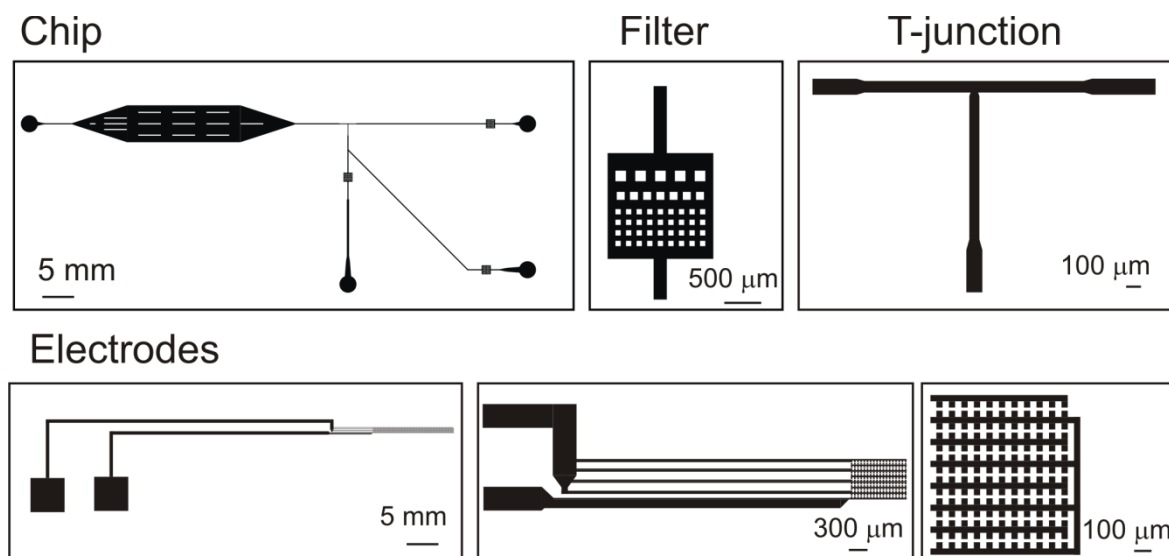
Figure 4-2 Chip and electrodes design. Chip design comprised three inlets, one outlet and one hexagonal chamber. The chamber contained rectangular pillars in order to prevent roof from collapsing. Each inlet channel was provided of a filter made of squared spaced pillars. The T-junction was made of three narrowed channels shaped as forming the letter T. Interdigitated electrode design took inspiration from (90).

A silicon master was produced by spinning AZ4562 photoresist onto a silicon wafer at 4000 rpm for 30 s. After baking the substrate for 5 min at 90 °C on a hotplate, the resist was exposed to UV light through a photomask for 16 s and was developed in a 1:4 solution of AZ400K developer: DI water. The silicon wafer was subsequently dry etched in a STS-IPC system to a depth of 50 µm. To prevent PDMS adhesion to the resulting silicon master, the silicon surface was silanised by vapour deposition of 1H,1H,2H,2H-perfluorooctyl-trichlorosilane overnight. PDMS was then poured onto the silicon master at a 10:1 ratio of base to curing agent, degassed in a vacuum desiccator chamber and cured at 70 °C for 2 h. The devices were then peeled from the mould and punched with a sharpened flat-end needle to create inlet and outlet ports.

The PDMS devices and glass slides were exposed to oxygen plasma for 18 s and then put in contact. The plasma treatment parameters were: 18 s, 50 W, 0.2 mBar and 250 sccm using a Gala Instruments PlasmaPrep5 barrel asher. The device microchannels were flushed with undiluted Aquapel followed by air, to improve the wetting of the fluorinated oil inside the channels. PTFE tubing (30, Cole Parmer) was then connected to the channel inlets and outlets.

Microelectrodes were fabricated on glass substrate using standard photolithography, metal evaporation and lift-off techniques. The inverse electrode design was patterned onto a glass substrate using S1818 photoresist, following a similar procedure to that used for AZ4562, using a bake time of 1 min, an exposure time of 4.5 s and a 1:1 dilution of Microposit developer. A 10 nm titanium, 60 nm gold layer was then deposited onto the substrate by electron beam evaporation using a MEB 400S system, before lifting-off the unwanted metal regions by immersing the sample in acetone and briefly sonicating. In order to avoid electrolysis at the electrodes, a 60 nm passivation layer of HSQ was spin-coated over the electrodes, using a 25% v/v dilution in methyl isobutyl-ketone and spinning at 2000 rpm for 30 s. The glass slides were then baked in a 180 °C oven for 1 h.

## 4.3.2 Device operation

Syringe pumps (New Era Pump System Inc., Farmingdale, UK) were used to control the flow rates of the continuous (1 µl min$^{-1}$) and dispersed phases (0.5 µl min$^{-1}$ for each inlet), resulting in stored droplets approximately 100 µm in diameter and constricted by the depth of the channel (50 µm). In these working conditions the Ca number for the system was equal to 3[3]. Once the flow rates were stable, a TTi TG120 function generator (2 MHz bandwidth) was used to apply a 1 MHz, 20 V square waveform, to the interdigitated electrodes. The devices were mounted on an inverted microscope (AXIO Observer A1, Zeiss, UK) and images were acquired using a CoolSNAP HQ$^2$ CCD camera (Photometrics, Tucson, USA). All fluorescence images were acquired using a Zeiss 20X dry objective (0.17 NA) and the appropriate filter set (XF100-2 and XF108-2, Omega Optical, UK) for the fluorophore being imaged. Data was processed and analysed using Matlab (version 7) and ImageJ software.

---

[3] Ca number was calculated by knowing the mean velocity of continuous phase (8.33x10$^{-3}$ m s$^{-1}$), its dynamic viscosity (4.11 g s$^{-1}$ m$^{-1}$) and the interfacial tension between the fluorinated oil and DI water (11.10x10$^{-3}$ ± 1.1 g s$^{-2}$).

### 4.3.3 Antibody conjugation to microbeads, calibration procedures and non specific adsorption assay.

Binding supports selective to the specific protein were produced by coating Superavidin$^{TM}$ microbeads with biotinylated antibody. Antibodies were biotinylated according to the manufacturer's protocol (step 1 of Figure 4-3). The antibody was dissolved in bicarbonate buffer, pH 8.5, at a concentration between 2 mg ml$^{-1}$ and 10 mg ml$^{-1}$. An aliquot of the biotinylating reagent equal to 1/10 the weight of the antibody was added to the solution. The solution was incubated at room temperature for 2 h and purified by overnight dialysis using a mini-dialysis unit. The resulting concentration of biotinylated antibody after purification was estimated by performing a colorimetric Bradford assay (91).

When conjugating biotinylated antibodies to superavidin beads, an antibody concentration five times greater than that required to cover the surface of the microbeads was used (the binding capacity of the beads was supplied by the manufacturer and equal to $2 \times 10^7$ binding sites). The biotinylated antibodies were incubated with the beads at room temperature for 2 h in a 0.1 M sodium bicarbonate buffer, pH 8.5 with gentle mixing. After incubation, the antibody coated beads were washed three times in PBS with 0.01% v/v Tween, before being blocked by incubation in PBS with 1% v/v BSA for 30 min to minimise non specific adsorption of potential contaminants. After this step, the beads were again washed three times in PBS with 0.01% v/v Tween and were then stored at 4 °C in PBS containing 0.05% v/v sodium azide until use (step 2 and 3 of Figure 4-3).

Six different dilutions of a fluorescent secondary antibody (FSA) solution were prepared to produce an immunoassay calibration curve (step 4 of Figure 4-3), each containing 1% BSA. The buffer solution with the highest concentration of FSA was chosen to correspond approximately to that required for full surface coverage of one functionalised bead per droplet. The addition of BSA was necessary to minimise the adsorption of antibody to the channel surface, protein non specific adsorption being a particular problem when low antibody concentrations were used. These experiments were carried out both on- and off-chip to compare the sensitivity of the fluorescence measurements between the two methods.

For off-chip experiments, beads were incubated with an anti-mouse IgG FITC-conjugated solution with gentle mixing. After 2 h, beads were washed three times in PBS with 0.01 % v/v Tween. For each of the six different FSA concentrations, a 5 µl solution was placed between a coverslip and a microscope slide, and images were acquired for 10 beads.

For on-chip experiments, FSA solutions and functionalised beads were encapsulated in droplets, using a fresh device for each of the six different concentrations. Immediately after droplet storage, fluorescence images were acquired every 30 min, with the intensity being measured for 10 beads at each time point (an unmeasured droplet was used for each intensity acquisition as control). Once a bead and fluorescent fusion proteins were encapsulated in a droplet, proteins specifically bound to the antibody-conjugated bead, increasing the fluorescence signal from the bead with time. Transport of antigens to the bead surface was due both to convective motions that caused fluid mixing inside the droplet during droplet transport (92) (which lasted 2-3 minutes) and to diffusion, which occurred over longer time scales when the droplets were stored inside the chamber.
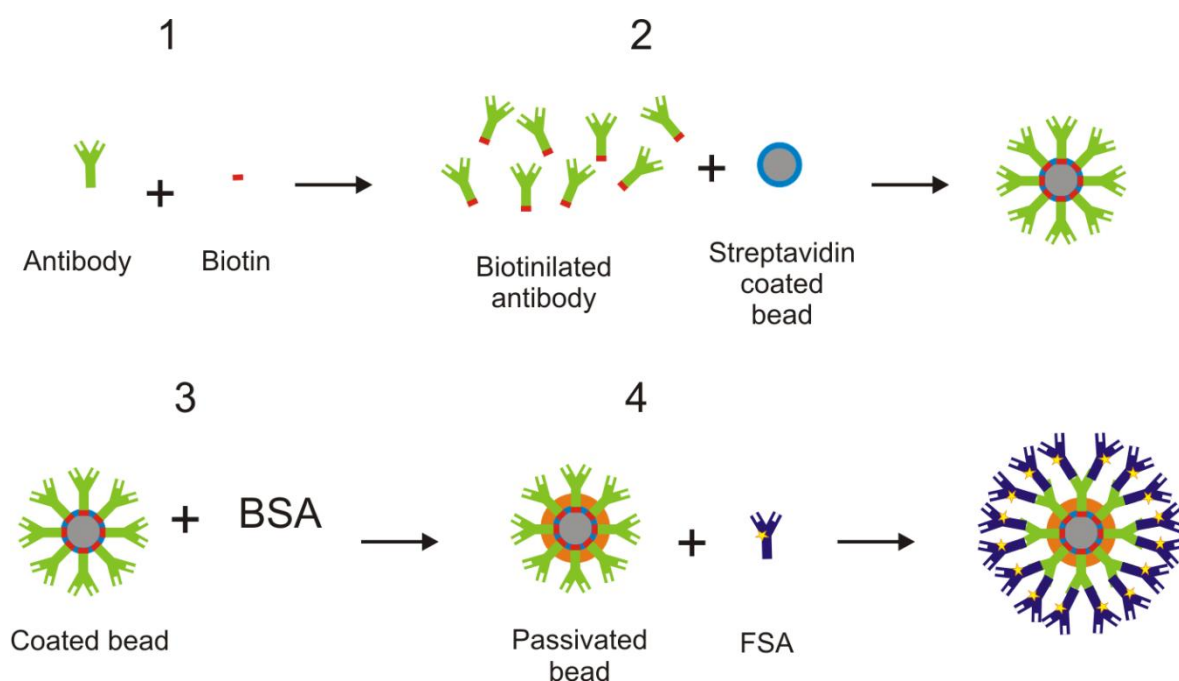


Figure 4-3 The coating bead protocol and calibration measurements required the following steps: 1) Antibody biotinylation; 2) conjugation of biotynilated antibody with streptavidin coated beads; 3) incubation of coated beads in BSA solution for preventing non specific adhesion on top of uncovered portions of the bead; 4) incubation of the coated bead with the Fluorescent Secondary Antibody (FSA) solution.

In this study non specific adsorption was also taken into consideration. This was measured on-chip experiments. Functionalised beads were encapsulated in droplets containing known concentrations of: only specific FSA (anti-mouse FITC-conjugated), only non specific FSA (anti-rabbit IgG FITC-conjugated) and mixed solution of specific and non specific FSA (anti-mouse IgG TRITC-conjugated and anti-rabbit IgG FITC-conjugated).

## 4.3.4 HEK-293 cell and MCF-7 cell lysis protocols

Human embryonic kidney (HEK-293) cells were transfected with a mammalian expression vector for HRas-mCitrine (plasmids were a kind gift from Professor Philippe Bastiaens, from Department of Chemistry at the Technische Universität Dortmund) by Dr. M. Sandison. 24 h prior to transfection, HEK-293 cells were plated out at $3\times10^6$ cells in a 75 cm$^2$ cell culture flask. The cells were transfected using 10 µg plasmid DNA and 22 µl GeneJuice transfection reagent (Merck, UK) per flask according to the manufacturer's instructions.

For on-chip lysis, cells were harvested 48-72 h after transfection. The growth media was removed and the cells were washed with PBS, before they were detached from the surface of the culture flask by gentle agitation. After counting the cell density, they were transferred to a centrifuge tube, pelleted at 1000 rpm in a benchtop centrifuge and resuspended in an appropriate volume of isosmotic medium (0.6 M D-sorbitol) to prevent cells swelling (93), at a final concentration of $4\times10^6$ cells ml$^{-1}$ for on-chip injection.

A stable human breast cancer (MCF-7) cell line expressing the fusion protein EGFP-actin and neomycin resistance was kindly prepared by Miss M. Chanasakulniyom (Biomedical Engineering Division, The University of Glasgow).

MCF-7 cells were seeded in 60 mm dishes with $5\times10^5$ cells per dish and incubated for 24 h prior to transfection. Cells were transfected with 20 µg of pEGFP-Actin plasmid DNA (provided by the Beatson Institute for Cancer Research) using a calcium phosphate transfection kit (Invitrogen). To isolate stable transfectants, the cells were trypsinized and replated in media containing 0.5 mg ml$^{-1}$ of Geneticin G418. The media was changed every 3-4 days for several weeks to remove cell debris and to allow colonies of resistant cells to grow. To select the

desired colonies, homemade cloning rings (made of plastic pipette tips) were dipped in grease and placed over the marked colonies. The colonies in the cloning area were trypsinized and transferred to 96 well plates. The individual colonies were propagated for several weeks in selective media. Thereafter, the stable transfected MCF-7 cells were cultured in DMEM containing 0.5 mg ml$^{-1}$ of Geneticin G418 to ensure cell line integrity.

For on-chip lysis, cultured MCF-7 cells were detached from the surface using trypsin and suspended in PBS. The cell suspension was washed twice with PBS, pelleting at 1200 rpm for 5 min, and finally suspended in 0.6 M D-sorbitol at a concentration of 4x10$^6$ cells ml$^{-1}$ prior to on-chip injection.

For off-chip lysis, cells were transferred to a centrifuge tube 48 hours after transfection and pelleted at 1000 rpm, before washing three times with PBS. The cell pellets were then resuspended in lysis buffer (150 mM NaCl, 50 mM Tris pH 7.4, 1mM EDTA, 1% Triton X-100) supplemented with protease inhibitors (Roche complete mini EDTA-free). The cells were lysed on ice using a probe sonicator by applying 30 short pulses (~1 s). Cell debris was pelleted at 14000 rpm, using a refrigerated microfuge, and the supernatants were frozen at -80 °C in aliquots until required. Lysate solutions were used at three different dilutions in PBS: 1/10, 1/50 and 1/100.

## 4.3.5 Western Blot Analysis

Western blot analysis was employed to measure the HRas-mCitrine (~50 kDa) concentration in the HEK-293 lysate. Blots were prepared by Dr. Sandison. The concentration was measured from 8 separate lysate samples run on 5 different blots, along with 10 samples of a purified glutathione *S*-transferase (GST, ~26 kDa) solution, run on 10 different blots. The concentration of the latter, which was used as a standard, was measured by Bradford assay to be 0.4 mg ml$^{-1}$ and 20 µl samples of either cell lysate or a 2% dilution of GST were run per lane.

Samples containing 20 µl of either HRas-mCitrine lysate or purified GST standard along with 5 µl of protein loading buffer (containing 20% glycerol, 2% SDS, 5% β-mercaptoethanol, 0.5% bromophenol blue and 63 mM Tris) were heated at 99 °C for 5 min, before running on a 10% SDS-PAGE gel, along with ColorPlus

prestained molecular weight markers (New England Biolabs), until the point the bromophenol blue just ran off the gel. The proteins were then transferred to Immobilon P membranes (Millipore, UK) using a semi-dry blotter (0.8 mA per cm$^2$ for 90 min). Following transfer, the membranes were blocked for 1 h in a solution of 5% non-fat milk powder in PBS, before washing twice in PBS containing 0.05% Tween-20 (PBS-Tween). All washes were 5 min long and carried out on an orbital shaker in approximately 100 ml wash buffer.

The membranes were then incubated with the primary antibody solution (5 µl anti-HRas or anti-GST and 5 ml 5% w/v non-fat milk powder in PBS-Tween) for 1 h on a roller mixer. After washing 6 times in PBS-Tween, the membranes were incubated with the secondary antibody solution (as before, except containing anti-mouse-peroxidase), again for 1 h on a roller mixer. Following a further 4 washes, the western blots were imaged by enhanced chemiluminescence using Pierce ECL Western Blotting kit (following the manufacturer's instructions) and a imaging system (G:Box, Syngene, UK).

### 4.3.6 Fluorophore intensity normalisation

In order to compare the fluorescence intensities acquired from the different fluorophores used (Fluorescein, EGFP, mCitrine and TRITC), filter sets and acquisition times, an intensity normalisation algorithm was written in Matlab by Dr. Michele Zagnoni. Information regarding the properties of the fluorophores used (extinction coefficient, fluorescent quantum yield and brightness) were available in literature (94, 95) and are reported in Table 4-1.

Table 4-1 Fluorescence properties fluorophores.

| Protein | Ex (nm) | Em (nm) | Extinction coefficient (M$^{-1}$ cm$^{-1}$) | Fluorescence quantum yield | Brightness EC*QY |
|---|---|---|---|---|---|
| *Fluorescein* | 495 | 519 | 75000 | 0.92 | 69 |
| *EGFP* | 488 | 507 | 56000 | 0.60 | 34 |
| *mCitrine* | 516 | 529 | 77000 | 0.76 | 59 |
| *TRITC* | 544 | 572 | 80000 | 0.15 | 12 |

The excitation and emission spectra for fluorescein isothiocyanate (FITC), enhanced green fluorescent protein (EGFP), tetramethyl rhodamine iso-thiocyanate (TRITC) and mCitrine fluorophores were each normalised to give a maximum peak value of 1. The mercury lamp emission spectrum and the excitation (transmission), dichroic (reflection and transmission) and emission (transmission) spectra of the filter sets were all obtain from Omega Optical. As the same objective was used in all experiments and the CCD camera acquisition spectrum was uniform across the range of wavelength in the experiments, their optical properties were not considered during normalisation.

The intensity normalisation between fluorophores was performed by assigning one dye as a reference (FITC) and normalising the fluorescence intensity acquired from the other dyes to the intensity of this reference. The normalised intensities, $I_{NX}$, were therefore calculated as:

$$I_{NX} = \frac{I_{OUT\_REF}}{I_{OUT\_X}} \frac{T_{REF}}{T_X} \frac{F_{F/P\_REF}}{F_{F/P\_X}}$$

$$4.1$$

where $I_{OUT\_REF}$ and $I_{OUT\_X}$ are the light intensities acquired at the camera, $T_{REF}$ and $T_X$ are the acquisition times and $F/P_{REF}$ and $F/P_X$ are the fluorophore-protein molar ratios of the reference dye chosen and the dye being normalised respectively (obtained from the datasheet).

## 4.4 Results and discussion

### 4.4.1 Bead preparation

10 μm diameter beads (as binding supports) were coated with biotinylated antibody (anti-H-Ras, Millipore) as described in Figure 4-3 and then incubated with a FSA able to bind to the anti-H-Ras. Knowing the concentration of beads in the solution and their binding capacity, coated beads were incubated with different dilutions of FSA. After a 2 h period of incubation the beads were washed and imaged under a fluorescence microscope. The imaging revealed that the beads became fluorescent, demonstrating the success of the protocol and the bead's selectivity (Figure 4-4). Plain beads were also imaged as a control

under fluorescence and showed to have an intrinsic background fluorescence level (IBF) which was taken in consideration for all the investigations.
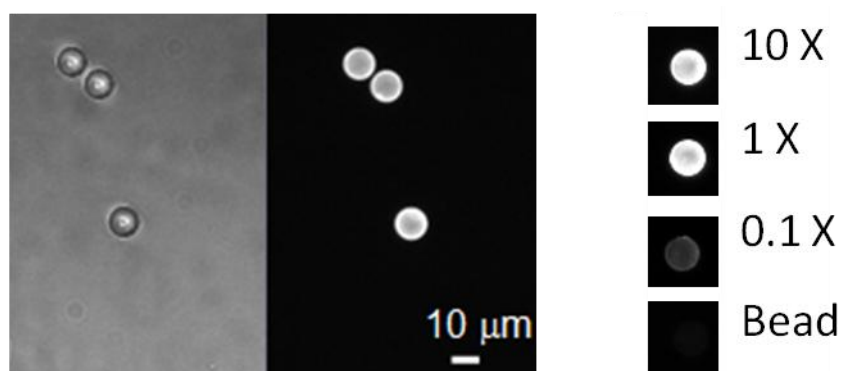


Figure 4-4 Beads coated by antibody: on the left, bright field and fluorescence images of beads after incubation with a dilution of FSA. On the right, fluorescence images of 10X, 1X, 0.1X FSA dilutions and intrinsic fluorescence level of a non coated bead.

## 4.4.2 Droplet generation

A single emulsion was generated by actuating three syringe pumps connected to the chip device fabricated as described in the Methods section. Emulsions were imaged using a camera connected to a microscope. The experimental set up used in the experiments is shown in Figure 4-5.
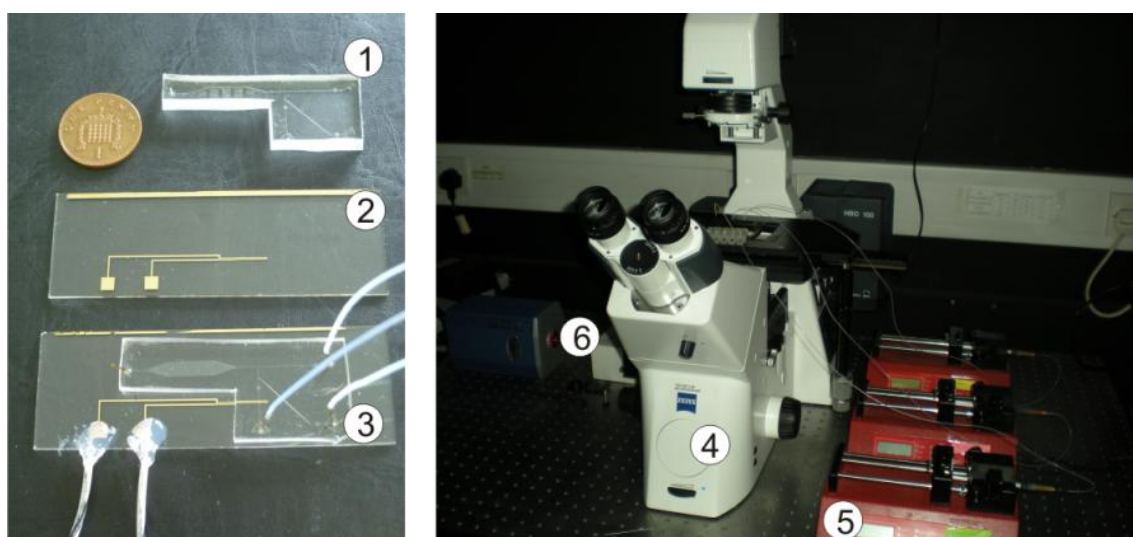


Figure 4-5 Experimental setup: 1) PDMS chip, 2) coverglass with electrodes, 3) PDMS chip bonded to the glass slide with fluidic and electric connections, 4) inverted microscope, 5) syringes loaded onto syringe pumps, 6) CCD camera.

The flow rates of the oil phase and aqueous phases were set respectively to 1 and 0.5 µl min$^{-1}$. In these conditions droplets of water in oil were produced at a rate of 20 droplets per second (Figure 4-6 A).

Due to the laminar flow in the microfluidic channel (Re equal to 0.09)[4], the transport of substances from one aqueous stream to another was negligible, as shown in Figure 4-6 B. The two aqueous solution were mixed only after droplet formation because of convective phenomena that originate at the interface of a W/O drop moving inside the channel (92).

The chamber was filled in approximately 2 minutes (although droplets were allowed to flow for 5 min to achieve a steady condition for cell injection). After this period, the flow was stopped. Typically, droplet volumes decreased by 25% with respect to the initial volume after 5 h, due to water absorption into the PDMS (96-98). The storage area allowed for the collection of approximately 2000 droplets, with almost 20% of these containing a single bead (Figure 4-6 C).

Analysis of micrographs of emulsion stored in the chamber showed monodispersity of the emulsion with a mean diameter equal to 92.8 µm and a CV equal to 3.8%. Distributions of droplets diameter and number of encapsulated beads within each droplet are presented in Figure 4-7. Droplets never assumed a spherical geometry because confined in a channel 50 µm height.

---

[4] Re number was calculated by knowing the mean velocity of continuous phase ($3.40 \times 10^{-3}$ m s$^{-1}$), its dynamic viscosity (4.11 g s$^{-1}$ m$^{-1}$), its density (1.87 g cm$^{-3}$) and the hydraulic diameter of the micro channel given by 4 times the ratio between the area (50 µm x 70 µm) and the perimeter of the channel (2x50 µm + 2x70 µm).
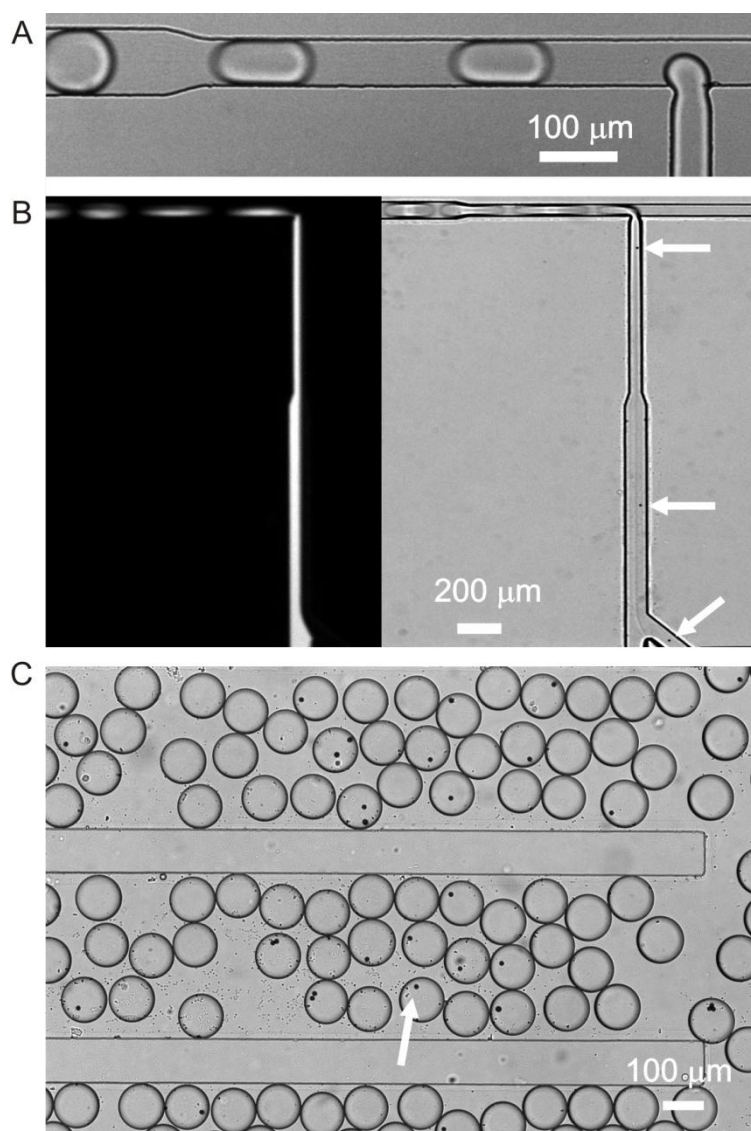
Figure 4-6 Droplets generation: A) Image showing droplet formation at the T-junction; B) Fluorescence and bright field images showing laminar flow at the Y-junction. The fluorescent phase flowing was a FSA solution. White arrows indicate functionalised beads within the aqueous stream; C) bright field image of droplets stored in hexagonal chamber. In the picture, 20% of the emulsion was encapsulating 1 single bead (white arrow).

A



B
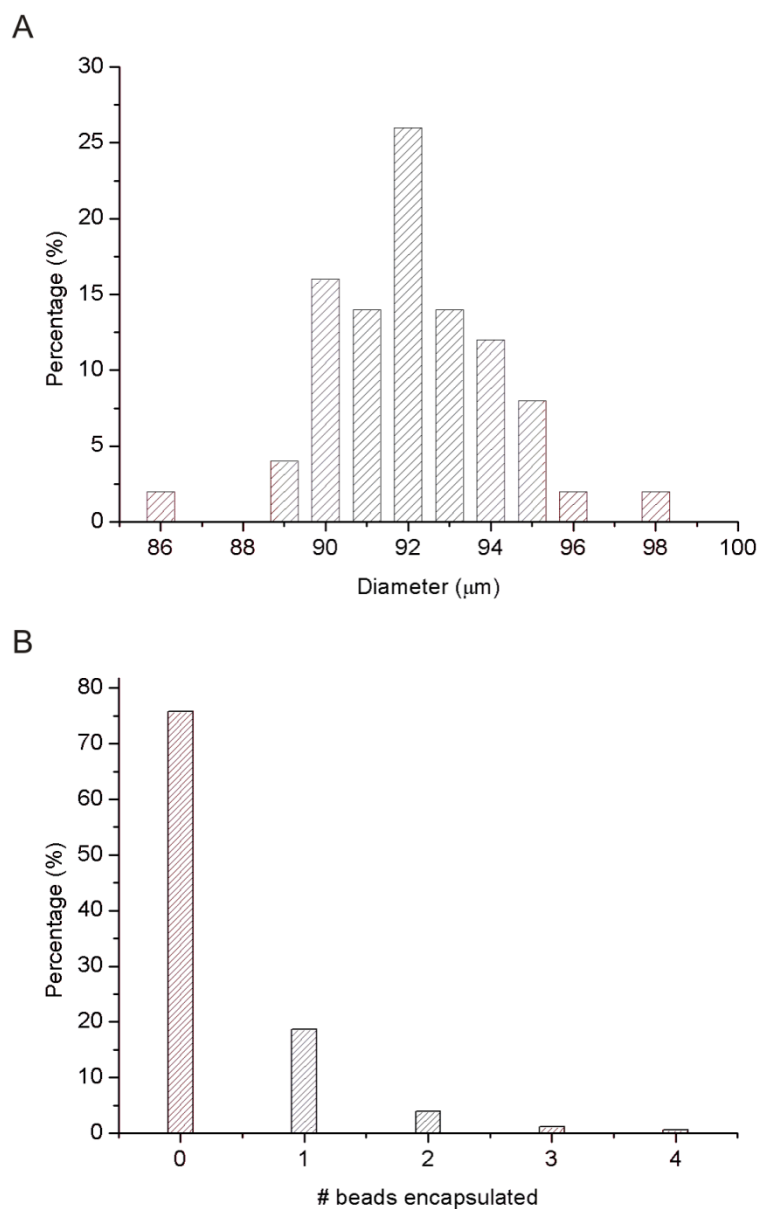


Figure 4-7 Emulsion characterization. A) Distribution of droplet diameter with average set on 92.2 μm and a CV equal to 3.8%. Bin size equal to 1 μm. B) Distribution of number of beads encapsulated in each droplet. Only 19% of droplets resulted in encapsulating one bead. Measurements were taken on a population of 200 droplets.

## 4.4.3 Calibration protocol

The capture and detection of antigens by antibody functionalised beads was carried out both on and off-chip, using known concentrations of fluorescent secondary antibody calibrants, in order to determine the sensitivity of both droplet and conventional bead-based immunoassays (Section 4.3.3). The calibration curve obtained from the on-chip experiments was later used to determine the concentration of fluorescent fusion proteins from fluorescence measurements obtained during experiments using cells and cell lysates.

Once a bead and fluorescent fusion proteins were encapsulated in a droplet, proteins specifically bound to the antibody-conjugated bead, which increased the fluorescence signal from the bead over time. An example of a fluorescence image from beads encapsulated in droplets stored in the microfluidic chamber is given in Figure 4-8. As described in Figure, the fluorescence signal ($\Delta I$) was calculated as the difference between the average value of the fluorescence intensity ($I$) from the bead and the average value of that obtained from the background (from an intensity line plot passing across the centre of each bead). Antigen concentrations significantly above saturation levels were avoided.
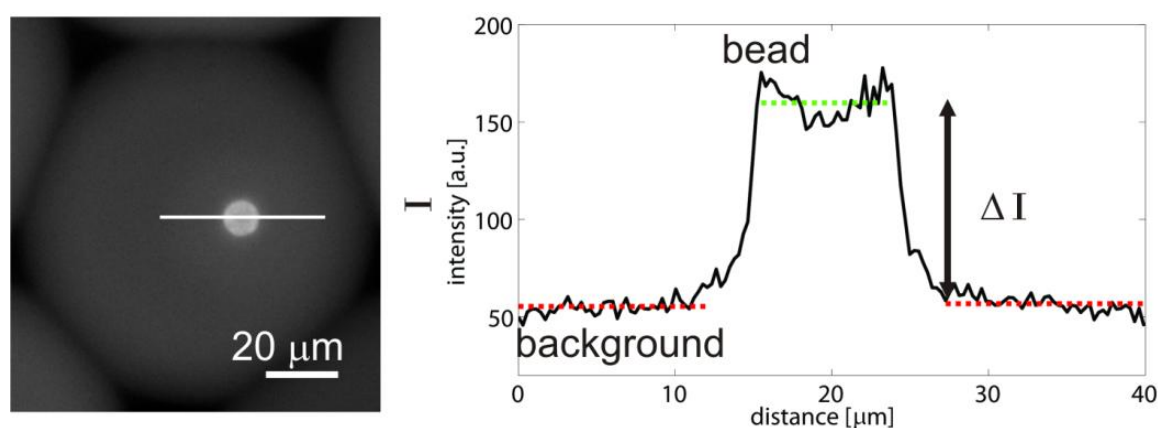


Figure 4-8 Fluorescence measurements of protein capture. On the left, fluorescence image of microdroplets stored inside the chamber after an incubation period of 1 h. On the right, the method used to measure fluorescence intensity data for immunoassay analysis. The white line, which runs through both the centre of the bead and the surrounding background, shows the position of the line plots acquired. The fluorescence intensity, ΔI, was calculated as the mean bead intensity (upper dashed line) minus the mean background intensity (lower dashed line).

The calibration curves in Figure 4-9 A show the mean values of the normalised fluorescence intensity[5] acquired after 2 h of incubation, as a function of FSA concentration, for both on and off-chip experiments. As expected, the fluorescence intensity acquired from beads (coated with mouse anti-HRas) encapsulated in droplets was lower than that detected from the off-chip experiments, presumably due to light scattering resulting from the multilayer emulsion system (glass-HSQ-oil-water). However, both curves have a sigmoidal shape, with the top right plateau of the sigmoid corresponding to the fluorescence from a saturated bead and the bottom left plateau stemming from

---

[5] Derived from the calculation of $I_{NX}$ discussed in Section 4.3.6 and referred to FITC fluorophore.

the combined intrinsic fluorescence of the bead and the droplet system. From these experiments, a detection limit of 55.2 pM was obtained for the immunoassay both on-chip and off-chip detection.
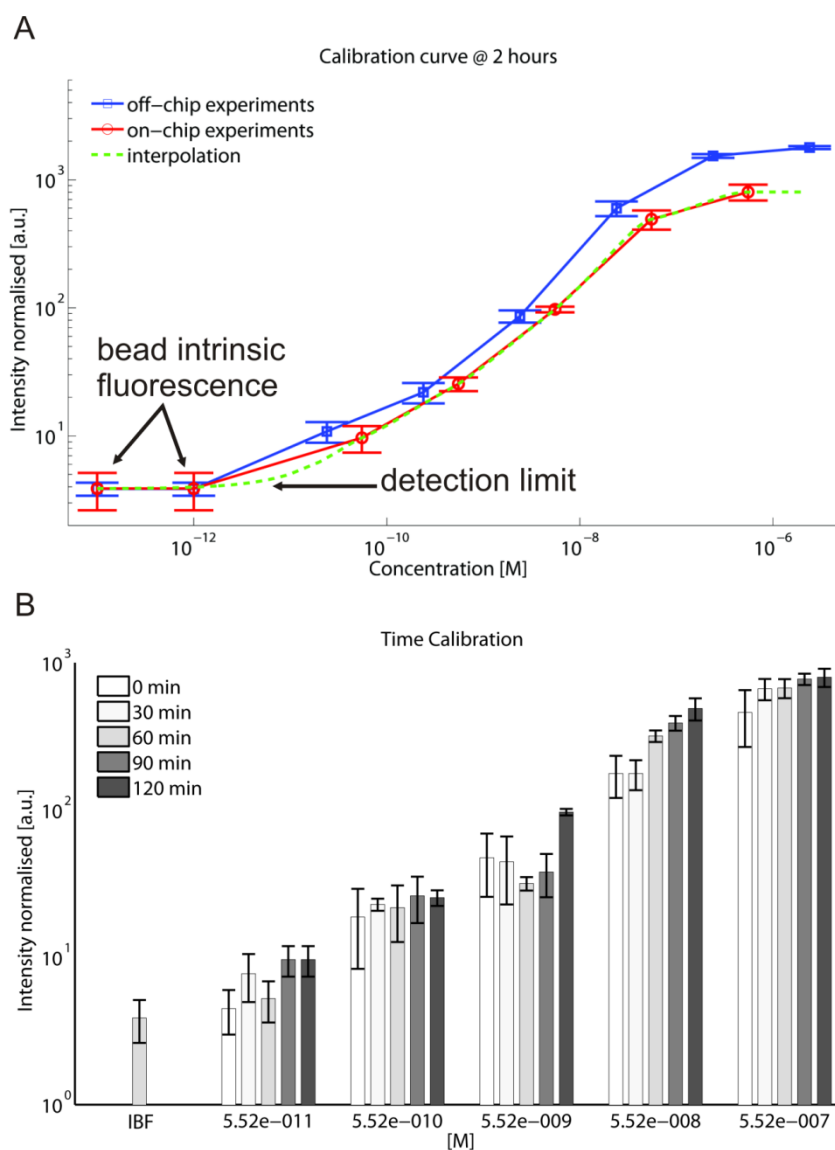


Figure 4-9 Calibration curves and immunoassay time response: A) off-chip (blue) and on-chip (red) calibration curves obtained by incubating beads with several known FSA concentrations. The values correspond to the mean intensity levels acquired after 2 hours of incubation. The dashed line (green) represents a data interpolation for on-chip experiments, obtained by applying a Piecewise cubic Hermite algorithm in Matlab; B) Time courses of the mean, normalised, fluorescence intensity levels, obtained from on-chip experiments, compared to the intrinsic fluorescence of a bead encapsulated in a droplet (IBF) for different FSA concentrations. Molar concentrations of FSA below approximately 50 pM could not be resolved.

The primary difference between the off-chip and on-chip experiments was that no washing steps could be carried out within the droplets. Thus, all proteins that

were encapsulated within a droplet, but not bound to a bead, remained within the aqueous phase and the level of bead fluorescence intensity acquired depended on the rates of mass transport and subsequently, the binding kinetics of the antibody-antigen used. In all cases, it was therefore important to ensure that the fluorophore concentration was within the linear binding range and that sufficient time was allowed for mass transport to reach equilibrium.

Figure 4-9 B shows the normalised fluorescence intensities obtained from the on-chip calibration experiments as a function of time, compared to the intrinsic bead fluorescence (IBF). For each experiment, the variation in the fluorescence intensity showed a trend that increased with time until an equilibrium condition dependent upon the antibody-antigen binding kinetics was reached. It should be noted that time *t=0* corresponds to the point that, following filling of the storage chamber, the flow was stopped. Therefore, at this stage the beads had already been incubated with the FSA solution for 2-3 min. For concentrations >50 pM, the initial measurements showed fluorescence intensities that were significantly greater than the IBF level and increased with FSA concentration. This rapid response was largely due to convective movements within the droplets, which occurred during the transport of a droplet from the T-junction to its resting position in the chamber. Such convective motion enhanced the mixing between the two aqueous phases (the bead suspension and the FSA solution). Due to the emulsion stability, time course measurements could be taken over many hours.

## 4.4.4 Non specific adsorption assays

The time dependence of the fluorescent measurements and the level of non-specific adsorption were also characterised. To assess the level of non-specific adsorption by the functionalised beads, on-chip experiments were carried out using solutions containing positive (TRITC-conjugated anti-mouse or FITC-conjugated anti-mouse) and negative (FITC-conjugated anti-rabbit) secondary antibody controls.

Experiments were carried out using single antibody (only specific antibody and only non specific antibody) and mixed solutions of antibodies (specific and non specific antibodies in droplet) as shown in the cartoons of Figure 4-10. The antibody concentrations were 1 µM in all cases, which is approximately the

concentration required for saturation of the available binding sites on the functionalised beads (determined from Figure 4-9 A). Time lapsed fluorescence intensity images were again acquired every 30 min for 2 h.

As shown in Figure 4-10, whether the antigens were encapsulated in droplets separately or mixed, the level of non-specific adsorption was substantially lower than specific antigen binding. Fluorescence intensity due to non-specific adsorption was estimated to be <12% of the specific binding level obtained. Whilst the latter followed the same time-course as seen in previous experiments, the level of fluorescence intensity obtained from non-specific antigen binding remained approximately constant throughout the 2 h incubation period.
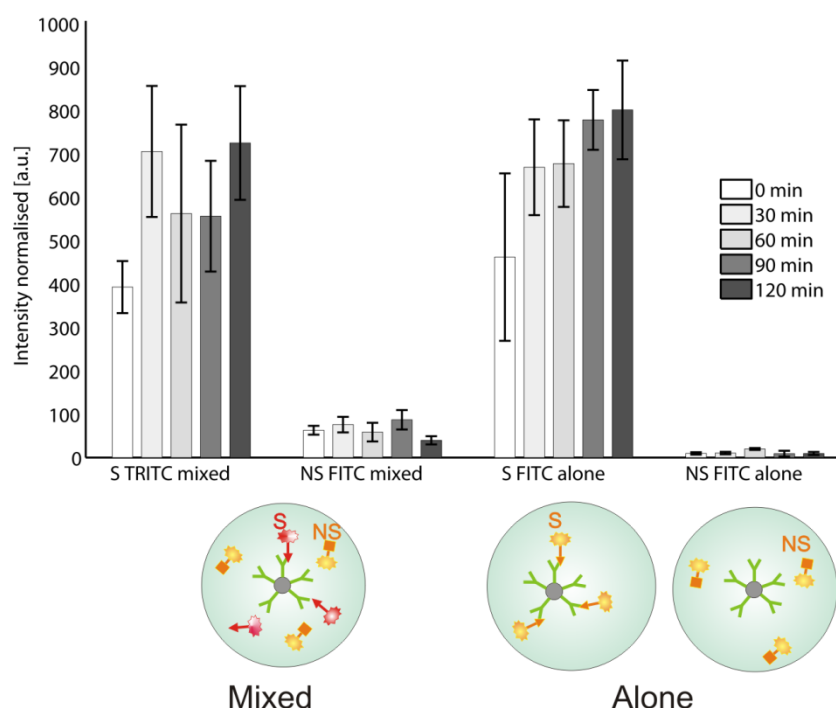


Figure 4-10 Time dependent specific (S) vs. non-specific (NS) adsorption of FSA, for 1 µM solutions. The graph shows mean intensity levels obtained from droplet encapsulation of a solution containing only non-specific (anti-rabbit) antigens, only specific (anti-mouse) antigens and a 1:1 mixture of both specific and non-specific antigens.

### 4.4.5 RAS Cell lysate assays

Experiments using a cell lysate prepared off-chip were also performed, to compare the on-chip results with those obtained by Western blot analysis and to

assess the performance of the immunoassay when using complex, biologically relevant samples.

Clarified cell-lysate from HEK-293 cells expressing HRas-mCitrine was prepared off-chip as described in Methods section. As their high concentration of detergent (1% Triton X-100) was sufficient to cause emulsion instability, undiluted lysate solutions could not be used. Therefore, three cell lysate dilutions - 1:10, 1:50 and 1:100 lysate:PBS - were prepared and injected into the device from inlet C (Figure 4-1).

The intensity levels acquired from single anti-HRas functionalised beads encapsulated in droplets were always much greater than the detection limit of the assay and showed a time dependence similar to that obtained in the calibration experiments (Figure 4-11 A).

Quantitative results were obtained by comparing the intensity levels from the cell lysate experiments with the normalised, interpolated calibration curve (Figure 4-11 B), assuming similar $K_D$ values. These resulted in concentrations of 2.1 nM HRas-mCitrine for the 1:100 dilution, 2.7 nM for the 1:50 and 11.0 nM for the 1:10. Using an average of the 1:100, 1:50 and 1:10 measurements gives an approximate concentration of 151.6 nM for the undiluted lysate.

To validate the results obtained from the on-chip procedure, a series of Western Blots were performed using the same clarified cell lysate along with a protein standard (purified glutathione *S*-transferase).

The results gave a HRas-mCitrine concentration of approximately 390 nM, which corresponds to a value 2.5 times higher than the concentration obtained on-chip. Differences may arise from losses due to non-specific adsorption within the device and tubing. As cell lysate solutions contain a multitude of proteins in addition to the one being detected, these results demonstrated the robustness and reliability of the on-chip immunoassay.
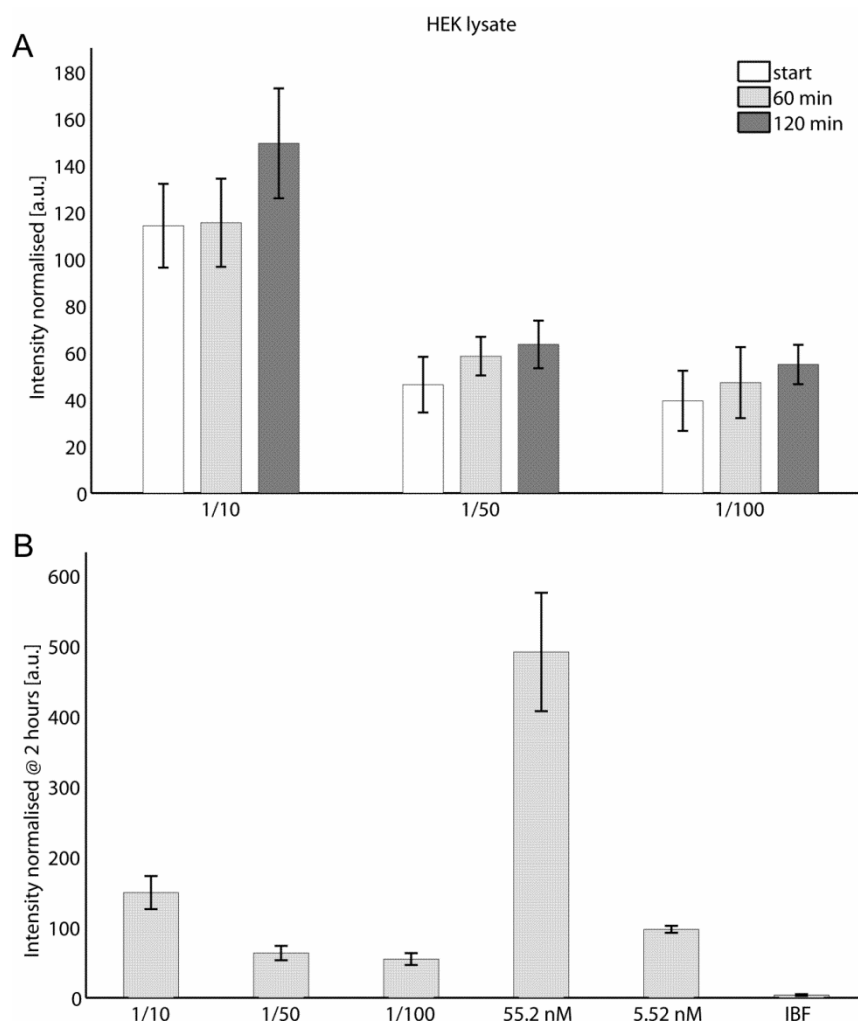
Figure 4-11 On-chip HEK-293 lysate experiments: A) Time-dependent, mean, normalised fluorescence intensity obtained from 1:10, 1:50 and 1:100 lysate:PBS solutions; B) Mean, normalised fluorescence intensity acquired after 2 h incubation, comparing the cell lysate dilutions to calibration experiments and to the intrinsic bead fluorescence (IBF) level. Data are representative of at least 5 experiments.

## 4.4.6 On-chip cell electro-lysis assays

Finally, both HEK-293 (expressing HRas-mCitrine) and MCF-7 (expressing Actin-EGFP) cells were electrically lysed on-chip and the concentration of fluorescent fusion proteins measured.

Cell lysis on chip was achieved by applying a 20 V magnitude square wave with a frequency of 1 MHz, typically resulting in cell trapping efficiencies >95%. For the conditions used (1 MHz, 20 V, 0.6 M D-sorbitol), the electric field strength was sufficient to cause the lysis of all cells captured at the electrodes (Figure 4-12), resulting in the release of their intracellular contents into the surrounding medium, which was subsequently encapsulated within droplets. Cell lysis resulted from the permanent electroporation of the plasma membrane (99) and

was caused by electrically-induced mechanical stresses. Lysis occurred over time scales in the order of hundreds of milliseconds. On average, 80 cells min$^{-1}$ were lysed using this protocol.
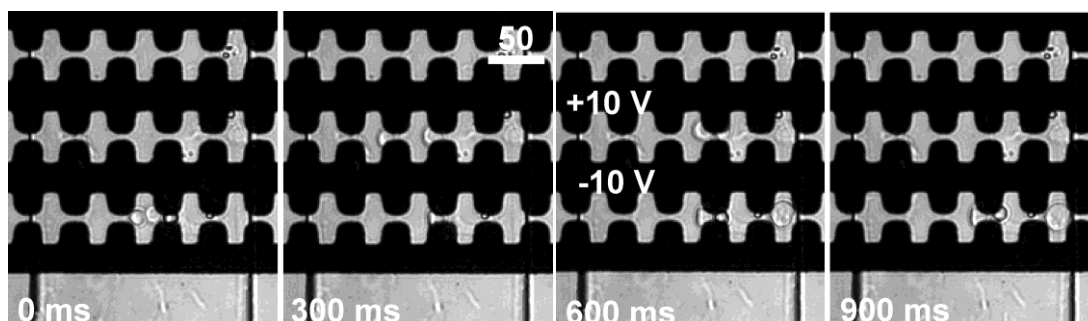


Figure 4-12 On-chip cell lysis. A typical time sequence of cell trapping/electroporation at the interdigitated microelectrodes (of which there were seven rows in total), showing more than one trapped cell at the electrodes at the same time. Scale bar is in μm.

Whilst cell lysate and antibody dilutions prepared off-chip were homogenous, leading to the formation of droplets containing the same number of fluorescent molecules, during on-chip cell lysis a non-uniform stream of fluorescent molecules was released into the flow. This was due to two factors: 1) the level of fluorescent fusion protein expression varied from cell to cell; 2) the number of cells being lysed at the one time was variable, typically 1-3 cells were trapped by the electrodes at the same time (Figure 4-12). For the cell suspension concentration used, rarely periods in which no cells were trapped at the electrodes were observed. Variability in the amount of cellular lysate between droplets was compensated for by averaging the signal from at least ten drops for each sample and time point.

After electro-lysis, cell fluorescence decreased to 30-50% of its original value for both cell lines. An example of the lysis of a HEK-293 cell expressing HRas-mCitrine is shown in Figure 4-13. It would not be expected that all the intracellular molecules of interest would be released into the surrounding media, with a significant number of proteins being, for instance, membrane-associated (it is known that modification of Ras can produce a membrane-anchored form) or attached to cytoskeletal components (actin being a key component of the cytoskeleton). For the flow rates and electric fields used, cells detached from the electrodes 0.3-1 s after trapping and lysis. However, the

decrease in cell fluorescence typically occurred in the first 500 ms. When detached from the electrodes, cell debris was either absorbed onto the channel walls prior to the Y-junction or occasionally encapsulated in droplets. Droplets encapsulating visible cell debris were not selected for analysis.
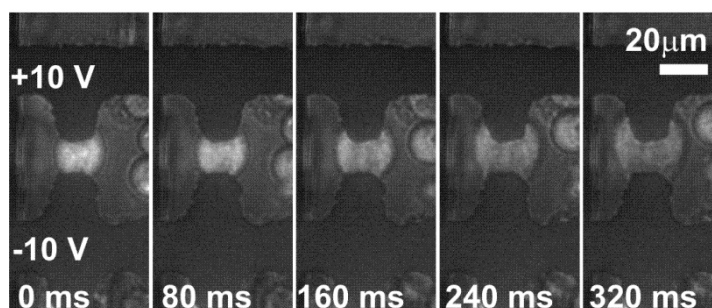


Figure 4-13 Ras expressing cell lysis. It can be seen that the cell diameter increased with time due to the effect of rupturing the plasma membrane.

## 4.4.7 RAS capture from cell lysed on chip

HEK-293 cells expressing HRas-mCitrine were used to validate the on-chip cell lysis procedure in combination with immunoassay for the detection of cytoplasmic proteins. Typically, 1000 cells were loaded and injected into the chip. Cells were electrically lysed using the on-chip microelectrodes and the immunoassay results obtained are shown in Figure 4-14.

Although expression levels varied widely from cell to cell (as is normal for a population of transiently transfected cells), the majority of the HEK-293 cells expressed high levels of the HRas fusion protein. These high levels are known to be rather cytotoxic and a number of dead cells were observed in the initial cell suspension, leading to a corresponding high background fluorescence level. The cells were also susceptible to lysis under mechanical stress, preventing extensive washing before being loaded into the chip. Experiments were therefore carried out with lysis electrodes both active and inactive, to enable a comparative measurement.

Figure 4-14 shows the immunoassay time courses obtained. By measurement of the difference in intensity with the microelectrodes inactive (the non-lysed case) and with the electrodes active (and lysing the flowing cells), along with comparison to the calibration curve, protein quantification was possible.

Intensity values for the non-lysed case corresponded to a HRas-mCitrine concentration of 3.5 nM, whilst the value obtained when lysing the cells was 13.0 nM, giving a value of approximately 10.5 nM for the contribution due to the cells lysed on-chip. This is in close agreement with the value from the Western Blot data.
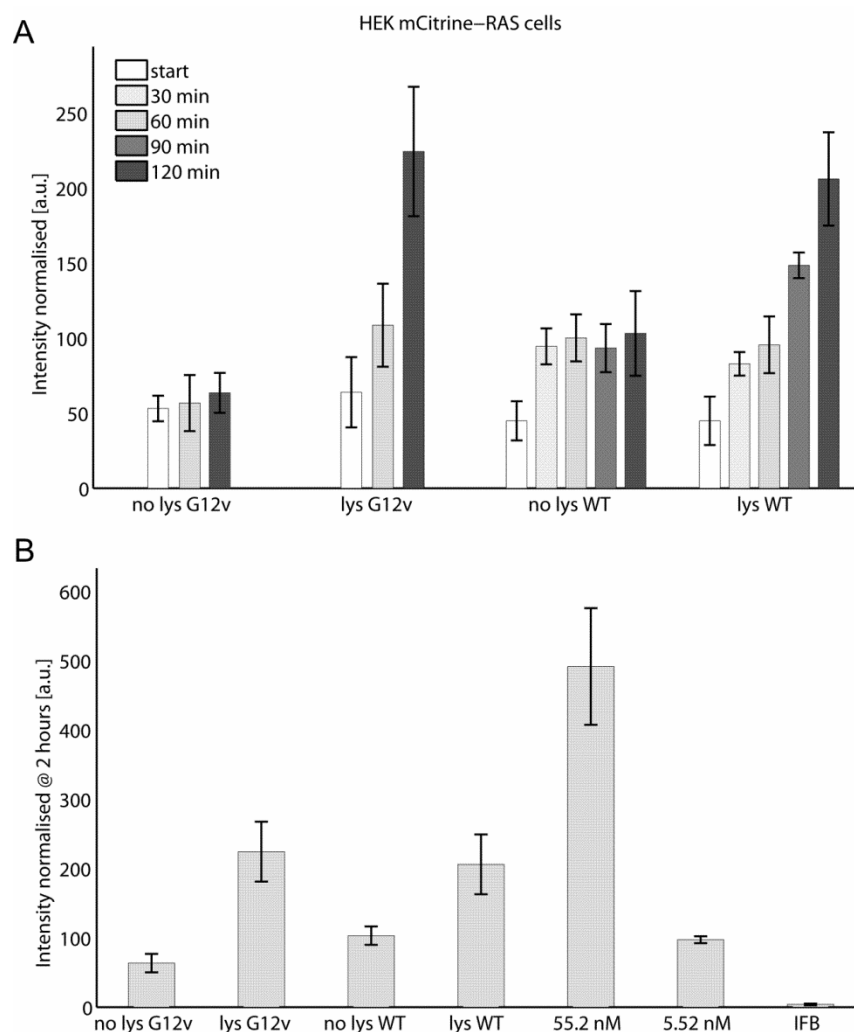


Figure 4-14 Detection of HRas-mCitrine in on-chip cell lysis experiments: A) Time dependent, mean, normalised fluorescence intensity levels obtained for both lysed and unlysed HEK-293 cells; B) Normalised fluorescence intensity levels acquired after 2 hours of incubation, comparing the on-chip cell lysis experimental data to calibration experiments and to the intrinsic bead fluorescence. Data are representative of at least 5 experiments.

Approximately 80 cells per min were lysed and 20 droplets per second produced within the device, giving on average the content of 0.066 cells per droplet. Knowing that the volume of a droplet was approximately 260 pl, it resulted that 0.066 cell in a 260 pl volume was equivalent to approximately $2.6 \times 10^5$ cells ml$^{-1}$,

which was approximately 0.026 times smaller than the cell concentration used to produce a lysate ($1\times10^7$ cells per ml) using the Western blot technique. The concentration of the HRas protein measured by Western Blot was approximately 390 nm HRas-mCitrine. A 0.026 dilution of this would therefore be in the order of 10 nM (exactly 10.14 nM).

## 4.4.8 Actin-EGFP Capture from cell lysed on chip

Finally, MCF-7 cells expressing actin-EGFP were used to further validate the combined on-chip lysis and immunoassay system for the detection of cellular proteins.

Actin is present both in monomeric and polymeric forms inside a cell, each form of which will clearly result in different levels of fluorescence when captured by a functionalised bead. Therefore, beads conjugated to anti-EGFP antibodies were suspended in one of two different buffer solutions prior to injection into the chip, either PBS or G-actin buffer. Whilst the former does not affect levels of polymerised actin, the latter promotes its depolymerisation. The results obtained when using these two buffer solutions, which exhibited different trends, are shown in Figure 4-15 A.

When G-actin buffer was used, the intensity levels were lower than when using PBS, confirming filament disassociation. Instead, when no action was taken to disrupt actin polymerisation, the intensity levels increased over time, reaching equilibrium after approximately 2 h. When the electrodes were inactive (and therefore no cells were lysed), the level of bead fluorescence remained at the same level as the intrinisic bead fluorescence.

By comparing the results from the on-chip MCF-7 cell lysis experiments with the calibration curve, actin-EGFP concentrations could be estimated (Figure 4-15 B). The intensity values obtained when using G-actin buffer corresponded to the saturation of the bead, whilst the values obtained when using PBS corresponded to intensity level well above the bead saturation. In the first case, the results suggest that monomeric and small filaments of actin-EGFP were captured by the beads; whilst in the second case, longer filaments of actin-EGFP were instead

bound, enabling the captured protein level to be well above that of monolayer coverage for an individual protein.
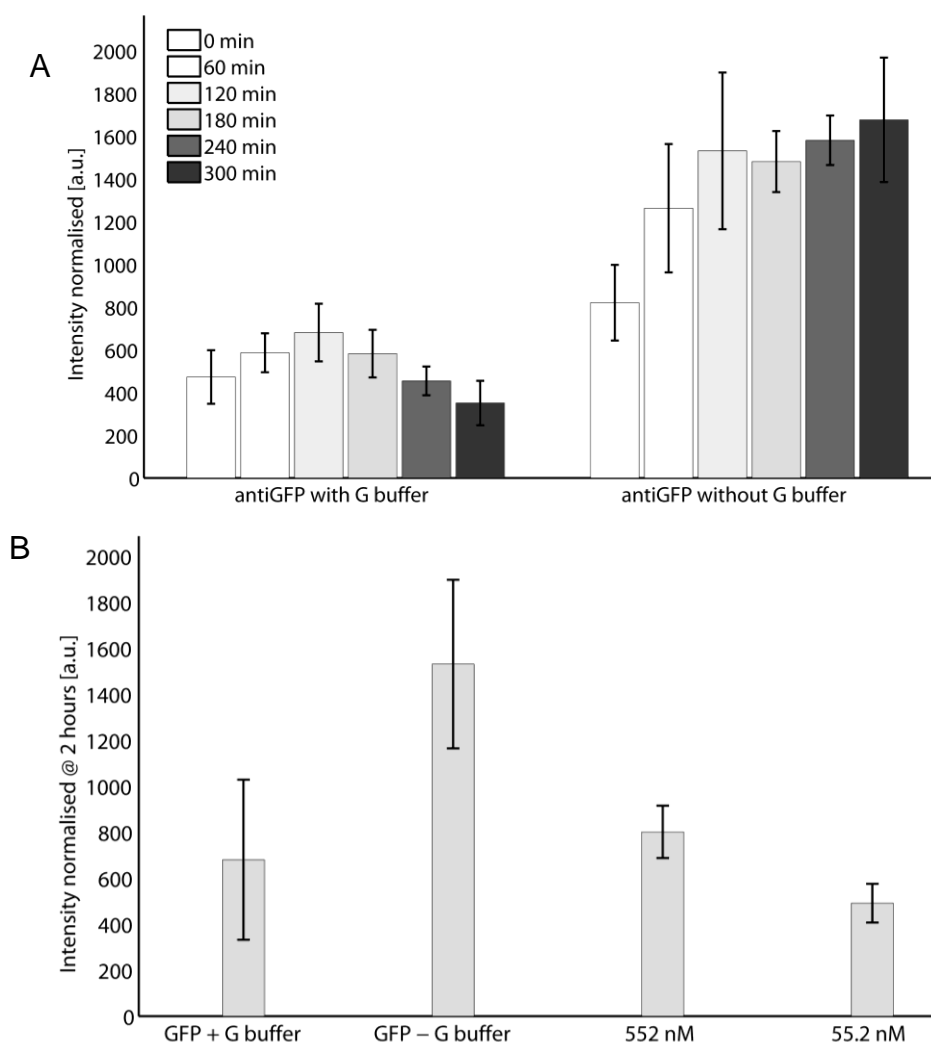


Figure 4-15 On-chip MCF-7 cell lysis experiments: A) Time dependent, mean normalised fluorescence intensity levels obtained from on-chip electrically lysed cells expressing actin-EGFP. Two immunoassays were performed, both using antiGFP-conjugated beads but each using a different buffer solution, either G-buffer (left) or PBS (right); B) Mean, normalised fluorescence intensity levels acquired after 2 h incubation, comparing experimental data from the on-chip cell lysis experiments to calibration experiments. Data are representative of at least 5 experiments.

## 4.5 Conclusions and future perspectives

In this work, a droplet microfluidic system for performing quantitative on-chip immunoassays with integrated cell lysis was presented. By taking full advantage of the efficiency and functionality of microfluidic devices, similar results to those obtained by Western blot were achieved in shorter times, using a reduced

number of cells. Whilst lysate solutions are typically produced from several million cells, less than a thousand cells were required to obtain reliable results using the on-chip immunoassay. This is valuable for the analysis of rare cell populations. The system, as it was conceived, had a detection range of five orders of magnitude, spanning from 50 pM to 1 µM, with analysis times typically in the order of two hours.

On-chip purification or washing stages were not required, greatly simplifying the device geometry and the complexity of operations. Nonetheless, droplet-based microfluidics can provide a library of operations that can be implemented for such purposes or for incorporating additional functionalities. For example, electrocoalescence of different droplet populations (90) and subsequential splitting (16) can be readily implemented within the channel network. Furthermore, multiplexed immunoassays could be carried out by injecting a library of encoded beads functionalised with a range of different antibodies.

# 5  Artificial cell models

Chapter 5 describes the use of a droplet-based microfluidic system for double emulsion formation, aiming to mimic living cells in their basic functions of compartmentalisation and protein production. The emulsion was used for cell-free protein expression which occurs in an aqueous environment enclosed within an oil membrane, separating the inner from the external aqueous environment. This Chapter focuses on the characterization of the microfluidic device used for double emulsion droplet formation and expression of proteins within the double emulsion system. Part of the material presented in this Chapter was published in *ChemBioChem* journal (2012), Volume 13, pages 792-795 and presented at the international conference EMBL 2012 (Heidelberg, Germany, July 2012).

## 5.1 Introduction and proposed approach

This Chapter demonstrates the combination of microfluidic droplet-based technology with cell-free protein expression system for the production of a bacterial protein within an artificial cell model.

In order to develop the idea associated with the "artificial cell" as an engineered entity that mimics the living cell in any of its part and/or function, synthetic biology procedures were used in combination with a microfluidic platform. Commercially available cell-free gene expression kits, together with DNA templates carrying the genes of the proteins of interest, were used in this research. An optimised *E. coli* extract (100), an optimised reaction buffer containing ATP regenerating system (101) and amino acids, that allow high-level synthesis of the desired protein, were encapsulated within the microdroplet and incubated in order to increase the protein yield. Figure 5-1 shows the concept already described, by other research groups, for the production of green fluorescent protein (GFP) both in single (29) and double emulsion (44), red-

shifted GFP (rsGFP) (102) and organophosphorus (OpdS) hydrolase enzyme (43). The droplet encapsulates the genome and the biological machinery required for protein synthesis. The information encoded into DNA, the "so-called" genotype, is translated into proteins, as the "phenotype".
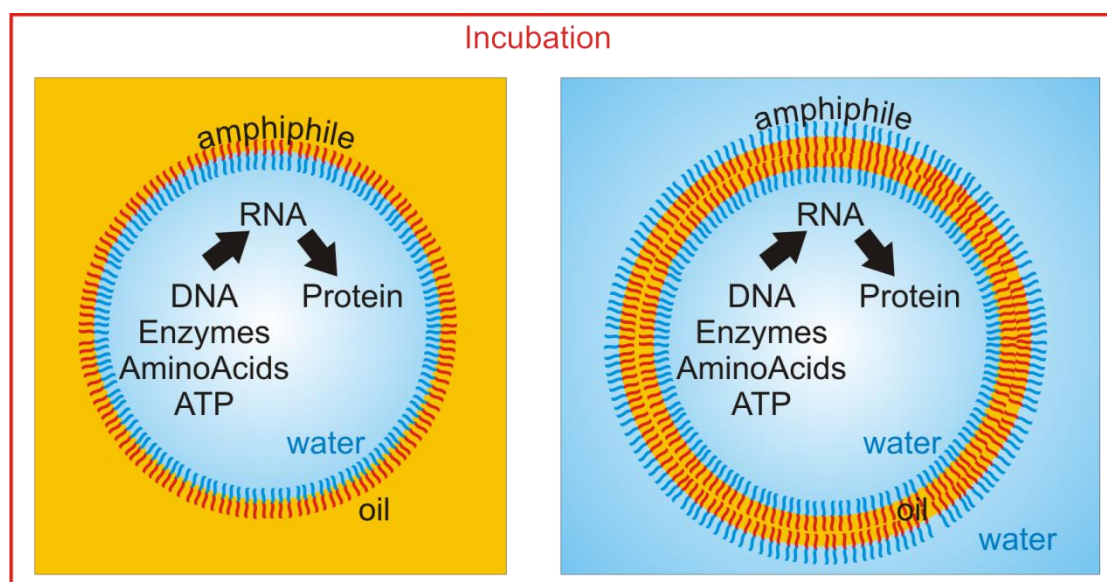


Figure 5-1 Microfluidic droplet of water in oil (left) and of water in oil in water (right) encapsulating a cocktail of bacterial ribosomes, nucleotides and enzymes which allows the in vitro transcription/translation process. This system requires incubation to increase the yield of protein production.

In this work the production of a cytoskeletal bacterial protein within a stable microdroplet was achieved for the first time. An industrial glass microfluidic device made of two X-junctions was used for the production of water in oil in water double emulsion. The droplets of the emulsion encapsulated the "living" components and through an opportune incubation step the protein of interest was expressed.

The protein in consideration is called MreB, which is present in all rod-like bacteria. Firstly described in 1988, a few years later its similarities with the actin protein were discovered (103). MreB is a monomeric protein of 36.9 kDa which polymerises forming patches in presence of ATP or GTP. MreB monomer's affinity to each other is much higher than the affinity between actin monomers and it polymerises forming linear polymers instead of helical structures as with actin. It has been estimated that in *Bacillus subtilis* the critical concentration, the value above which the MreB starts to polymerise, is around 5.6 μM, two

orders of magnitude lower that the actin one (550 μM) (104) while in *E. coli* and *Thermotoga maritima* this value goes respectively down to 6 nM (105) and 3 nM (106). On average in *E.coli* there are 8000 molecules of MreB (107), which means that, considering its average volume between 0.6-0.7 $\mu m^3$, the concentration of MreB per cell is equal to ~20 μM. Competitive inhibitors of ATP like the S-(3,4-dichlorobenzyl)isothiourea, also known as A22, can decrease the critical concentration value for polymerisation by four times with consequences on properties such as depolymerisation and formation of amorphous structures, rather than linear ones (108).

MreB naturally assembles in the bacterial membrane environment as discrete patches that lie just beneath the membrane (109). It has been demonstrated that the MreB moves along the membrane with a speed equal to 0.1 $\mu m\ s^{-1}$ (110). Recent investigations have found that these patches move circumferentially around the cell and interact with the peptidoglycan (PG) elongation machinery made of cell-wall synthesis enzymes (PG hydrolase which synthesize the PG layer and penicillin-binding proteins that polymerise and crosslink the PG subunits) and plasma membrane proteins (MreC, MreD, RodA and RodZ), (109). The interaction with the membrane, in *E. coli*, it is mediated by hydrophobic residues clustered on one side of an N-terminal amphipatic helix which form the predicted membrane-binding surface (111).

The MreB is not only responsible for organizing the machinery of cell wall synthesis (111), but also plays an important role in the maintenance of the bacterial shape (107, 112). Studies on E. coli and *Bacillus subtilis* have found that MreB genes are responsible for their rod like shape (107, 113); in fact when mutations or deletion of the MreB genes occur the cells change their morphology becoming spherical and assuming an inflated shape (103). At present the role of this protein within bacterial cells has not been completely elucidated.

This work aimed to produce platforms where proteins, like MreB, whose functions are not completely understood, can be expressed and studied within the microfluidic platform. In this pilot study, using a bottom up approach, *E. coli* MreB was linked to a red ~30 kDa fluorescent protein mRFP1 (also abbreviated as RFP) (114) and expressed within an artificial cell model made of a double emulsion droplet. It was found that the protein, within the artificial chassis, did not denature and behaved as if a native protein. The MreB spontaneously

polymerised forming patches and showed preference towards the hydrophobic oily membrane. In the same experimental conditions, as a control, the water soluble protein RFP was expressed and remained dispersed within the droplet. Moreover fluorescence recovery after photobleaching (FRAP) analysis showed that MreB-RFP molecules insert themselves within the hydrophobic membrane and that for the most part do not leave this place creating space for new unbleached molecules.

## 5.2 Materials and methods

### 5.2.1 Materials

Double emulsions were prepared by using a combination of hydrophobic and hydrophilic microfluidic systems (3000301 and 3000158, Dolomite, UK) connected to each other through a polytetrafluoroethylene (PTFE) gasket and held together by a metallic frame (3200088, Dolomite, UK). Mineral oil (M3516, Sigma, UK) 2% (w/w) Span 80 (85548, Sigma, UK) and DI water were used as the continuous or discontinuous phases in the characterisation experiments. FITC (Sigma, UK), BODIPY 505/515 (Invitrogen, UK) and DiI (Invitrogen, UK) were used as dyes for imaging. Solutions were delivered using PTFE tubing (3200063, Dolomite, UK) directly connected to plastic syringes controlled by syringe pumps (NE-300, New Era Pump Systems, UK). A solution containing the DNA was loaded into a 100 µl glass syringe (Hamilton, CH). Protein expression experiments were performed using Expressway™ Cell-Free *E.coli* Expression kit (Invitrogen, UK) and DNA plasmids. DNA plasmids were cloned using pEXP5-NT/TOPO cloning reaction (Invitrogen, UK) and One Shot TOP10 chemically competent *E. coli* cells. The concentration of the expressed protein was using a colorimetric detection assay using a BCA™ protein assay kit (23227, Thermo Scientific, UK) and a spectrophotometer (U 2000, Hitachi, UK). Depolymerisation assay used A22 compound (475951, Merck Millipore, UK).

### 5.2.2 Droplets generation

Double emulsions were generated by using a hybrid chip comprising a hydrophobic network (supporting a continuous oil phase), interfaced with a

hydrophilic network (supporting an aqueous phase). The overall geometry adopted can be represented as two linked cross flows, in which droplets of an internalised or segmented aqueous phase were produced with a hydrophobic membrane environment using two successive pinched flows. Aqueous and oil phases were shaped in a continuous flow to generate first a single and then a double emulsion. At the first cross-junction, two parallel streams of oil, perpendicular to a stream of watery solution, helped in the breaking up into droplets of the water-in-oil (W/O). Each droplet was carried to the second cross-junction where two streams of water pushed the droplet, surrounded by the oily phase, into a channel full of water. At this point the droplet of water was dispersed in an oil phase, itself dispersed in another watery phase forming the W/O/W droplet (Figure 5-2).
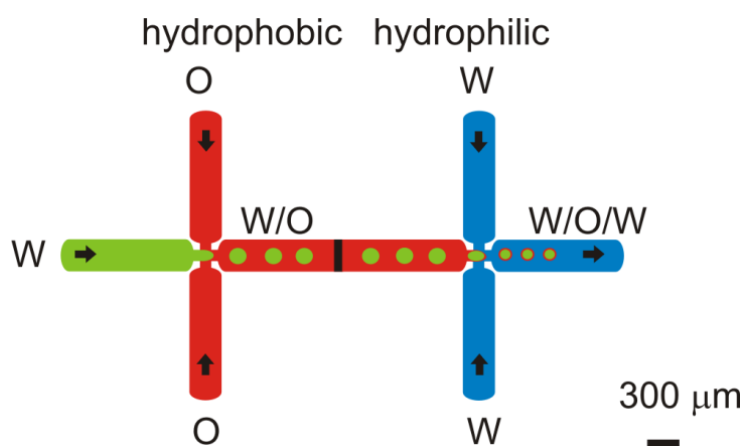


Figure 5-2 Double emulsion generation. The microfluidic system is made of two glass chips with different wetability characteristics. The two chips are joined by a PTFE gasket. The flows are marked as O (oil) and W (water) for the hydrophobic and hydrophilic flows.

The chip was fabricated by Dolomite using an isotropic wet etching of two pieces of glass which then underwent thermal bonding. Details of the chip design are showed in Figure 5-3. The channels are 100 µm deep.

By optimizing the fluid flow rates it was possible to control the thickness of the oily membrane and the number of W/O/W droplets originating from one W/O droplet. Figure 5-4 shows the experimental setup prior to an experiment.
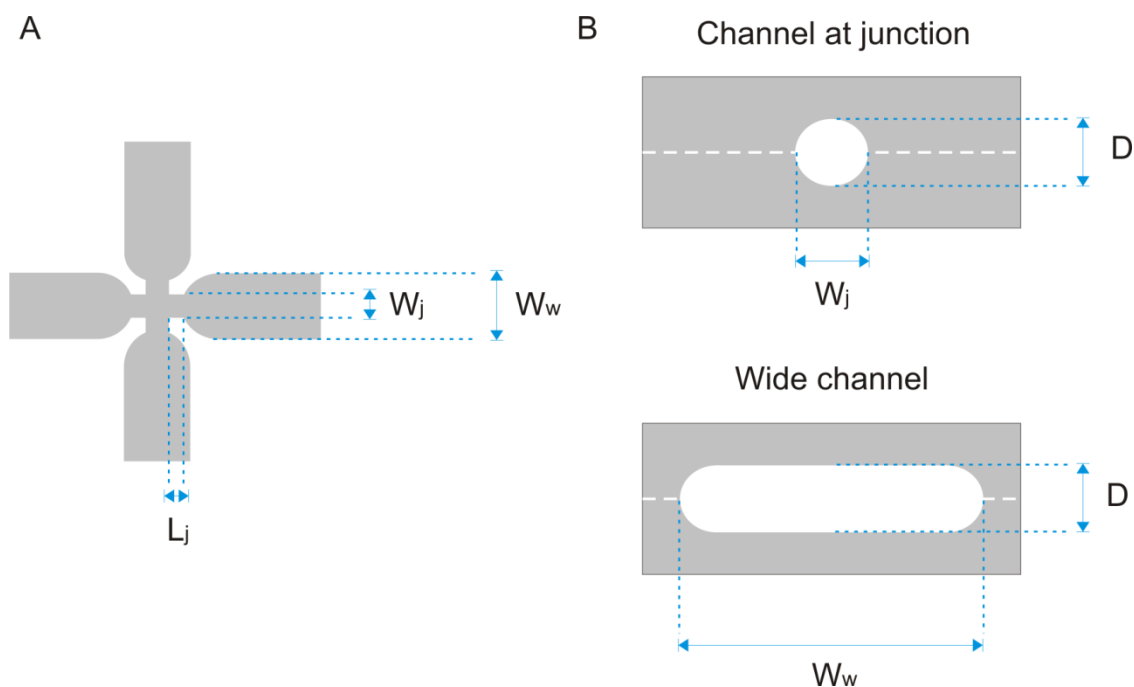
Figure 5-3 Chip geometry. A) Cross junction width $W_j$= 105 μm, $W_w$= 300 μm, $L_j$= 190 μm; B) channel section of the channel at the junction and of wide channel depth D= 100 μm.
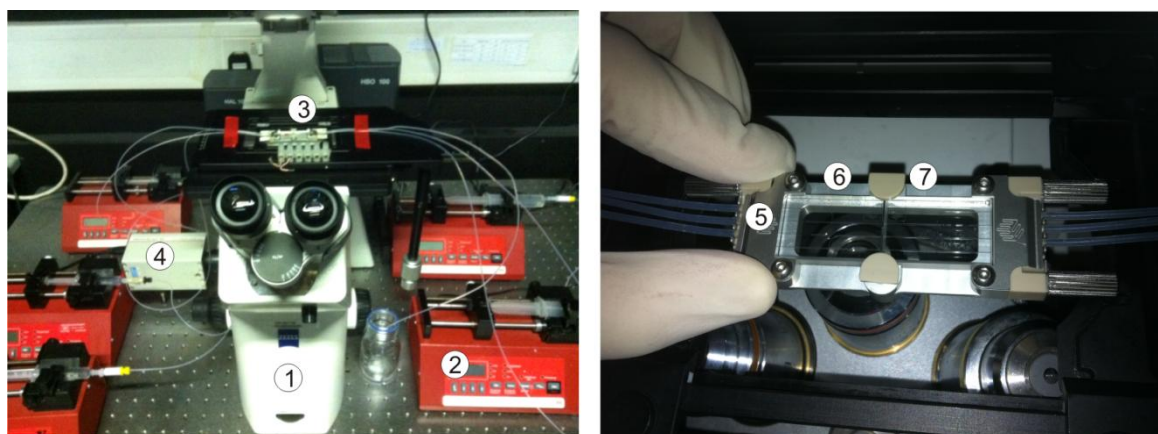


Figure 5-4 Experimental setup. On the left, 1) inverted microscope, 2) syringe pumps, 3) microfluidic droplet generator, 4) high speed camera. On the right: photograph of the chip for the generation of double emulsions. The chip is composed of a metallic frame 5) holding together two glass devices respectively 6) the hydrophobic and 7) hydrophilic one.

## 5.2.3 Cloning procedures

Two different DNA templates were designed, namely MreB linked to RFP to study the protein's phase separation at the membrane, and the water soluble RFP as a plasmid control. The fusion protein gene *MreB-RFP* with GS linker and the *RFP*

gene alone were PCR-amplified from plasmid pSB1A2_BX(*MreB-RFP*)[6] using Platinum® Taq DNA Polymerase High Fidelity (Invitrogen, UK) and primers MreB_NT_for and MreB_NT_rev or RFP_NT_for and RFP_NT_rev.

The general protocol for the polymerase was followed with an additional final 30 min extension step at 68 °C. After gel extraction (Qiagen, UK) the PCR products were used in pEXP5-NT/TOPO® Cloning reactions (Invitrogen, UK) to obtain the plasmid pMreB-NT containing the N-terminal $His_6$ tagged fusion protein gene *MreB-RFP* with GS linker and the control plasmid pRFP-NT containing the *RFP* gene with an N-terminal $His_6$ tag.

TOPO® Cloning reaction protocol consisted in gently mixing and incubating for 5 min at room temperature 1.75 µl of PCR product, 1 µl of salt solution, 2.25 µl of DI water and 1 µl of TOPO® vector.

50 µl of One Shot® TOP10 chemically competent *E. coli* cells were used for cell transformation. Cells were thawed on ice and supplemented with 2 µl of TOPO® Cloning reaction before beeing gently mixed. Cells were then heat-shocked for 30 s at 42 °C without shaking, immediately transferred to ice, supplemented of S.O.C. medium (2% Tryptone, 0.5% Yeast extract, 10 mM NaCl, 2.5 mM KCl, 10 mM $MgCl_2$, 10 mM $MgSO_4$, 20 mM glucose) and incubated at 37 °C for 1 h with shaking. Afterwards 10-50 µl of bacterial culture was spread on prewarmed LB agar plate containing 100 µg $ml^{-1}$ ampicillin and incubated overnight at 37 °C. Surviving colonies were selected for DNA plasmid collection and ready to use.

Figure 5-5 shows the plasmid structures designed with CLC Genomics Workbench V5.1 while Table 5-1 shows primers used in DNA manipulation. Plasmids were designed with the help of Dr. Louise Horsfall (University of Glasgow).

---

[6] Details of construction of pSB1A2_BX(*MreB-RFP*) plasmid are shown in Appendix II.
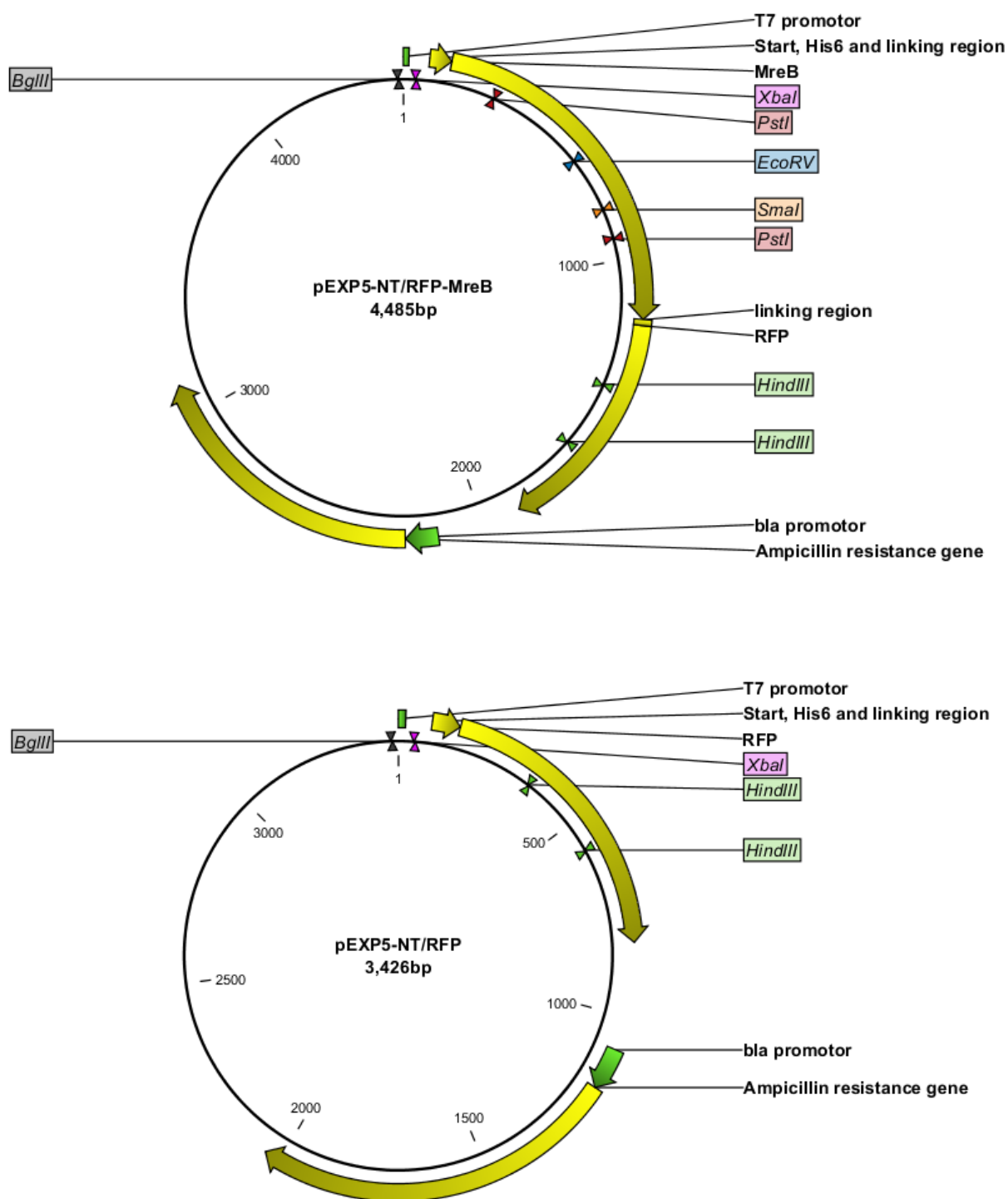
Figure 5-5 Before plasmid reconstruction, which involved the insertion of MreB-RFP and RFP genes into separate plasmids, pEXP5-NT/TOPO plasmids contain a T7 promoter for high-level expression of recombinant protein (bases 1-17), ribosome binding sites (RBS) (bases 68-73), Polyhistidine region for easy column purification or Anti-Hist Western blot analysis (bases 92-109), restriction and ligase enzyme insertion sites, Ampicillin resistance gene (Amp) (bases 498-1358), T7 transcription terminator site (bases 159-287).

Table 5-1 Primers used in DNA manipulation.

| Target | Primer | Sequence |
|--------|--------|----------|
| *E.coli* cDNA | MreB_forward | CGC<u>GGATCC</u>ATGTTGAAAAAATTTCGTGGCA |
| | MreB_reverse | AGGAAGCCATGCTACCGCTGCCGCTACCCTC TTCGCTGAACAGG |
| *BioBrick BBa_E1010* | RFP_forward | AGCGGTAGCATGGCTTCCTCCGAAGACGT |
| | RFP_reverse | CCG<u>CTCGAG</u>TTATTAAGCACCGGTGGAGTG |
| | GS linker | GGTAGCGGCAGCGGTAGC |
| *pSB1A2_BX (MreB-RFP)* | MreB_NT_for | ATGTTGAAAAAATTTCGTGGCATGTTTTCC |
| | MreB_NT_rev | TTATTAAGCACCGGTGGAGTGAC |
| | RFP_NT_for | ATGGCTTCCTCCGAAGACGTTATC |

## 5.2.4 Cell-free protein expression

MreB-RFP and RFP (control) plasmids were used for protein expression both in bulk and in droplet. Experiments in bulk were useful to establish the concentrations of the two expressed proteins.

1 µg of DNA plasmid was mixed with 20 µl *E. coli* extract, 20 µl of IVPS *E. coli* Reaction Buffer, 1 µl of T7 Enzyme mix, 1 µl of 75 mM methionine, 1.25 µl of 50 mM amino acid, RNase-free DI water, shacked for few seconds and then mixed with a feeding solution containing 25 µl of IVPS Feed buffer, 1 µl of 75 mM methionine, 1.25 µl of 50 mM amino acid, RNase-free DI water.

The solution was kept on ice until it was either loaded into a 100 µl glass syringe or incubated in a vial in a standard shaking incubator (300 rpm) at 32 °C for 2 h. When droplets were produced, they were collected into a vial, incubated at 32 °C and inspected under microscope.

Depolymerisation experiments with A22 were performed as follows. After 2 h of incubation at 32 °C the MreB-RFP expression solution was mixed with a solution containing A22 (2 mg ml$^{-1}$) in a ratio 1:1 and then incubated overnight for 12 h.

Afterwards droplets were generated and incubated for 12 h at 32 ℃ then imaged.

## 5.2.5 Imaging

Imaging was performed on an inverted microscope (AXIO Observer A1, Zeiss), 10X and 20X objectives (Zeiss), a CCD camera (Motion Scope M2, Redlake, UK) and a digital CCD camera (Coolsnap HQ$^2$, Photometrics, USA). As soon as it was produced, the double emulsion was always collected into a vial and 50 µl was deposited between two cover slips, one with an etched depression (N/A144, Academy, UK). In some cases, water soluble FITC and DiI oil soluble dyes were used to enhance the contrast between inner watery droplet and oily membrane.

Cross-section images of the emulsion were acquired using dual-channel confocal imaging performed on a laser scanning confocal system (L5M 510 Meta, Zeiss), with a Zeiss Axiovert 200 M inverted microscope, using a 40x objective lens (LD Plan, Neofluar, NA 0.6).

The FITC 495/519 water soluble dye and the BODIPY 505/515 oil soluble probe were excited using the 488 nm spectral line of an Argon laser, whilst the DiI oil soluble dye and the MreB-RFP were excited by the 543 nm spectral line of a HeNe laser. The fluorescent emission of each species was detected using separate photomultiplier tube (PMT) channels, then merged to form the final image. A Band Pass (BP) 505-530 nm filter applied to detection channel for FITC (excitation/emission maxima=495/519 nm) and BODIPY (excitation/emission maxima=505/515 nm), while a 560 nm long-pass filter was applied to DiI detection (excitation/emission maxima=549/565 nm) RFP detection (excitation/emission maxima=584/607 nm) channels.

FRAP experiments were performed on the same laser scanning confocal microscope with a 63X/1.4 NA oil-immersion objective at 32 ℃ using an air-stream stage incubator. Bleaching was performed with a rectangular spot on a cropped area of 12.5 µm x 12.5 µm using a 543 nm spectral line from a 1.2 mW HeNe laser operating at 80% laser power. Fluorescence recovery was monitored at low laser intensity (50% of its maximum power) at every 10 minutes intervals for the first 2 h of the experiment. Fluorescence images were quantified using ImageJ software.

# 5.3 Results and discussion

## 5.3.1 Double emulsion generation

The production of a double emulsion for biological experiments required first the characterization of the device by observing it working at optimized flow rates. By tuning the flow rates of the fluids, different patterns of emulsion, with relative contributions of oil and aqueous phases were achieved. To systematically observe those patterns the flow rates of two fluids were kept constant and the flow rate of the third one was varied.

Keeping the flow rates of the water and oil constant at the first junction allowed observing the effect that a variation in the second water flow rate caused. The water flow rate at the second junction was varied from 0 to 200 µl min$^{-1}$, while flow rates of the water and oil at the first junction were respectively set at 2 µl min$^{-1}$ and 1 µl min$^{-1}$. These flow rates allowed the formation of droplets both at the first and second junction and reasonable low volumes of biological solution (100 µl) were used in the double emulsion generation. Lower flow rate values at the first junction, caused a backward second water flow which prevented the formation of single emulsion.

When the droplets of water in oil were produced, they moved into the second chip by passing through the gasket connection without any disturbance (Figure 5-6) where they arrived at the second X-junction and met the outer water phase.



Figure 5-6 Micrograph of the microfluidic channels in the connection point where droplets produced at the hydrophobic chip (on the left part) migrate to the hydrophilic chip (on the right part). A PTFE gasket seals the two chips. Scale bar equal to 100 µm.

At this point, according to the flow rates of the outer water, the droplets followed different destinies. For outer water flow rates lower than 5 µl min$^{-1}$ the oil and the second water phase flowed as parallel streams and the water droplets continued to be dispersed into the oil phase. For higher flow rates, the

droplets were split and encapsulated into oil droplets forming the double emulsion. During the formation of W/O/W droplets oil droplets and very small oil droplets called "satellites" were also formed. Figure 5-7 shows the formation of W/O/W droplet for inner, middle and outer flow rates equal to 2 $\mu$l min$^{-1}$, 1 $\mu$l min$^{-1}$ and 10 $\mu$l min$^{-1}$ respectively. This flow rate combination caused the partitioning of the W/O droplets into two W/O/W droplets not perfectly identical. Ca number[7] at the second junction was equal to 1.6x10$^{-3}$.
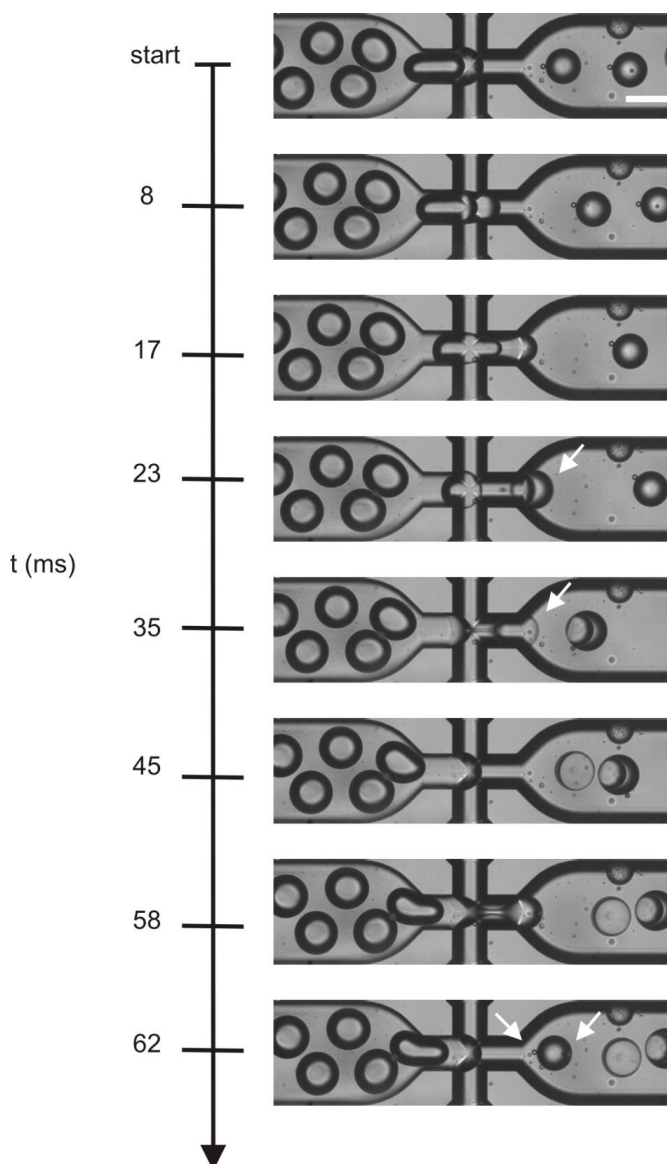


Figure 5-7 Temporal sequence of frames during the double emulsion formation. Arrows indicate the formation of W/O/W droplets (at 23 and 35 ms) and the formation of oil droplets and satellites (at the 62 ms). For the chosen flow rate combination each droplet resulted divided into 2 W/O/W droplets. Scale bare equal to 100 $\mu$m.

---

[7] Ca number was calculated knowing the velocity of the continuous phase (1.6x10$^{-3}$ m s$^{-1}$), the viscosity of the continuous phase (1.0x10$^{-3}$ g s$^{-1}$ m$^{-1}$) and the interfacial tension between the continuous and dispersed phase (10.1x10$^{-3}$ ±1 g s$^{-2}$).

By increasing the flow rate of the external water flow the number of W/O/W droplets originating from one W/O droplet increased as shown in Figure 5-8 A. How the W/O droplet partitioned into different W/O/W droplets influenced a property of the emulsion called "dispersity" which is defined as a measure of the heterogeneity of the size of the droplets. Figure 5-8 B shows the formation of W/O/W droplets, just after the second junction, for some of the flow rates taken in consideration.
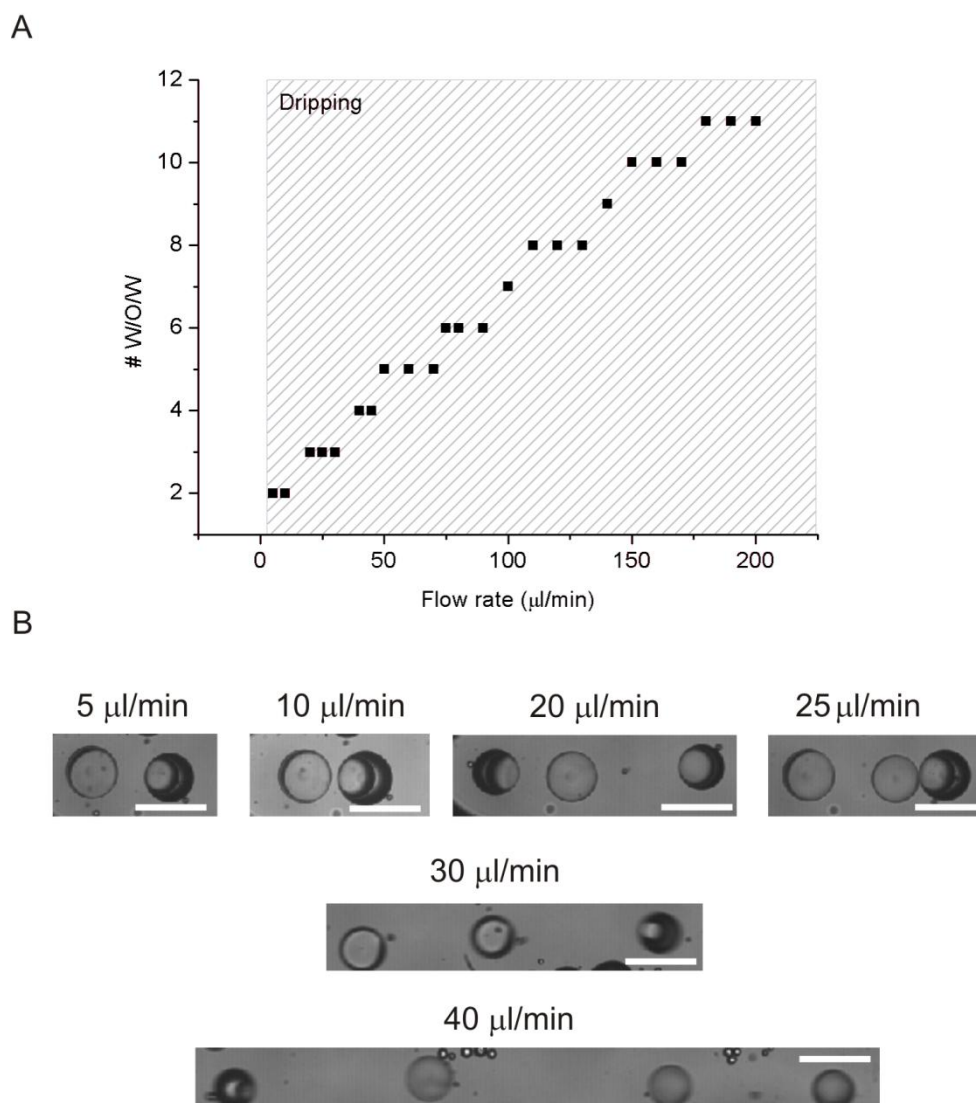


Figure 5-8 A) Effects of external flow rate variations on the W/O/W number produced for each single emulsion. The formation of W/O/W begins at 5 µl min$^{-1}$ (dripping regime). B) Partitioning of the W/O into different number of W/O/W droplets at different flow rates of the external water phase. Scale bar equal to 150 µm.

Intuitively, an increase in the flow rates determined a decrease in the W/O/W dimension (both inner and outer droplets). In some cases the partitioning created W/O/W droplets with an inner water droplet having a diameter three

times smaller than the outer diameter. In this analysis a few microliters of each emulsion produced were imaged. The diameters of the collected droplets were measured taking into consideration only the droplets which respected the following rule

$$D_{outer} / D_{inner} \leq 4/3$$

where $D_{outer}$ and $D_{inner}$ are respectively the diameter of the droplet of oil and the inner droplet of water. Figure 5-9 A shows the trend of the inner and outer diameters and their difference at the different flow rates used. In Figure 5-9 B micrographs of the emulsions obtained are presented.
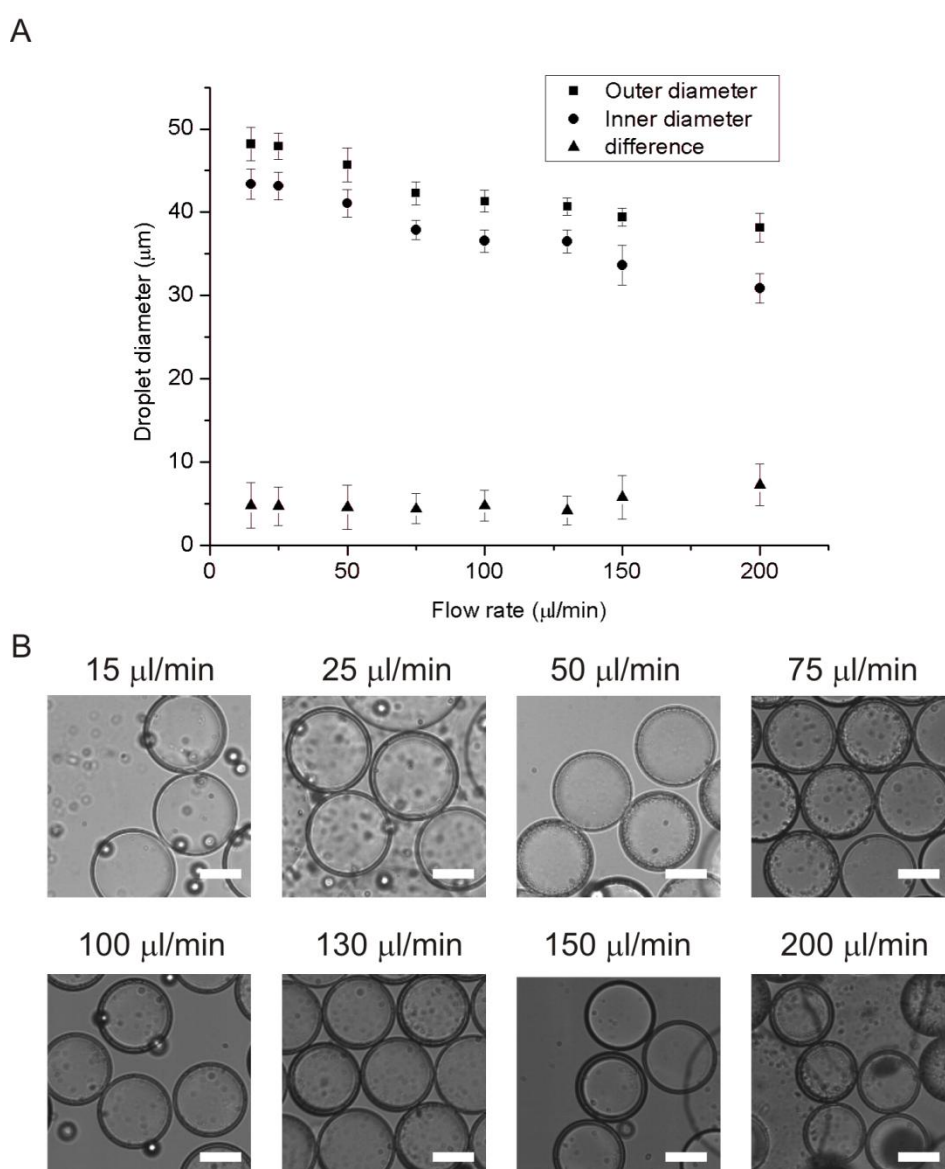


Figure 5-9 Effects of external flow rate variations on W/O/W dimensions: A) the inner diameter (circle) and outer diameter (square), with the difference shown as a triangle. Inner and middle phase flow rate were kept constant at 2 µl min$^{-1}$ and 1 µl min$^{-1}$ respectively. B) Micrograph pictures of W/O/W double emulsions, the scale bar is equal to 25 µm.

The combination of flow rates chosen for the cell-free expression experiments was 2 µl min$^{-1}$, 1 µl min$^{-1}$ and 100 µl min$^{-1}$ (inner, middle and external phase). This combination produced a reasonable[8] monodisperse emulsion with the smallest amount of oil droplets (4% over 300 droplets). Figure 5-10 shows a confocal microscopy of the emulsion where different dyes were dispersed in the oil and inner water phase in order to obtain a better contrast between the watery inner droplet and the oil phase. Figure 5-11 shows the distribution of inner and outer diameter of W/O/W emulsions generated at flow rates equal to 2 µl min$^{-1}$, 1 µl min$^{-1}$ and 100 µl min$^{-1}$ (inner, middle and external phase).
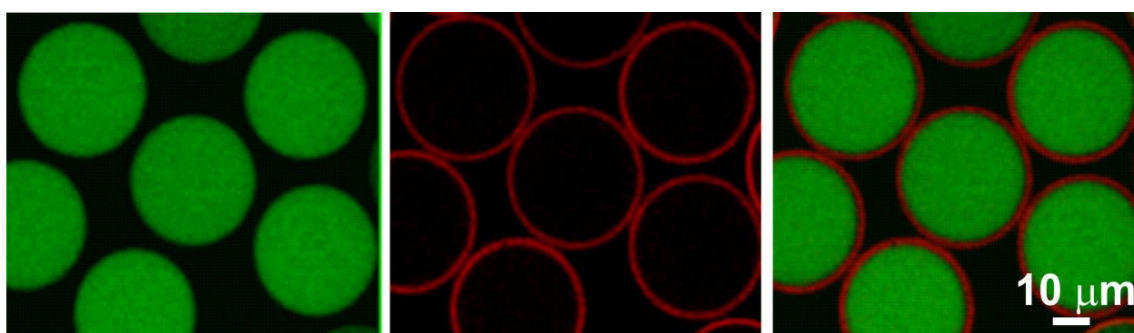


Figure 5-10 Dual-channel confocal microscopy of W/O/W double emulsions made in an aqueous solution: The inner aqueous (green) and interfacial hydrophobic phases (red) consisted of 100 nM FITC (fluorescein isothiocyanate) in deionised water and mineral oil (Sigma) with 2% (w/w) Span 80 and 2 nM DiI (dialkyl-carbocyanine iodide), respectively. The relative balance of flow rates used to deliver respectively inner, middle and outer phases were 2 µl min$^{-1}$, 1 µl min$^{-1}$ and 100 µl min$^{-1}$; the hydrophobic membrane was visualised by incorporation of the hydrophobic dye, DiI. The variation in the size of the aqueous phase was 3.6% (mean diameter 37.4 µm), and of the overall microdroplet was 3.1% (mean 41 µm), giving a mean membrane thickness of ca. 4 µm.

The effect of different temperatures on the double emulsion stability was also evaluated. W/O/W emulsions generated at flow rates equal to 2 µl min$^{-1}$, 1 µl min$^{-1}$ and 100 µl min$^{-1}$ (inner, middle and external phase) were stored at 37 °C, 30 °C, 20 °C, and 3 °C and observed after 24 h. Bright field microscopy images taken soon after droplet generation and after 24 h incubation were analysed in order to observe the percentage of shrinkage of the inner droplet. Droplets incubated at 37 °C showed shrinkage of their inner droplets equal to 22% with respect to their initial size. Emulsions stored at 30 °C and 20 °C did not show any coalescence, but an overall shrinkage of <10% was observed with

---

[8] Coefficients of variation of the inner and outer droplets were respectively 3.6% and 3.1%, in agreement with what found in literature (23).

respect to their original size, after 24 h. Emulsions stored at 3 °C remained stable for five months and no coalescence or shrinkage was observed. Data not showed.
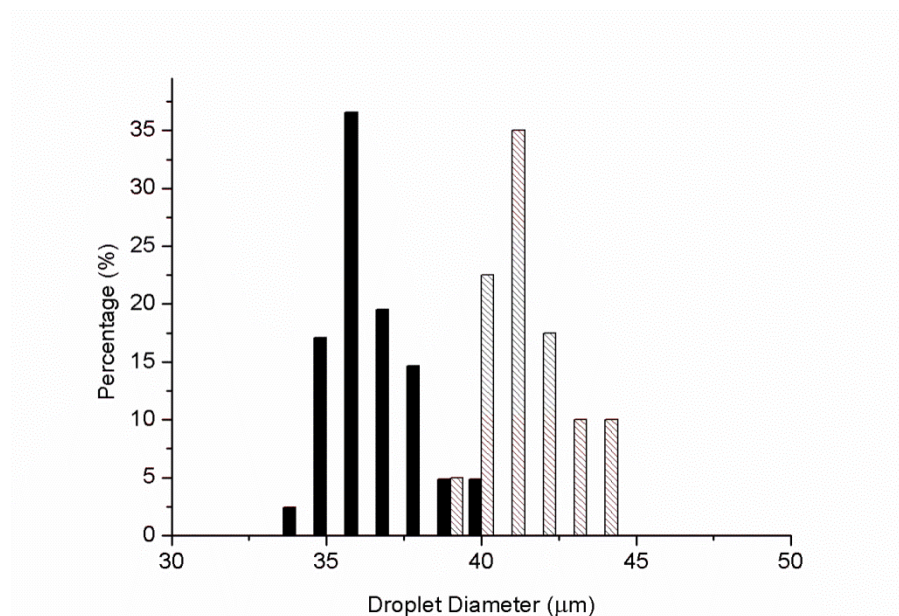


Figure 5-11 The distribution of the inner (black) and outer (grey) diameter of the emulsion produced using flow rates equal to 2 µl min$^{-1}$, 1 µl min$^{-1}$ and 100 µl min$^{-1}$ for respectively inner, middle and external phase. The mean diameter of the inner compartment was 37.4 µm with a c.v. of 3.6% whilst that of the outer membrane (whole drop) was 41.0 µm with a c.v. of 3.1%, indicative of a membrane region with an average thickness of 3.6 µm. Bin size equal to 1 µm.

## 5.3.2 Protein expression

Both the fusion protein (MreB-RFP) and water soluble protein RFP used as a control, were expressed in droplets. Droplets were produced as previously described, incubated at 32 °C and monitored under a fluorescence microscope over time. Their expression level was monitored using time lapse fluorescence microscopy (Axiovert 200 microscope, Carl Zeiss). Images were captured every 10 min in the first hour and every 30 min for 11 h afterwards. Increases in RFP fluorescence indicated successful expression of both RFP and fusion protein MreB-RFP by cell-free expression. The mean fluorescent intensities were quantified using ImageJ and expressed as a function of time.

Both expressions of MreB-RFP and RFP (used as control) in droplets showed a trend that increased over time (Figure 5-12). Fluorescence values were expressed in arbitrary units and time zero in the graph corresponded to ~1 h

after generation, when the droplets were still. The expression rate of RFP was higher than MreB-RFP probably as a consequence of the smaller size of its coding sequences. The coding sequence of MreB-RFP is longer than RFP (1716 base pairs of DNA compared to 675 base pairs). As a consequence, at the transcriptional level, production of MreB-RFP mRNA is slower than production of RFP mRNA. The mRNA levels correspond to protein expression. Differences in protein concentrations are 20%–40% of those attributed to mRNA levels (115, 116). In addition to mRNA levels, ribosome density (the number of ribosomes on active mRNAs divided by transcript length) may also play a role in the production of proteins. The longer the transcripts are, the slower the translation process is. Moreover, the long transcripts require a number of bound ribosomes to produce new proteins, which also effects the synthesis rate (117).

In addition to the size of the encoding sequence, conformation change of RFP might have an impact on the fluorescence intensity of the MreB-RFP fusion protein. The fusion protein might cause structural hindrance or misfolding to RFP that effect RFP intensity.
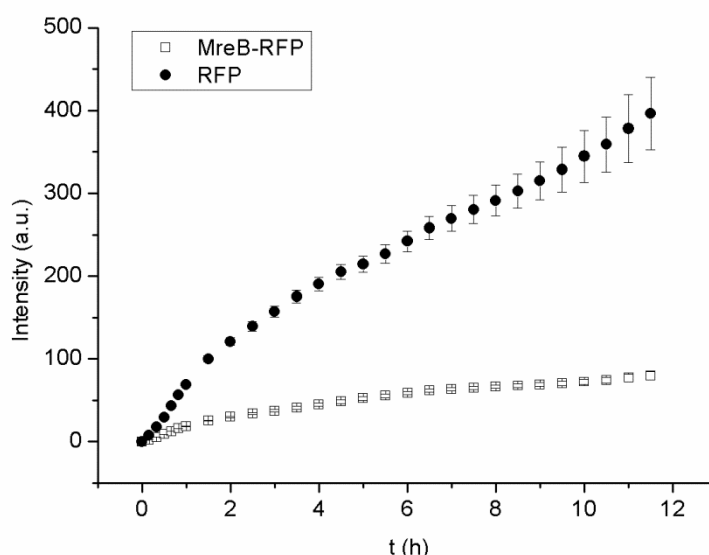


Figure 5-12 Cell-free MreB-RFP and RFP expression. Trend of fluorescent signal acquired during the protein expression of MreB-RFP and RFP alone. In both cases the curves show an increase with time. The fluorescence intensities of MReB-RFP and RFP at each time point are the result of 10 measurements. In both experiments exposure times had the same value of 300 ms. Time zero represents ~1 h after generation.

### 5.3.3 MreB-RFP aggregation at the interface

Fluorescence pictures taken by confocal microscopy showed that after 1 h of incubation, the RFP, as a water-soluble protein, remained dispersed homogeneously within the entire water droplet (Figure 5-13 A) whilst MreB had begun to localise at the water/oil interface (Figure 5-13 B).
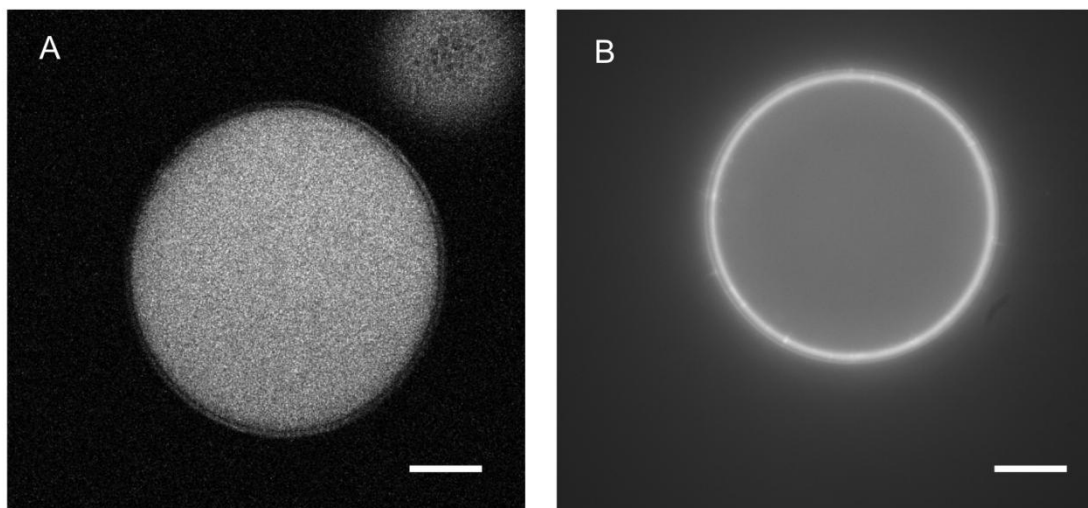


Figure 5-13 Cell-free protein expression in W/O/W double emulsions. Fluorescence micrograph of a W/O/W during the expression of (a) RFP as a soluble protein in the artificial cell cytosol, and (b) MreB-RFP, which has portioned at the hydrophobic interface. Scale bar equal to 10 µm.

After 14 hours of incubation droplets containing MreB-RFP showed the partitioning of the protein at the membrane and the formation of MreB-RFP aggregates at the water/oil interface while the RFP protein remained homogeneously dispersed in solution.

Figure 5-14 A shows a micrograph of a double emulsion droplet and Figure 5-14 B shows a confocal picture of a portion of the membrane. Precipitates of MreB-RFP were also visible at the bottom of the droplet. Figure 5-15 shows three confocal slices at the top, the middle and bottom part of the droplet.
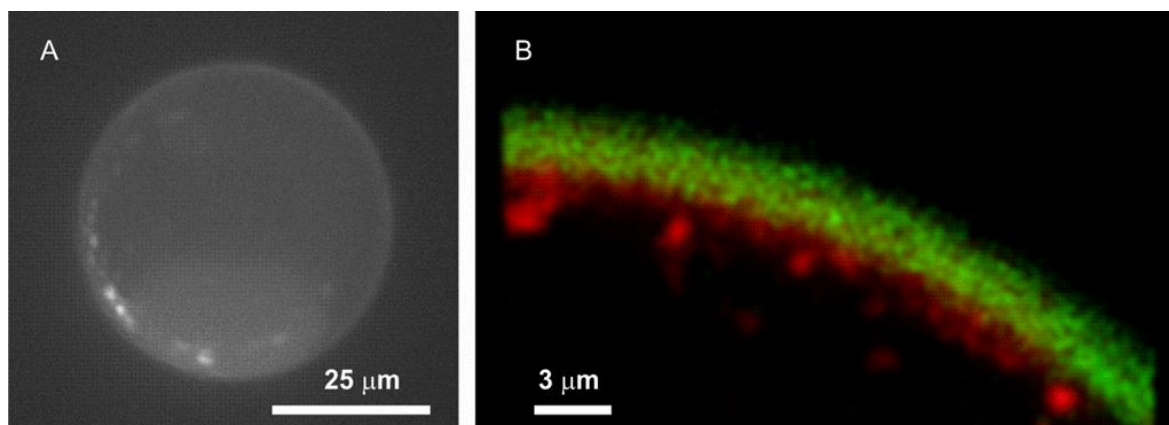
Figure 5-14 Expression of MreB-RFP within double emulsion. A) micrograph of double emulsion droplet 14 h after generation; B) Confocal micrograph (3 μm thick plane) of a portion of droplet membrane. The RFP-tagged MreB forming aggregates localized to the oil-water interface. The image was created by forming the W/O/W droplets with 100 nM BODIPY dispersed in the oil phase and MreB-RFP in the segmented phase. Fluorescence was detected in separate channels.
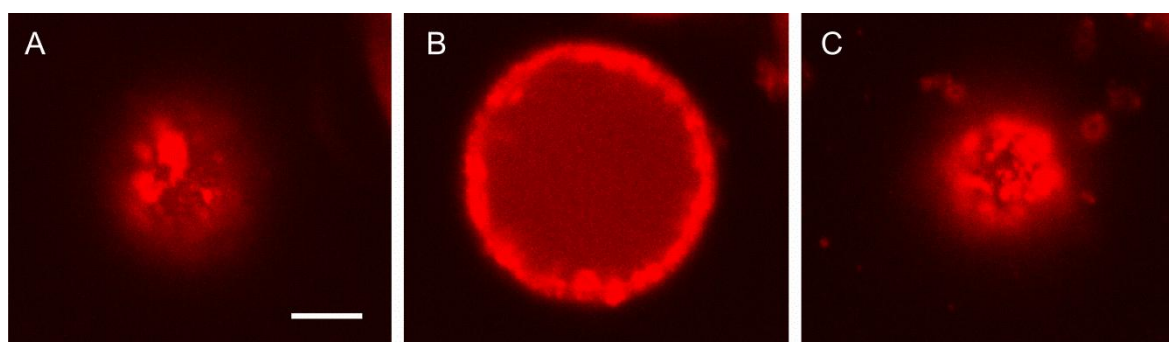


Figure 5-15 Confocal scanning images of top (A), middle (B) and bottom (C) part of the droplet 24 h after droplet generation and incubation. Fluorescence spots denote the formation of protein patches that seem to show preference towards the hydrophobic part of the droplet. Scale bar equal to 10 μm.

MreB-RFP partitioning is due to the amphipathic region present in the MreB, as it was demonstrated that a stable mutant of *E. coli* MreB that lacked the N-terminal amphipathic helix does not bind strongly to the membrane while the wild-type *E. coli* MreB does (53). One implication is that once the MreB-RFP adsorbs at the water/oil interface, it might be difficult to dissociate from the interface. Moreover it is likely that the formation of aggregates occurred due to the polymerisation of the MreB monomers. The MreB concentration in bulk was estimated as approximately 27 μM, which was above the protein polymerisation threshold and of the same order of magnitude as the concentration present in average bacteria (~20 μM). By comparison the RFP concentration was also measured after cell-free expression and it was observed that using the same

amount of plasmid, under the same experimental conditions, the amount of protein produced was two times higher (~43 µM).

In order to assess whether the formation of patches was due to polymerisation of MreB-RFP, a polymerisation perturbing compound, known as A22, was adopted in this study. After 12 h from droplet generation and 24 h of incubation at 32 °C with A22 solution, the MreB-RFP once again showed a tendency to adhere to the hydrophobic membrane (Figure 5-16 A) but did not show any patch formation (Figure 5-16 B).
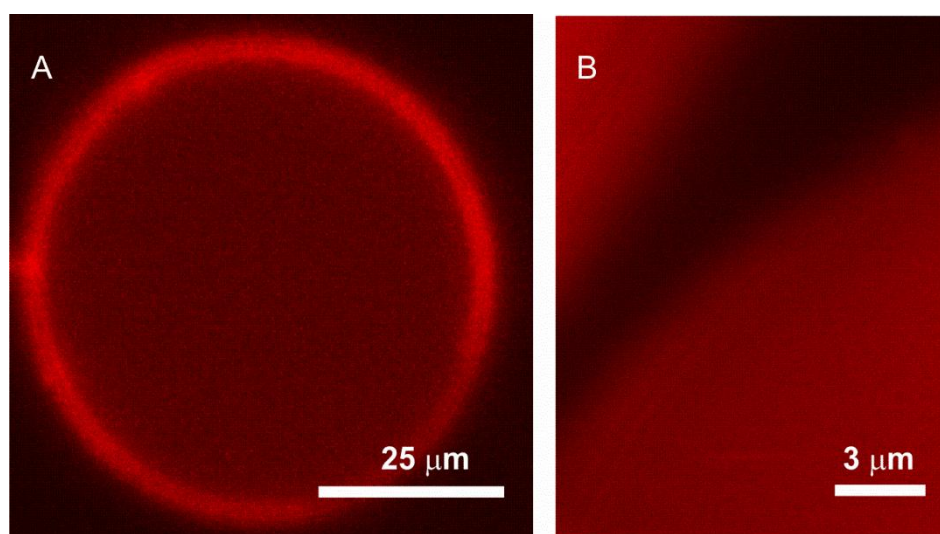


Figure 5-16 Confocal fluorescence microscopy of a droplet containing MreB-RFP protein solution incubated with A22 (2 mg/ml) in a ratio 1:1 for 12 h at 32 °C. A) The MreB-RFP molecules deposit to the hydrophobic membrane. B) Detail of droplets at the membrane does not show any aggregation due to polymerisation.

In order to further investigate the behaviour of MreB-RFP at the water-oil interface, MreB adhesion to the membrane was further investigated by FRAP (fluorescence recovery after photobleaching) analysis. Droplets containing cell-free MreB-RFP expression system were generated, as previously discussed, and incubated at 32 °C for 24 h. After incubation, a portion of the droplet membrane was photobleached by 1.2 mW HeNe focused laser beam (543 nm wave length) at 80% of full power for 1.5 min and later on periodically imaged using 50% of the maximum power. Intensity of membrane over time was measured using ImageJ. Two membrane area intensities were measured, respectively the bleached area ($I_b$) and the non bleached one ($I_m$) (Figure 5-17). It was observed that just after 1 h from the photobleaching event 4.4% of the non bleached membrane

fluorescence had recovered. This value increased to 7.5% after 2 h and 11.4% after 6.8 h. Quantification of FRAP analysis is graphically represented in Figure 5-18 where the plotted intensity is the ratio between the intensities of bleached membrane (Ib) and non bleached one (Im). This experiment used three measurements whose mean value was plotted. Fluorescence recovery did not reach more than 12% of the initial level suggesting that the space within the membrane for new MreB-RFP molecules was filled. This behaviour demonstrates once again the propensity of this protein to stay in contact with the hydrophobic phase, as an analogue of a membrane.
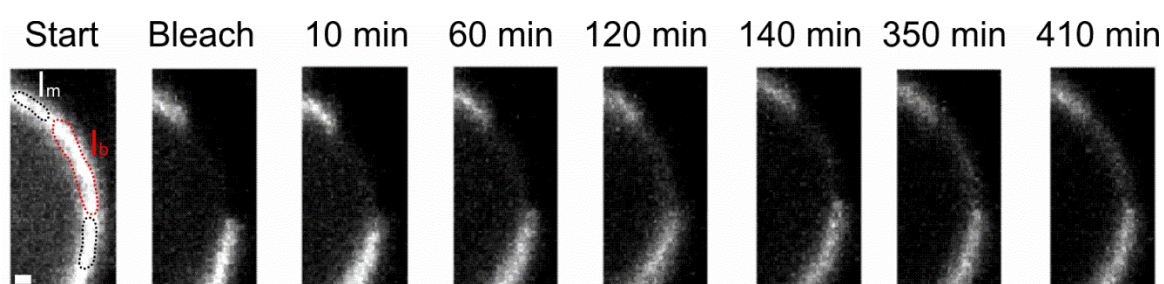


Figure 5-17 FRAP experiment on a portion of hydrophobic membrane of a double emulsion droplet 40 μm diameter. Start point corresponds to 24 h after droplet generation. During the experiments two areas within the membrane were monitored $I_m$ (black dotted area) and $I_b$ (red dotted area). During the experiment the droplet was incubated at 32 °C. Scale bar equal to 2 μm.
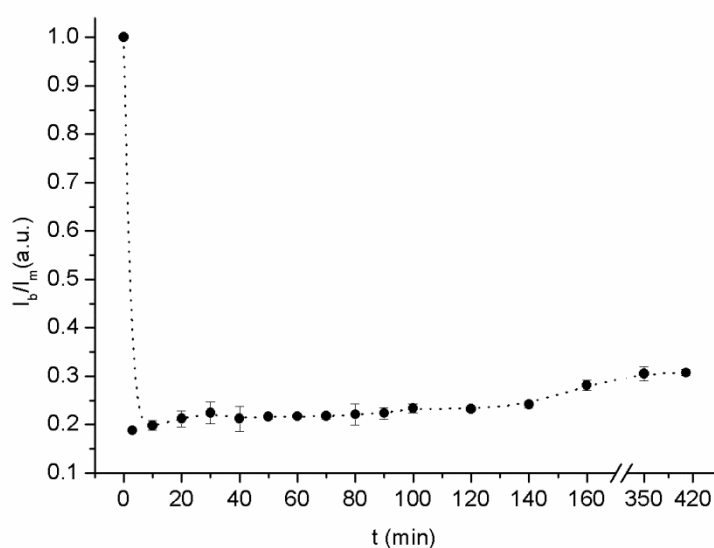


Figure 5-18 Quantification of FRAP analysis obtained over three measurements. Droplets have mean diameter equal to 40 μm.

## 5.4 Conclusions and future development

This chapter presented the formation of a monodisperse double emulsion that acts as a cell model which mimicked their capacity of protein production and the presence of a membrane that separates the inner from the outer environment.

This study demonstrated the cell free expression of a protein construct with a fluorescent marker, whose native form is known to show a preference for aggregation within artificial hydrophobic membranes. It was demonstrated that also in synthetic systems like a double emulsion, the membrane related protein MreB shows an intrinsic membrane affinity. The protein not only aggregated at the water-oil interface, but also polymerised in a manner and at concentrations which are consistent with in vivo studies.

Moreover FRAP experiment showed that the MreB not only adhere to the hydrophobic surface but also insert within the membrane. Further investigation could assess the coefficient of diffusion for this protein within the membrane and compare the values obtained with experiments in vivo. It was estimated that the MreB linked to a yellow fluorescent protein (YFP, 27 kDa) (118) has a coefficient of diffusion equal to 1.11 $\mu m^2$ $s^{-1}$ or 0.95 $\mu m^2$ $s^{-1}$ according to its globular or filamentous status (118).

Finally, these studies demonstrated the compatibility of double emulsion systems with cell-free expression of soluble and structural membrane-related proteins, which opens up avenues for future investigations of the MreB with vesicles of nanometer thick membranes such as polymersomes.

# 6 Polymersomes as chassis for protein expression and triggered release

Chapter 6 describes the approach adopted to form monodisperse polymeric shells, also known in literature as polymersomes, used as scaffolds for cell-free protein expression and, more interestingly, for controlled protein release. The nanometre shell thicknesses, the chemical compositions of used polymers, which add to the membrane biocompatibility and biodegradability properties, and the uniformity of shells produced using microfluidic methods allow interesting applications in the biomedical and synthetic biology fields. Part of the material presented here has been published in Angewandte Chemie International Edition journal (2012), Volume 124, Issue 26, pages 6522–6526.

## 6.1 Introduction and proposed approach

In the previous Chapter the idea to use droplet-based microfluidic systems for the production of monodisperse double emulsions used as artificial cell models for protein investigation was demonstrated. It was shown how double emulsion droplets can work as synthetic compartments which mimic one or more properties of natural cells and provide useful platforms for the study of protein properties for fundamental cell function (119).

In this chapter, the mechanism of how droplet-based microfluidic methods enable the fabrication of monodisperse polymersomes is presented, showing how it is possible to encapsulate active materials in polymeric vesicles. Stable cell-like polymersome structures made of biocompatible and biodegradable membranes were demonstrated. Similarly to the previous work, these systems can encapsulate the complete biological machinery required for protein

expression but, in contrast to the double emulsions due to the semi-permeability of the membrane, triggered release of the protein from the polymersomes through an osmotic shock can also be achieved. In this Chapter the cell-free expression of MreB is demonstrated.

To achieve the high efficiency of encapsulation of the biological machinery necessary for protein expression within the polymersomes, a capillary microfluidic device (63) to produce W/O/W double-emulsion droplets was established. The microfluidic device consisted of two tapered cylindrical capillaries inserted within a square capillary as shown in Figure 1 A. The first cylindrical capillary was modified to be hydrophobic and used for injection of the aqueous inner-most phase while the second cylindrical capillary was hydrophilic and used for collection of the double-emulsion droplets.

The double-emulsion droplets were prepared by one-step emulsification process and collected in an aqueous solution, resulting in polymersomes. To achieve this, first there was an evaporation of the solvent phase, where the polymer was dispersed, and then a subsequent separation of oil phase (dewetting of the hexane) due to a partial wetting between the watery core and the hexane shell, as described in (63). Finally the polymersomes were incubated at room temperature to evaporate the organic solvent on the top of the collection liquid and afterwards at 32 °C for protein expression. This produced polymersomes consisting of a bilayer membrane of PEG-b-PLA diblock copolymers Figure 6-1 B.

The membranes of the polymersomes were semi-permeable, facilitating a technique by which it was possible to trigger the release of the expressed proteins into the continuous phase using osmotic shock (63, 64, 120). An osmotic pressure difference between the inner core and continuous phase caused a flux of water through the membrane until the osmotic pressure difference became insignificant; this changed the size of the polymersome, causing a swelling. Negative osmotic shock was used to form a pore in the membrane as shown in Figure 6-2; continuous inward water flux, driven by the large difference in osmolarity, causes a radial strain above the critical value, inducing the formation of a pore at the weakest point on the membrane.
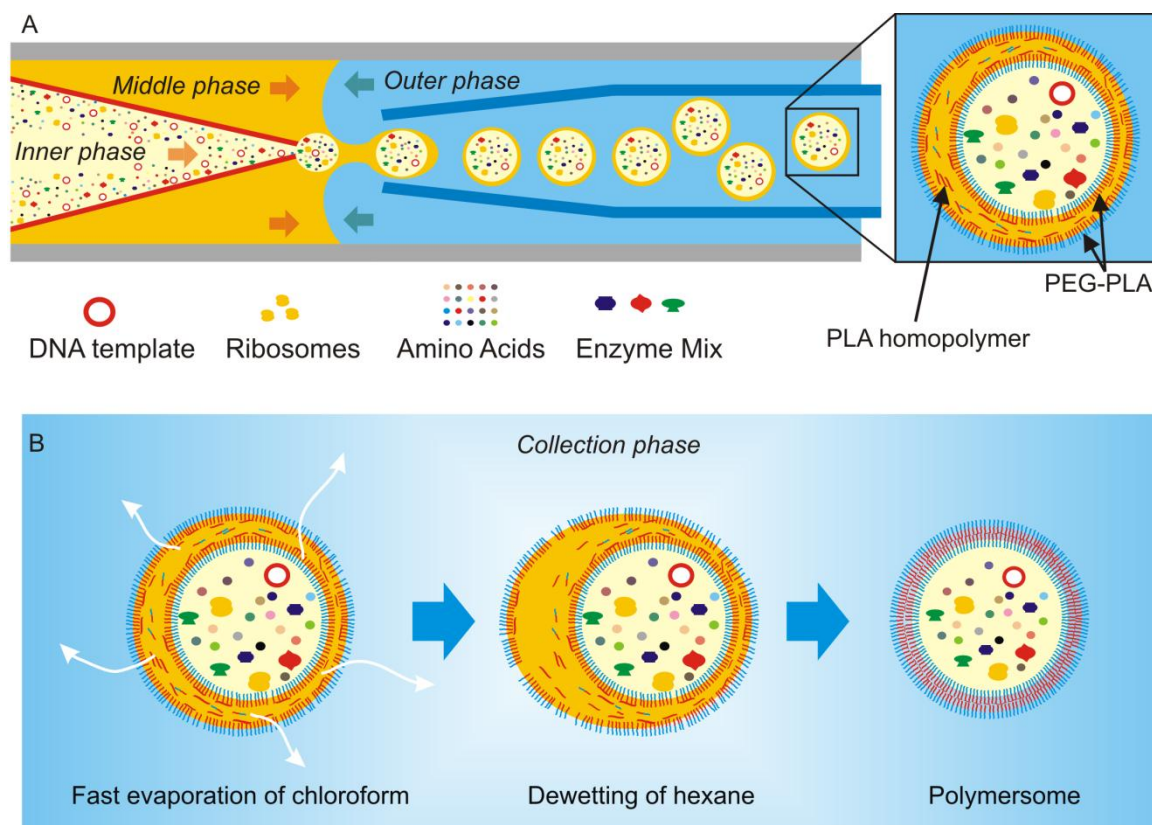
Figure 6-1 Polymersomes production. A) Schematic illustration of the microfluidic device used for polymersomes generation and the double-emulsion droplet just after generation. B) After generation the droplet showed fast evaporation of the chloroform present in the mixture, dewetting of amphiphile-laden oil phase on the surface of the innermost drops and separation of the oil, producing polymersomes with a PEG-PLA membrane. Polymersomes encapsulate all the ingredients required for protein synthesis (DNA, amino acids, Enzymes, ribosomes).
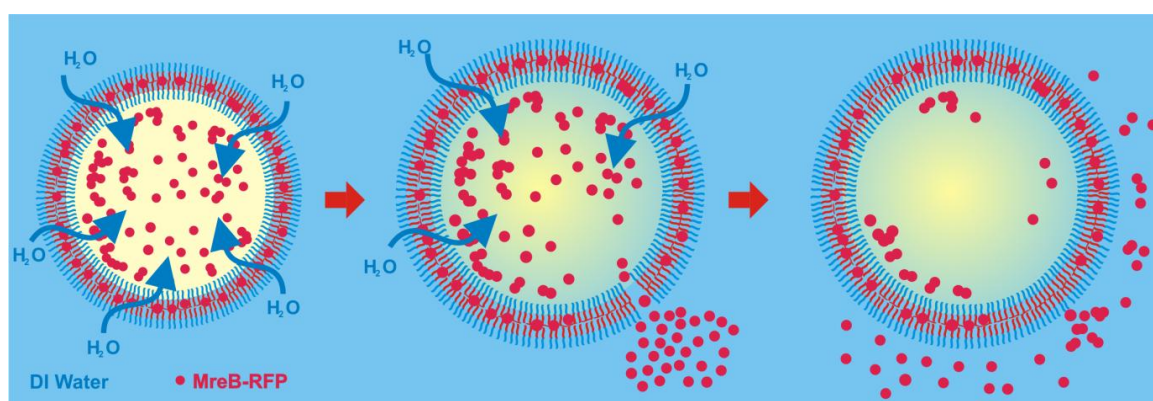


Figure 6-2 Protein release under osmotic shock. Schematic illustration of MreB-RFP release from polymersomes and subsequent self-sealing of their membrane in DI water. Due to the high osmolarity in the interior of the polymersomes, there is inward water flux through the membrane, swelling the polymersomes and triggering formation of holes in the membrane. Therefore, proteins expressed in polymersomes are released through the pores.

# 6.2 Materials and methods

## 6.2.1 Materials

Polymersomes were prepared using a capillary microfluidic device made of two cylindrical glass capillaries of 1 mm in outer diameter (World precision instruments, Inc., 1B100-6, USA) tapered and assembled within a square capillary of 1.05 mm inner dimension (AIT glass, USA).

Cylindrical injection capillary was treated with n-octadecyltrimethoxyl silane (Aldrich, USA) while the cylindrical collection capillary was treated with 2-[methoxy(polyethyleneoxy)-propyl] trimethoxyl silane (Gelest, Inc., USA).

The innermost aqueous solution contained a cell-free expression solution (Expressway, Invitrogen, USA) and the MreB-RFP plasmid. The middle oil phase was a mixture of chloroform (25693, Sigma, USA) and hexane (15671, Sigma, USA) with a volume ratio of 32:68 with 5 mg ml$^{-1}$ of PEG-(MW 5000)-b-PLA (MW 10000) (Polysciences, Inc., USA) and 2.5 mg ml$^{-1}$ of PLA (MW 15000, Polysciences, Inc., USA). The continuous phase was an aqueous solution of 10 wt% PVA (MW 13 000-23 000, Sigma-Aldrich, USA) and 0.1 M NaCl with 300 mOsm l$^{-1}$ (value similar to plasma osmolarity) while the collection phase is an aqueous solution of 0.15 M NaCl. A water-soluble green dye (FITC) was used as a model active material for the osmotic shock experiments. Osmolarities were measured using an osmometer (3300 Micro-Osmometer, Advanced Instruments, Inc., UK). Fluids were loaded into glass syringes (Hamilton, CH) controlled by syringe pumps (Harvard Apparatus, USA). The generation of double-emulsion drops was observed using a high-speed camera (Phantom V9, Vision Research, USA). The expression of MreB-RFP and the triggered release of the protein were evaluated by a confocal microscope (Leica, TCS SP5, UK). Images were analysed using ImageJ software.

## 6.2.2 Preparation of solutions

The innermost aqueous solution for the cell-free protein expression was prepared by mixing 1 µg of the plasmid for MreB-RFP with the components present in the cell-free expression kit, according to manufacturer's protocol, as

described in Section 5.2.4. The solution was kept on ice until it was loaded into the syringe. PEG(5000)-b-PLA(10000) was dissolved in a mixture of chloroform and hexane with a volume ratio of 38:62 at a concentration of 5 mg ml$^{-1}$ for the middle phase of double-emulsion droplets. The solution was agitated for 30 min before adding PLA homopolymer (MW 15000) to the mixture at a concentration of 2.5 mg ml$^{-1}$. The additon of PLA enhanced the stability of the bilayer in some experiments. A 10 wt% aqueous solution of PVA was used as the continuous or outer phase of double-emulsions.

### 6.2.3 Chip fabrication

Chip fabrication was performed by Dr. Shin-Hyun Kim (Harvard University, USA). Two cylindrical glass capillaries of 1.00 mm in outer diameter and 0.58 mm in inner diameter were tapered by axially heating and pulling the capillary using a pipette puller (Sutter Instrument Co, Model P-97, USA) to have small aperture (~20 μm). The glass capillary broke in two identical tapered glasses and their tips were smoothed using sandpaper in order to obtain the desired diameter (>20 μm).

The capillaries were assembled within a square capillary of 1.05 mm and the distance between the inner and collection capillary was controlled by hand under optical microscope. Prior to assembly, the cylindrical injection capillary was dipped in with n-octadecyltrimethoxyl silane (Aldrich, USA) for 30 sec to make it hydrophobic, while the cylindrical collection capillary was treated with 2-[methoxy(polyethyleneoxy)-propyl] trimethoxyl silane (Gelest, Inc., USA) to make it hydrophilic.

After dipping the capillaries were incubated for 10 min. The remaining fluids were then removed by blowing the capillaries with compressed air prior to assembly. The square capillary was bonded to the surface of a glass slide. Two 20G luer-stubs (Intramedic Luer Stub Adapters, Beckton Dickinson, Sparks, MD, USA) served as input connectors for the middle and outer fluids while the cylindrical capillary was directly connected to a tubing. Figure 6-3 shows the microcapillary device prior to an experiment.
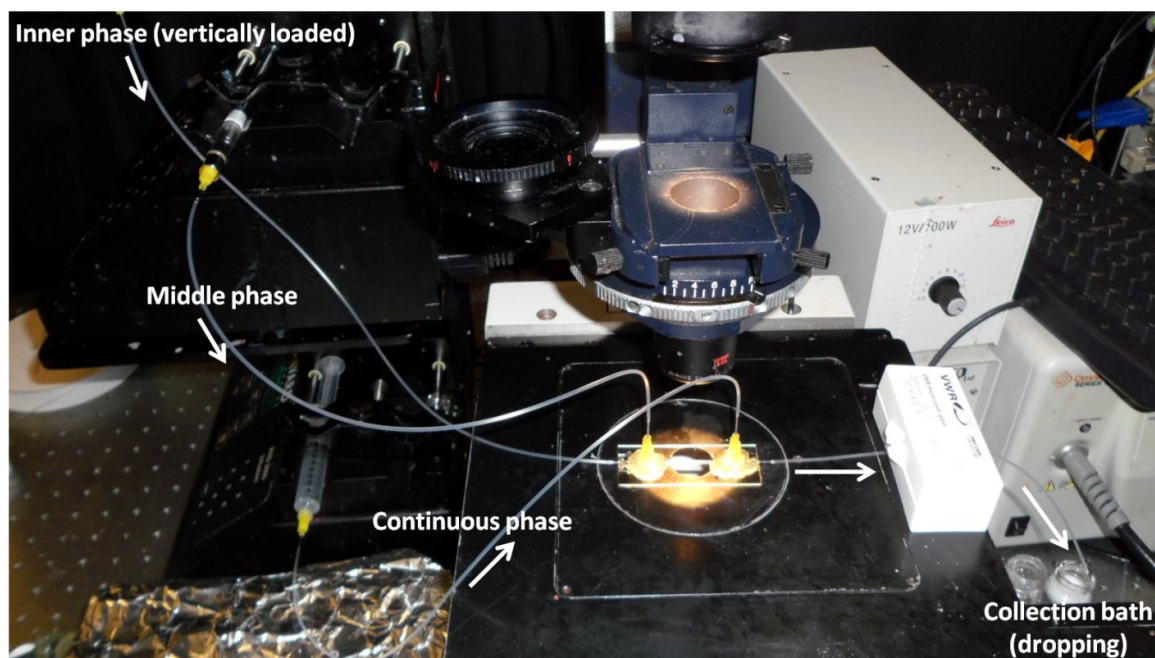
Figure 6-3 Capillary device placed on the stage of an inverted microscope and connected with tubing to the syringes containing the inner, middle and continuous phase. Once produced, double emulsions were collected into a vial called collection bath.

## 6.2.4 Polymersomes preparation

Polymersomes were prepared from double-emulsion droplets using a glass capillary device. The hydrophobic capillary was used to inject an aqueous mixture of the *E. coli* ribosomal extract, required for protein expression, with the MreB DNA plasmid; this formed the innermost drop of the polymersome. As a middle phase, a mixture of chloroform and hexane was used with poly(ethylene glycol) (PEG, MW 5 000)-b-poly(lactic acid) (PLA, MW 10 000) diblock copolymers and PLA homopolymer (MW 15 000). The PEG-b-PLA diblock copolymer served as the amphiphile, while the PLA homopolymer was added to enhance the stability of the resultant polymersomes (64). This mixture was injected through the interstices between the outer square capillary and the inner injection capillary. The outer phase, also called continuous, was an aqueous solution of 10 wt% poly(vinyl alcohol) (PVA, MW 13 000-23 000) and 0.1 M NaCl injected through the interstices between the outer square and inner collection capillary, forming a counter-flow to the innermost and middle phases, as shown in Figure 6-1 A.

The innermost, middle and continuous phases were injected into the device at flow rates of 700, 800 and 3000 µl h$^{-1}$ respectively. Polymersomes were collected

in a vial containing aqueous solution of 0.15 M NaCl and left open to evaporate the organic solvent on the top of the collection liquid. The suspension was left at room temperature for 1 h and then incubated for few hours at 32 °C.

# 6.3 Results and discussion

## 6.3.1 Polymersomes formation

Highly monodisperse double-emulsion drops were produced in a dripping mode by one-step emulsification (64) as shown as shown in Figure 6-4.
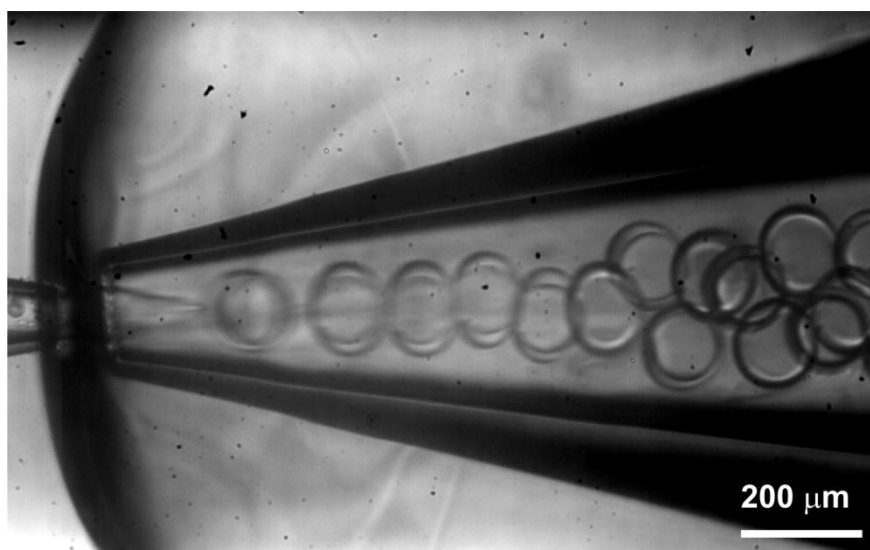


Figure 6-4 Optical micrograph showing the generation of W/O/W double-emulsion droplets; the flow rates used for the delivery of biological solution, oil and continuous phase were set respectively at 700, 800, and 3000 µl h$^{-1}$.

These double-emulsion droplets exhibited dewetting of the middle oil phase on the surface of the innermost droplets as the chloroform partitioned out of the droplet; thus, concentration of hexane, which is a poor solvent of PEG-b-PLA diblock-copolymers, increased, resulting in expulsion of the oil layer from two monolayers of diblock-copolymers at W/O and O/W interfaces. This dewetting induced a formation of unilamellar structures by overlapping the two monolayers (63) (64) (121). In addition, the dewetted middle oil phase was separated from the innermost drop, producing polymersomes consisting of a bilayer membrane of PEG-b-PLA diblock copolymers, with an excess of PLA homopolymer in the inner, hydrophobic region of the bilayer. The dewetting and separation of oil

droplets occured in ~5 minutes after droplet formation and because of this, the residual organic solvent in the membrane of polymersomes became small (below detection limits). The rate of injection of the innermost, middle and continuous phases into the device was found to be at flow rates of 700, 800 and 3000 µl h-1 respectively. The resultant monodisperse polymersomes encapsulating the aqueous solution for protein expression are shown in Figure 6-5 A a few minutes after generation, representing polymersomes on the bottom of the collecting vial. Polymersomes are not on the same plane and this deforms the Gaussian shape distribution in the diameter analysis (Figure 6-5 B).
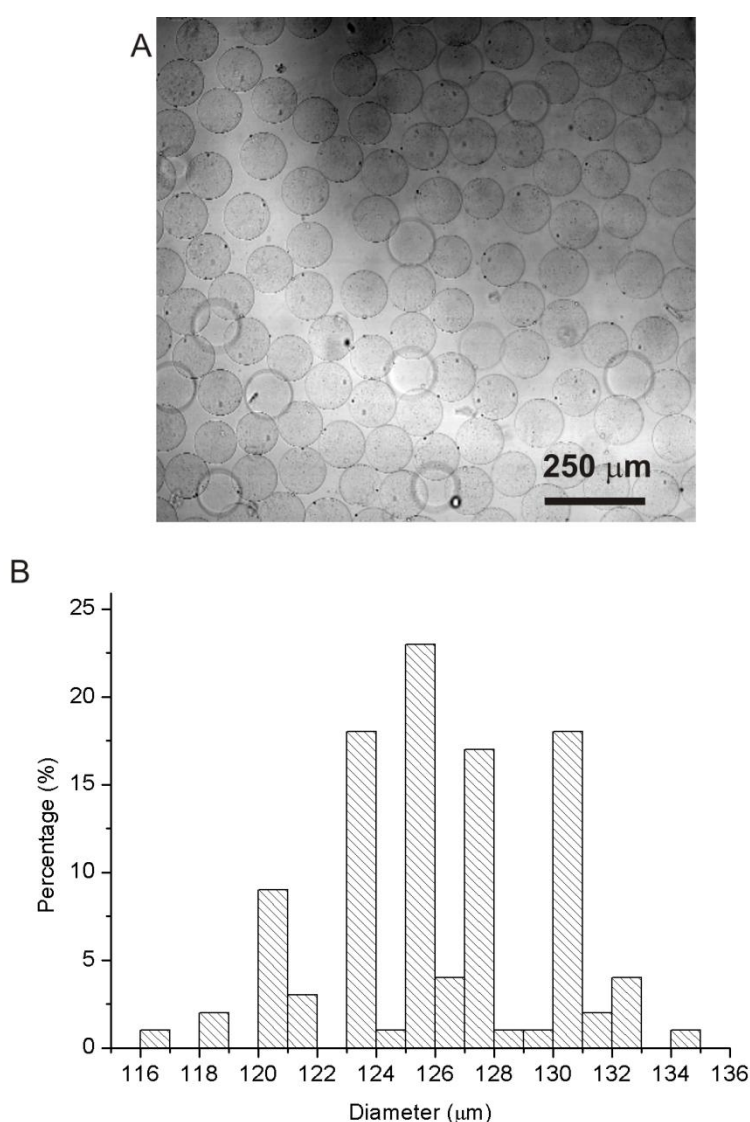


Figure 6-5 Polymersomes collected into a vial. A) Optical micrograph of monodisperse polymersomes produced using flow rates equal to  700 µl h$^{-1}$, 800 µl h$^{-1}$ and 3000 µl h$^{-1}$ for respectively inner, middle and external phase. B) Distribution of polymersome diameters. The mean diameter is 126 µm with a C.V. of 2.7 %. Histogram bin size equal to 1 µm.

According to the experimental rule that establishes a relation between polymersome membrane thickness *d* and copolymer molecular weight *MW* (50) as follows

$$d \sim MW^b \tag{6-1}$$

with $b \cong 0.55$, it was estimated that the generated polymersomes had a membrane thickness between 290-198 nm. This means almost two orders of magnitude bigger than a natural living cell membrane and one order of magnitude bigger than a prokaryotic cell membrane.

## 6.3.2 Protein expression within reinforced polymersomes

After generation the suspension of polymersomes was left at room temperature for 1 h in order to allow the complete sedimentation of polymersomes and the hexane dewetting and then it was incubated for a few hours at 32 °C. To observe and evaluate the protein expression in the polymersomes, fluorescence measurements were taken on several polymerosomes over the incubation time. All polymersomes imaged showed almost the same level of fluorescent signal at the same incubation time. Images were taken every 15 minutes for the first two hours of incubation. The resultant expressed MreB-RFP exhibited fluorescence, reaching a maximum after 2 h of incubation as shown in Figure 6-6.
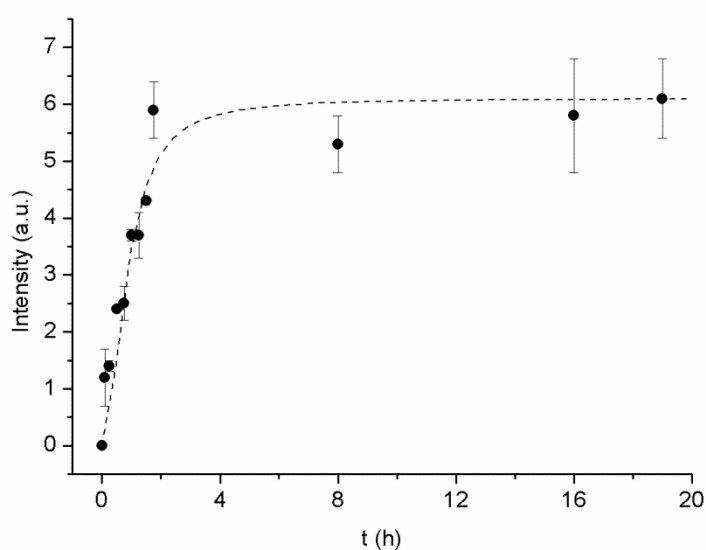


Figure 6-6 Fluorescence signal over time due to protein expression in polymersomes. After an initial linear increase, production of protein reaches a plateau at about 2 h of incubation at 32 °C.

In the first hour, the fluorescence signal increased linearly and reached a plateau after 2 h. This data was consistent with other kinetic studies performed on cell-free protein formation (122) and previous observation (123).

In addition, the polymersomes safely encapsulated the protein for 3 days after incubation. Although polymersomes were composed of biodegradable PLA, hydrolytic degradation did not affect the stability of the polymersomes in a period of two months (64). Instead, attachment of MreB to the membrane could physically interrupt the bilayer, making them unstable after 3-4 days.

Figure 6-7 A and B show confocal microscope images of the polymersomes after 2 h of incubation. The MreB-RPF proteins formed patches in the aqueous core of the polymersomes, with some protein attaching to the membrane, as shown by the arrows in the high magnification image in Figure 6-7 C.

The patch formation was attributed to the propensity of the MreB to polymerise and form filaments. Their adhesion was presumed to be due to a helical hydrophobic motif in the MreB proteins, which interacted with the hydrophobic portion of the membrane. The adhesion of the protein to the hydrophobic membrane was consistent with recent evidence suggesting that the binding activity of MreB to the *E. coli* membrane relies on the presence of hydrophobic residues clustered on one side of an amphiphatic helix of MreB, facilitating interaction between the protein and the membrane (53).
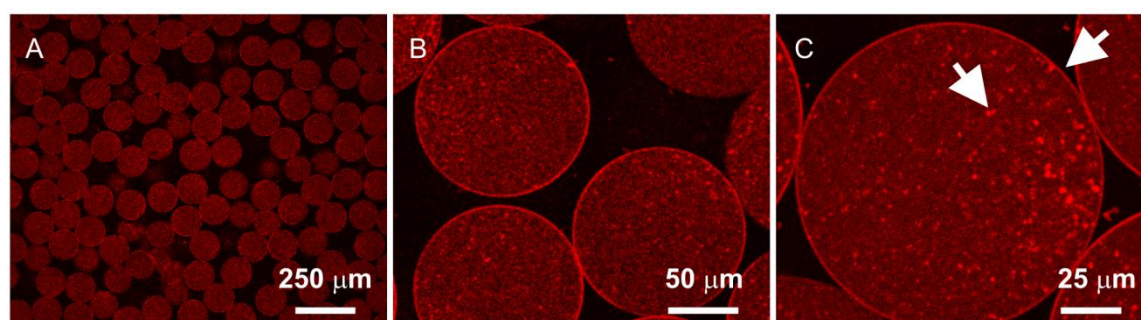


Figure 6-7 Confocal microscope images of reinforced PEG-PLA polymersomes, after 2 h of incubation at 32 °C, at different magnifications (A-C). Arrows indicate the formation of polymerised MreB-RFP patches dispersed in inner phase and the adhesion of the protein on the membrane.

In order to confirm that the fluorescence from the membrane was caused by the attachment of protein, observations of empty polymersomes with a confocal microscope and the same experimental conditions were performed, as shown in Figure 6-8.
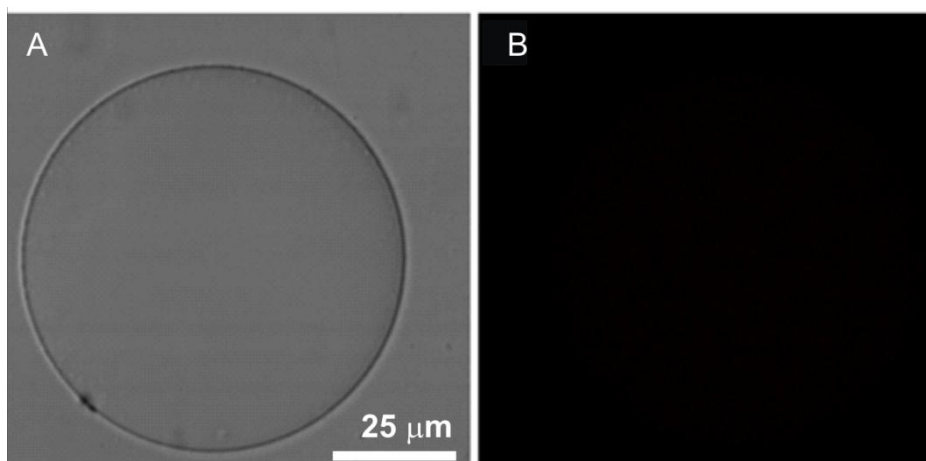


Figure 6-8 Bright field and confocal microscope images of empty polymersome. The polymersomes do not exhibit any fluorescence without expression of protein.

It was also observed that the addition of PLA homopolymer in the bilayer increased the hydrophobicity of the membrane, thereby increasing the adhesion of the MreB. By contrast, polymersomes composed of only PEG-b-PLA diblock-copolymers without the additional PLA homopolymer did not exhibit any adhesion of the expressed protein to the membrane, as shown in Figure 6-9 A. Moreover, the polymersomes were unstable and showed spontaneous breakage after protein expression without any osmotic shock, as shown in Figure 6-9 B.
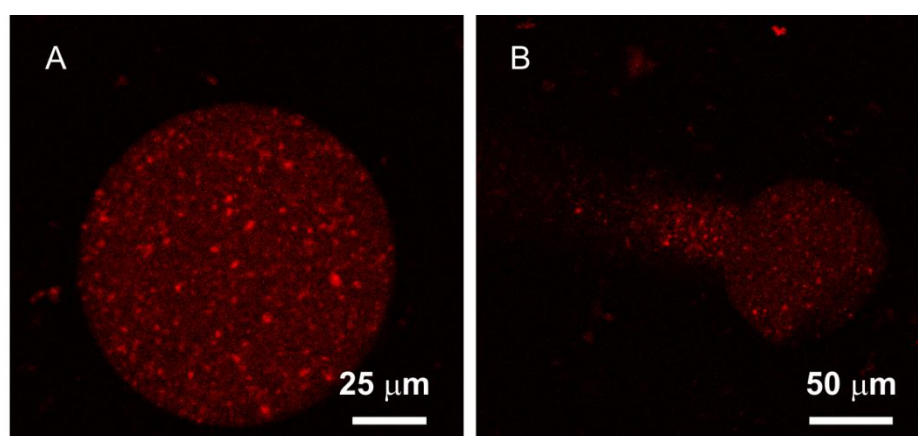


Figure 6-9 Lack of stability in PLA homopolymer-free bilayer membranes (no reinforced membranes). A) The membrane was hydrophilic and no strong adhesion of MreB on the membrane could be observed. B) Spontaneous breakage of the polymersome.

## 6.3.3 Protein release through osmotic shock

In order to obtain protein release from the polymersomes, they were transferred from 0.15 M aqueous solution of NaCl into DI water. It was observed that the diameter of polymersomes immediately increased, resulting in the formation of single pores in the membranes. As the bilayer polymer membrane was strengthened by PLA homopolymers, no disintegration of the overall structure was observed. Instead, a pore was produced and the MreB was released into the DI water, as shown in Figure 6-10 A and B; arrows denote the plume of protein released from the polymersomes. This release event was synchronised across many polymersomes, reflecting the uniformity in the size and structure of the produced polymersomes.
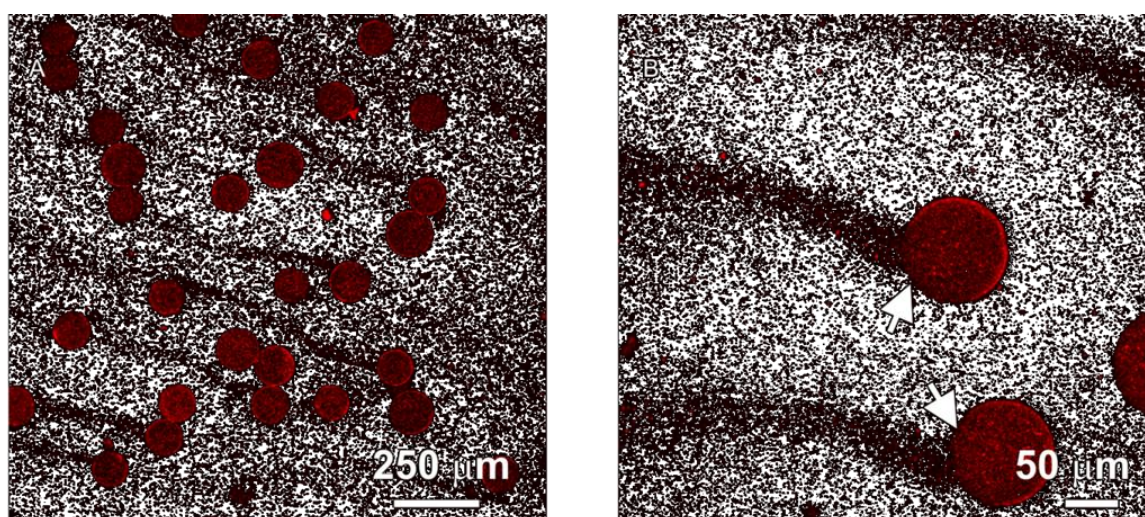


Figure 6-10 Protein release. A) Confocal processed micrograph showing polymersomes 4 h after their generation, immediately after their dispersion in DI water. B) Membrane ruptures occurred in a localized region as denoted by arrows.

After the protein was released, the interior of the polymersome exhibited significantly reduced fluorescence intensity, whereas the fluorescence intensity from the membrane remained constant, owing to the adhesion of the protein on the inner surface of the membrane, as shown in Figure 6-11 A and B where it is presented a comparison of polymersomes fluorescence before and 20 min after the addition of DI water.

After 20 min from the DI water injection most of the polymersomes did not rupture during the inflation due to the inward influx of water, and kept their

spherical structure whereas 20% of polymersomes showed substantial buckling of the membrane. Arrow in Figure 6-11 B shows a buckled polymersome in the suspension. This percentage did not increase after 24 h of incubation.
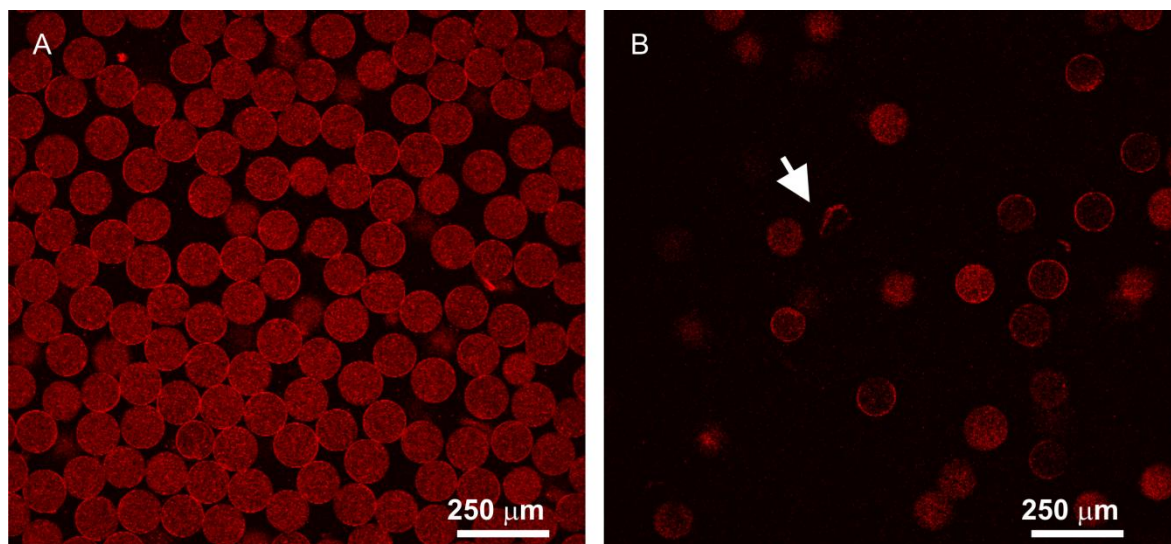


Figure 6-11 Comparison between polymersomes before (A) and after (B) 20 min from DI water addition.

Upon dispersion of polymersomes in DI water, fluorescence signal of polymersomes decreased due to release of the MreB-RFP. Figure 6-12 shows the decreasing fluorescence signal from polymersomes immersed in DI water in their first 30 min. The trend follows an exponential decay typical of a release curve. Measurements were done over ten polymersomes.

The fact that some fluorescence remained in the interior implies that not all of the proteins have been released, suggesting that the pore "heals" as the osmotic pressures are equalized (124). The fact that the pore was actually formed in the membrane was confirmed by adding the green dye molecule, FITC (MW 332.31 Da) to the DI water. It was observed that fluorescein will enter the interior of the polymersome. This was valid both for "round" polymersomes and for "buckled" (Figure 6-13). By contrast a picture showing matching osmolarity values between the inner and the outer polymersome is presented in Figure 6-14. It is clear that green water does not cross the membrane.
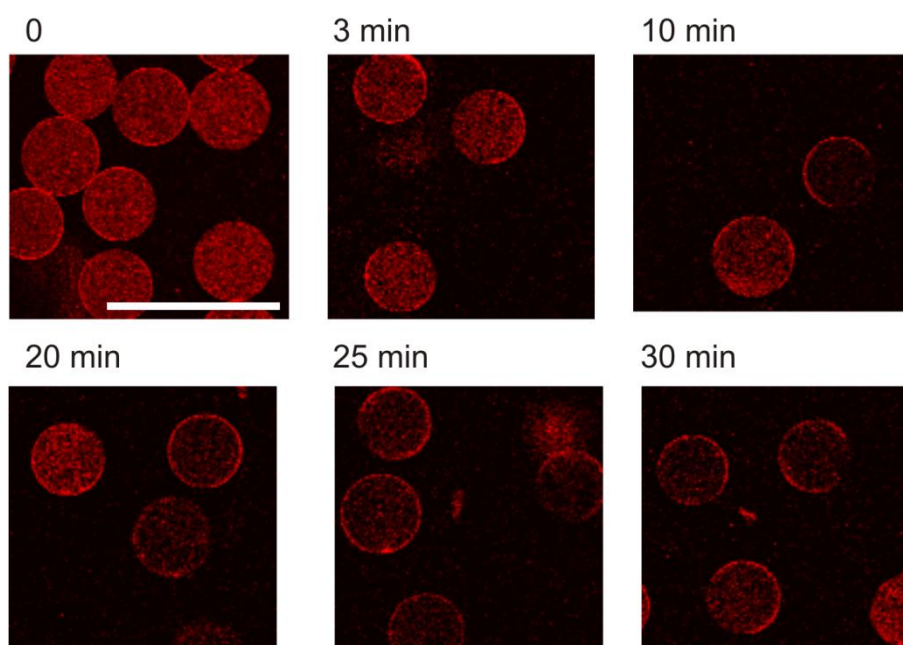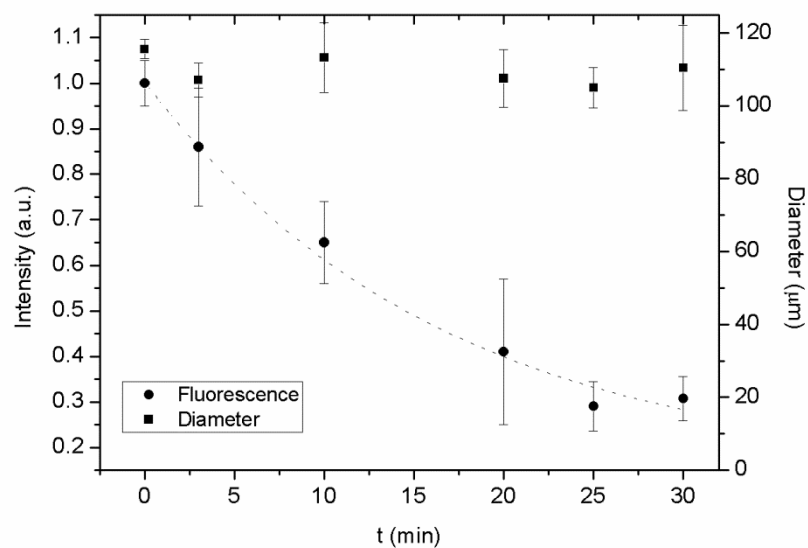
Figure 6-12 Fluorescence intensity and diameter trend over time during inverse osmotic shock. Time zero corresponds to an instant before DI water addition. Measurements were done over ten polymersomes. The confocal microscope images were included to show the protein release from the interior of polymersomes which exhibited reduced fluorescence intensity. The membrane's intensity remained constant due to the protein adhesion with exception in some portions from where the protein was released. Scale bar equal to 250 $\mu$m.
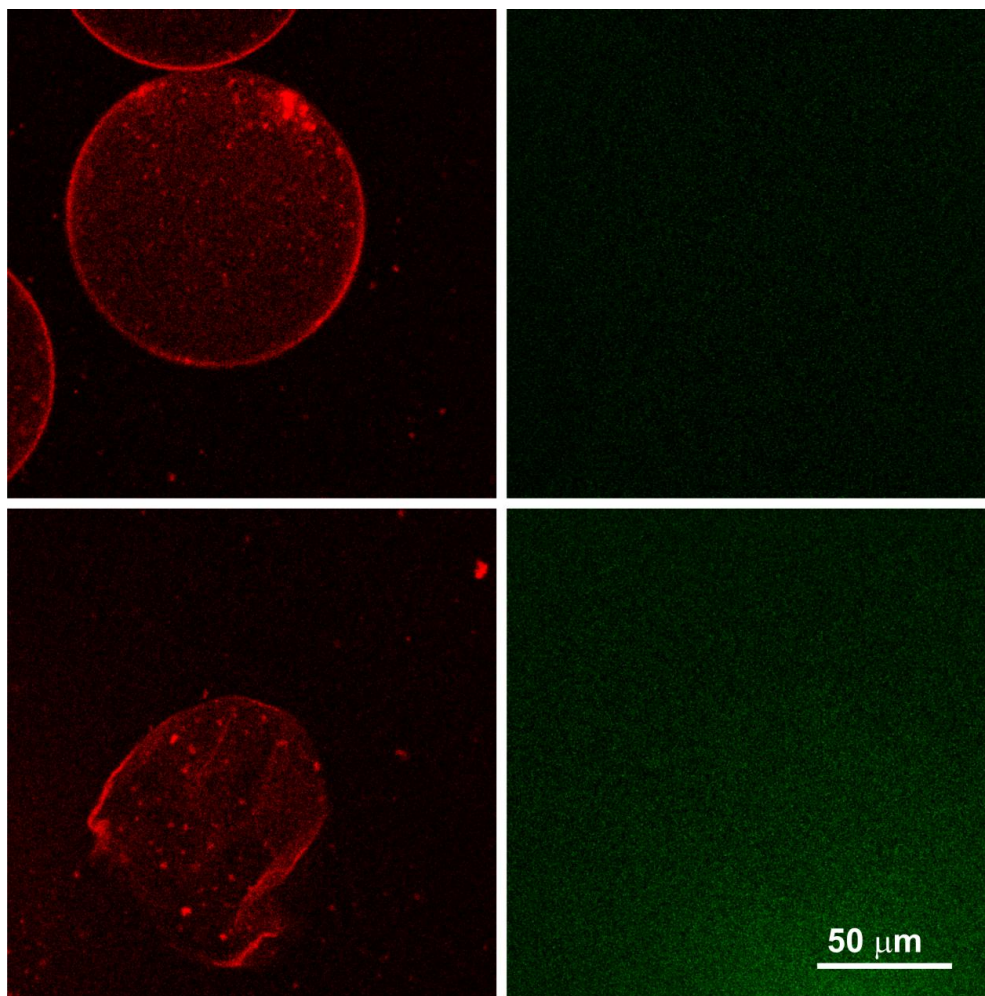
Figure 6-13 On the left, dual-channel confocal micrographs of round and buckled polymersomes after release of proteins. The proteins in inner phase of polymersomes were released to continuous DI water, while the proteins on the membrane remain. On the left, green dye molecules added to the DI water entered the inner phase of polymersome, confirming the formation of holes in the membrane after osmotic shock.
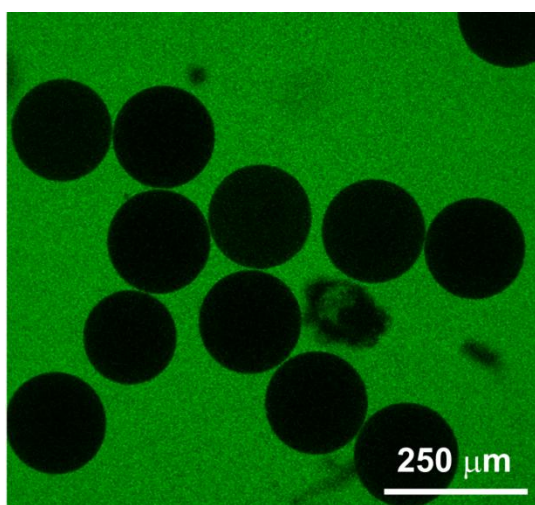


Figure 6-14 Polymersomes with inner and outer phase having the same osmolarities. Fluorescence picture showing there was no inward flux of outer solution within the polymersomes.

## 6.4 Conclusions and future perspectives

The microfluidic technique based on the formation of double-emulsion droplets enabled encapsulation of the protein expression machinery in monodisperse polymersomes without loss of material. The PLA homopolymer-reinforced polymersomes provided a stable compartment for protein expression, while their semi-permeability facilitated triggered release of expressed proteins through a negative osmotic shock. The stability, biocompatibility and biodegradability of the materials may provide new opportunities for studies and applications in *in-vivo* drug delivery and regenerative medicine, where *in-situ* production and release of specific proteins may be required.

Moreover, polymersome scaffolds are potentially useful as test systems for fundamental studies of "systems" approaches to biology (54, 125).

Ultimately, a promising application of this work will be the construction of polymersomes which mimic aspects of the *E. coli* cytoskeleton. This can be achieved by introducing other components of the bacterial cytoskeleton, in combination with PG deposits, in the polymersomes, thereby creating a protocell that has a reconstructed intracellular matrix and which might even be able to change shape.

# 7 Concluding remarks and future directions

In this thesis, droplet-based microfluidic applications concerning protein investigations and protein triggered release have been explored and developed. This Chapter summarizes the findings obtained during the research and indicates some of the avenues which could be explored in future.

## 7.1 Immunoassay in microdroplet

The first aim of this research was to develop a system capable of detecting the amount of specific protein produced by small populations of cells, which were directly lysed on-chip. The system which was developed was shown to be capable of reducing the time and amount of reagents commonly used for protein detection and quantification in a conventional Western blot. This result was achieved by:

- Using a fluorescent protein tagged to the protein of interest;
- Exploiting the affinity that antibodies have towards specific epitopes;
- Taking advantages of some of the interesting droplet-based microfluidic features, such as: small reaction volumes and fast reaction times due to fluid recirculation occurring within the droplets after their generation (92).

A comparison between the results obtained by using microfluidic chip and Western blot analysis is summarised in Table 7-1.

For the same concentration of H-RAS mCitrine detected, the microfluidic system used $10^4$ times fewer cells, a feature particularly appealing for conditions where rare cell populations (i.e. stem cells) need to be used. The microfluidic chip was

also shown to be significantly faster than Western blot analysis. From the moment of droplet generation to the processing the results, the immunoassay was completed in 3 h. This was 9 h faster than Western blot analysis. Preparation of 100 μl of anti H-RAS antibody coated beads was completed in 3 h and was enough to perform at least 50 experiments. Preparation of 8 non-disposable microfluidic chips required a total of 3 h. The most expensive biological reagent used was the antibody solution. In the microfluidic application 50 μl of antibody was used for a total of 50 immunoassay experiments. Each Western blot analysis used 5 μl of antibody per lane. Finally, each chip contained thousands of droplets affording the opportunity to carry out highly robust statistical analyses.

Table 7-1 Comparison of H-RAS mCitrine capture obtained by using microfluidic chip and Western blot analysis.

|  | Microdroplet | Western blot ("Gold Standard") |
|---|---|---|
| Protein Concentration detected (nM) | 10.00 | 10.14 |
| Number of cells | $10^3$ | $10^7$ |
| Time experiment (h) | 3 | 12 |
| Antibody (μl) | 1 | 5 |

Future exploitation of this work could lead to:

- An ELISA essay in droplet, in order to avoid the need to link a fluorescent protein to the protein of interest (Figure 7-1 A);
- Multiplexed immunoassays carried out by injecting a library of encoded beads functionalised with a range of different antibodies (Figure 7-1 B);
- An opportunity to increase the limit of detection to pM.
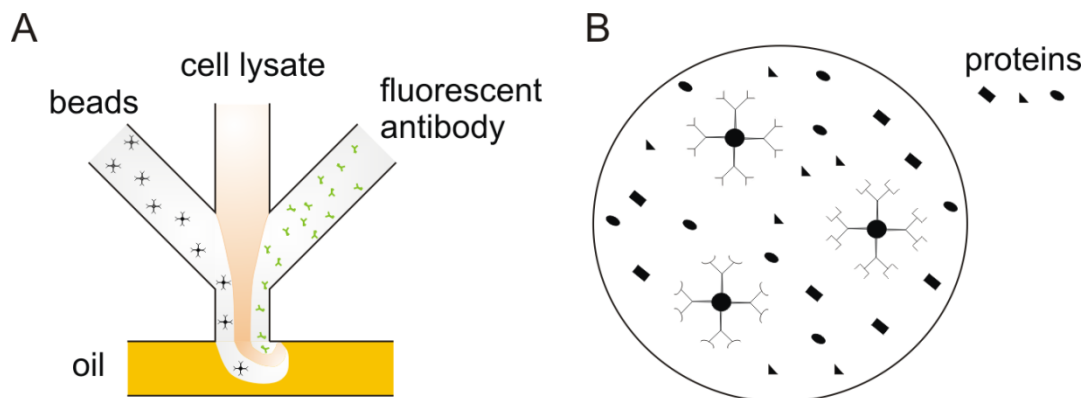
Figure 7-1 Future exploitation of the immunoassay in droplet could lead to the development of: A) an ELISA essay which could avoid the need to modify the protein of interest with a fluorescent marker and B) multiplexed immunoassays that would use a library of beads functionalised with different antibody able to link different proteins present in the cell lysate.

## 7.2 Microdroplets as artificial cell models

The second major application of this work focused on producing platforms capable of mimicking aspects of living cells, such as the presence of a membrane that separates the inner from the outer environment and the capability to produce proteins. Two different types of membranes were produced in this work, namely:

- Hydrophobic mineral oil (hydrocarbon chain);
- Polymeric vesicles of PEG-PLA.

Both types of membrane were produced through the use of double emulsion systems that allowed the production of thousands of monodisperse structures adopted for different applications.

Mineral oil membranes were produced by using a commercially available microfluidic system which has been characterised to control the thickness of the oil membrane. By tuning the flow rate of one fluidic phase during the droplet generation step, the oil membrane was varied from tens to a few micrometers in size. Such double emulsion platforms were used to observe and confirm scientific evidence on the MreB protein behaviour, whose understanding is still not completed by scientists.

MreB seems to have an influence on the rod-like shape of some bacteria and, in 2011, scientific evidence asserted that MreB has a preference towards

hydrophobic membranes due to the presence of an amphipathic helix in their structures (53). In a simple oil membrane system, through confocal microscopy and FRAP analysis, in this research it was observed that MreB molecules adhered to the oil membrane and they were even included within the membrane (Figure 7-2). Due to the capability of MreB monomers to polymerise, patches of proteins were also observed. Within the double emulsion system, MreB polymerised in a manner and at concentrations which were consistent with *in vivo* studies (104).
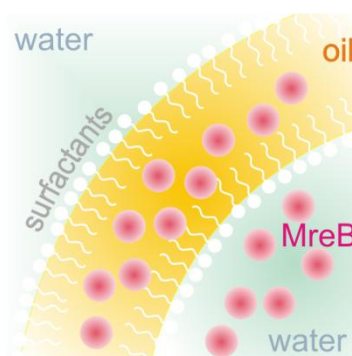


Figure 7-2 Representation of MreB units insertion into the hydrophobic oil membrane. The units of MReB (5.1 nm × 3.9 nm) (126) inserted into a few microns membrane space stabilised by a ~28 Å thick monolayer of surfactant SPAN 80 (127), formed at the interface with water.

Future investigations could involve using the double emulsion system to:

- Study the diffusion of the protein within the hydrophobic membrane;
- Prove other protein behaviour in a less complex environment than the cellular one;
- Add new features taking inspiration from the natural cells.

Following the same approach used for the production of protein within a double emulsion system, polymeric vesicles of PEG-PLA, reinforced with PLA homopolymer, were produced through the well characterised capillary device developed by Professor Weitz at Harvard University (24). Through control of the inner and outer polymersome osmolarities, the polymeric compartments were engineered so as to be compatible with the protein expression and stable for up to 3-4 days after their production.

Due to the nature of the chosen polymer, these systems have also proved to be reliable carriers for triggered release of their content. Their homogeneity in

size, derived from their production through microfluidic systems, and their water permeability property produced polymersomes acting as carriers for synchronised delivery. The delivery was triggered by a change in the osmolarity of the outer liquid phase where the polymersomes were stored. During the first 30 minutes from the osmotic shock the deliver followed an exponential decay, while the rest of the protein remained anchored to the membrane of the polymersome, estimated to be few hundreds of nanometers thick (Figure 7-3).
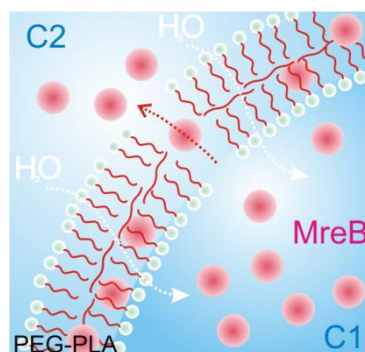


Figure 7-3 Representation of a portion of PEG-PLA vesicle (reinforced with PLA homopolymer) undergoing to osmotic shock. The nanometer thick bilayer is permeable to water molecules that enter into the polymersome to equalize the concentration of the interior of the polymersome (C1) and the external one (C2). The inward flux of water makes the polymersome swell until a point where the membrane undergoes to a rupture causing the release of the MreB protein.

For the first time the utility of microdroplets to function as a cell model capable to protein release has been showcased. This technique could be used:

- In the study of proteins relevant in the field of regenerative medicine such as: fibronectin, elastin and collagen;
- For the mimicking of living cells, due to their nanometer thick membrane. This could be achieved by introducing other components of the bacterial cytoskeleton, in combination with PG deposits, in the polymersomes, thereby creating a system that has a reconstructed intracellular matrix and which might even be able to change morphology;
- Assembly of multiple functional "protocells" each with particular responsive membranes to changes in pH, light, ionic concentrations.

# Appendix I

## Coverage of beads with antibody

The following calculations were necessary to establish the weight of secondary antibody needed to cover a bead.

Firstly, it is necessary to know the bead's number ($N_B$) used. This value is calculated knowing the density of beads in the purchased solution ($D_b$), the density of the bead ($\rho_B$) and the radius of the bead ($r_b$). Assuming the beads are modelled as perfect spheres of volume V, the number of beads contained in that volume can be calculated as follow:

$$N_B = \frac{D_b \cdot V}{\frac{4}{3}\pi r^3 \cdot \rho_B}$$

Knowing that each bead contains $2 \times 10^7$ binding sites (info from Bangs Lab) the number of binding sites ($n_b$) in a given volume $V$ is:

$$n_b = \left(2 \cdot 10^7\right) N_B$$

To establish the weight of antibody in grams ($w_{AB}$) required to cover completely all beads contained in the volume $V$, the following calculation is performed:

$$w_{AB} = \frac{n_B \cdot MW_{AB}}{N_A}$$

where $MW_{AB}$ and $N_A$ are the antibody's molecular weight and the Avogadro's constant respectively.

# Estimation of molecules within the droplet

These calculations were necessary to establish the number of molecules inside the droplet that are able to bind the bead.

To establish the molecules of protein inside the droplet it is essential to know the volume of the droplet ($V_D$) and the protein concentration of the initial delivered solution ($C_P$). Considering the droplet as a spheroid, its volume can be calculated using the equation below:

$$V_D = \frac{4}{3}\pi \left(r^2\right)\frac{h}{2}$$

where $r$ is the radius of the droplet and $h$ the height of the channel where the droplet is formed. Taking into account that the dispersed phase is made by the mixing of protein solution and buffer containing beads, only half the volume of a droplet contains protein solution. The weight of the secondary antibody solution ($w_{AB2nd}$) and the number of molecules ($n_{AB2nd}$) can be calculated as follows:

$$w_{AB2nd} = C_P \cdot \frac{V_D}{2}$$

$$n_{AB2nd} = w_{AB2nd} \cdot \frac{N_A}{MW_{AB2nd}} \cdot$$

# Appendix II

## Construction of the pB1A2_BX(MreB-RFP) plasmid

BioBrick ref BBa_I719015 was obtained from the Registry of Standard Biological Parts, which contains gene expression cassette of T7 promoter-RBS-mGFP-terminator in pSB1A2. This plasmid was reconstructed as pB1A2_BX by introducing *Bam*HI and *Xho*I sites between the RBS and terminator instead of m*GFP* gene. *MreB* gene was PCR-amplified from the genomic DNA isolated from *E.coli* strain KO11 using the TIANamp bacteria DNA kit (Tiangen, China).

The reporter gene *RFP* was amplified from BioBrick BBa_E1010, using RFP_forward and RFP_reverse primers. The fusion protein gene *MreB-RFP* was assembled by overlap extension PCR, with GS linker inserted between the two genes. Then the *MreB-RFP* fragment was inserted into pSB1A2_BX with *Bam*HI and *Xho*I, resulting in the vector pSB1A2_BX(*fusion protein*), which contained the target gene expression cassette T7 promoter-RBS-*MreB-RFP*-terminator (Figure 1). All the procedures have been performed under Miss Chen's supervision.
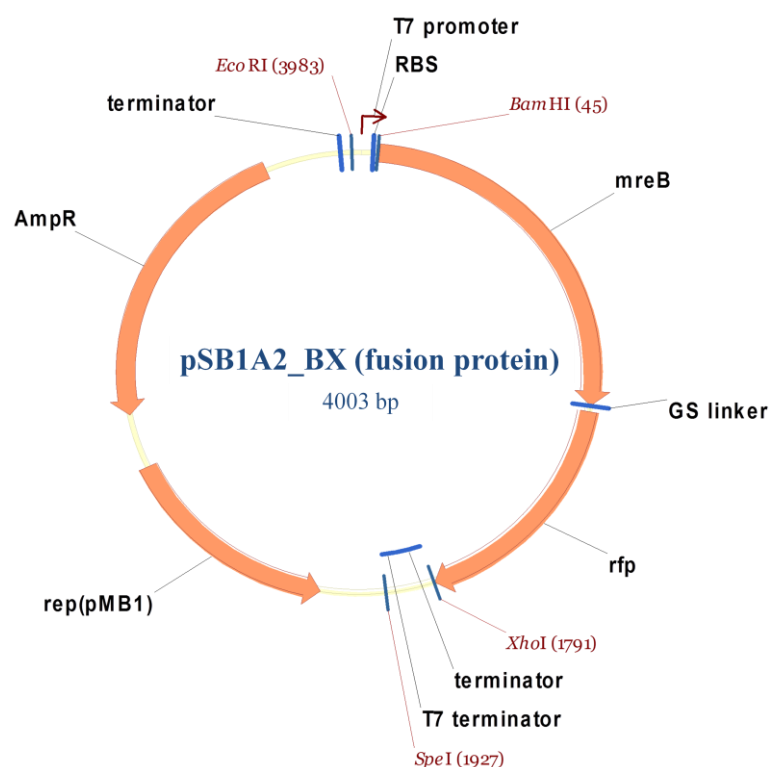


Figure 1 pSB1A2_BX(fusion protein) plasmid structure. This vector was designed by using Vector NTI software.

pSB1A2_BX(*fusion protein*) plasmid was transformed into BL21(DE3) via electroporation and selected by ampicillin resistance. The cells were inoculated overnight in 100 ml LB broth with an initial optical density at 600 nm ($OD_{600}$) of 0.1, incubated at 30 °C, 220 rpm. When the cell density reached 1.0, IPTG was added to a final concentration of 0.8 mM in order to induce the expression of the fusion protein. Upon adding IPTG, fluorescence detection was performed every hour. BL21(DE3) with pSB1A2_BX without fusion protein was used as control. As shown in Figure 2, in bacteria transformed with pSB1A2_BX(*fusion protein*), after addition of the IPTG promoter, the production of protein starts slowly for almost 3 h. After this phase, during the next 4 h it follows a linear trend until the 7th h when it gradually slow down and reaches a plateau after 11 h. Strains transformed with the plasmid control did not exhibit any meaningful fluorescence.
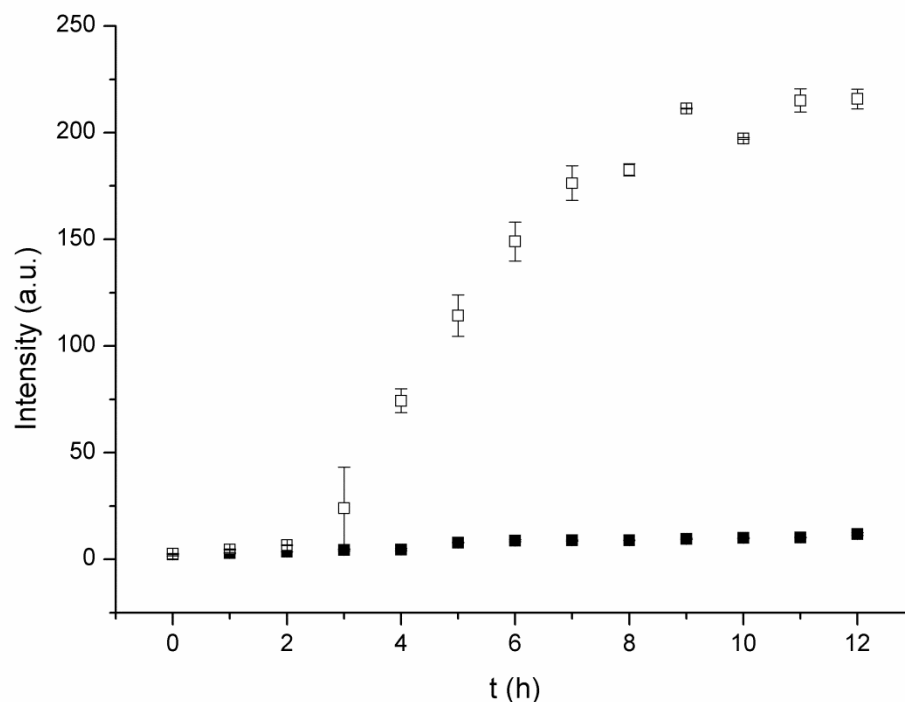


Figure 2 Fluorescence measurements over the time on cell culture inoculated with pSB1A2_BX(fusion protein) (white squares) and control plasmid (black squares).

Figure 3 shows the vials of the two cultures after incubation and the pellet of bacteria after spinning. Imaging of bacteria under confocal microscope showed the peculiar structure of MreB.
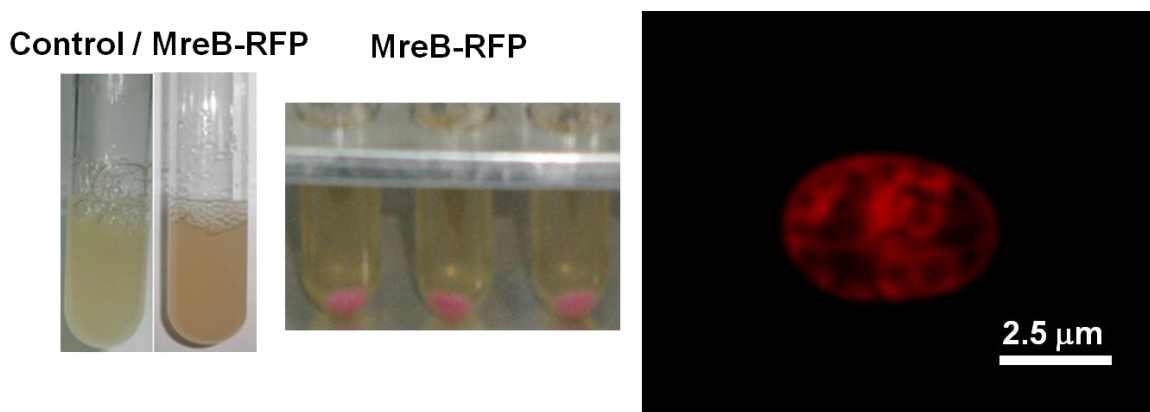
Figure 3 Cultures of *E.coli* expressing the control plasmid and the MreB-RFP plasmid (left). Pellets of bacteria expressing MreB-RFP after centrifugation of three vials (centre). Laser scanning confocal image of *E.coli* expressing MreB-RFP (right) taken by Miss Y. Chen.

## Plasmid amplification, restriction and ligation protocol

All primers were designed by 9Vector NTI software.

The plasmid was amplified by PCR technique. In a vial, all the components required for PCR were mixed. These included: 0.4 µl of DNA template (10 ng ml⁻¹), 0.4 µl of Primer F (Forward) 10 µM, 0.4 µl of Primer R (Reverse) 10 µM, 4 µl of Buffer, 0.4 µl of dNTP, 0.4 µl of dfu enzyme and 14 µl of DI water. After the reaction, gel electrophoresis was performed. All the DNA molecules subjected to 118 V for 20 min were separated according to their molecular weight in an agarose gel (1%) immersed in TAE (Tris-acetate-EDTA) buffer. After DNA separation, the gel was then immersed in an ethidium bromide (EB) solution, a substance able to attach to intercalate DNA and allows it to be visualised with UV light. The brightest column of the gel was cut and purified from the agarose gel (using Tiangen Midi purification kit) and its concentration was measured using a spectrophotometer (Nanodrop, Thermo Scientific).

Then the purified DNA was mixed with a restriction enzyme as (14 µl of plasmid, 2 µl of buffer, 0.5 µl of enzyme, 3.5 µl of DI water) and incubated at 37 °C. After 4 h the DNA was again separated by gel electrophoresis, purified and mixed with lygase enzyme (7.5 µl of plasmid, 2 µl of buffer, 0.5 µl of lygase) at room temperature for 20 min.

## E. coli transformation protocol

In order to insert plasmid into bacteria, membranes were permeabalised by thermal shock.

20 µl of DH5 α E.coli ($6\times10^8$ cell ml$^{-1}$) was suspended in 2 ml of LB media and shaken for 10 h at 37 ℃. After this time the vial containing the cells was centrifuged for 2 min and the remaining pellet was suspended in $CaCl_2$ for 5 min and mixed with the reconstructed vector. Then the vial was immersed in warm water (42 ℃) for 45 sec and then in ice bath for 2 min. 900 µl of LB media was added and incubated for 45 min at room temperature. In the mean time 1.5% of agar solid media containing a drug (Ampicillin) was prepared. Once solidified, the bacteria were spread on it and let them grow for 12 h.

## Plasmid extraction and purification protocol

The transformant E. *coli* colonies were extracted from the dishes using pipette and were put in the vials containing LB medium. The cells were centrifuged for 2 min. The supernatant was removed and 150 µl of solution 1 (made of 4.5 ml 20% glucose. 2.5 ml *1* M Tris-Cl, pH 8.0. 2 ml 0.5 M EDTA), 200 µl of solution 2 (made of 2 ml of 1 M NaOH, 1 ml of 10% SDS, 7 ml of $H_2O$) and 200 µl of potassium acetate (made of 29.5 ml glacial acetic acid at pH 4.8 adjusted with KOH pellets and 100 ml of water). EDTA and SDS have the function of protect the DNA from the DNAase and break the cell wall respectively. Potassium acetate interacts with the SDS and causes the precipitation of proteins while DNA remains in solution. The solutions were then centrifuged for 15 min and sodium acetate and 1 ml of ethanol were added in order to keep the pH above 9 and let the DNA precipitate. The solution was centrifuged at 4 ℃ for 10 min; afterwards 1 ml of 70% ethanol solution was added. The presence of DI water in ethanol was required to dissolve the salts present in the solution. Then the solution was centrifuged twice and dried in the oven to complete the ethanol evaporation. To the DNA 20 µl of DI water was added and a gel was run. Afterwards the DNA was purified and the plasmid was collected. A small amount of plasmid was sent to a company to be sequenced.

# Bibliography

1.     Zare RN, Kim S. Microfluidic platforms for single-cell analysis. Annu Rev Biomed Eng. 2010;12:187-201. Epub 2010/05/04.

2.     Beebe DJ, Mensing GA, Walker GM. Physics and applications of microfluidics in biology.  Annu Rev Biomed Eng2002. p. 261-86.

3.     El-Ali J, Sorger PK, Jensen KF. Cells on chips. Nature. 2006;442(7101):403-11.

4.     Weibel DB, DiLuzio WR, Whitesides GM. Microfabrication meets microbiology. Nat Rev Microbiol. 2007;5(3):209-18.

5.     Pamme N. Continuous flow separations in microfluidic devices. Lab Chip. 2007;7(12):1644-59.

6.     Mark D, Haeberle S, Roth G, von Stetten F, Zengerle R. Microfluidic lab-on-a-chip platforms: requirements, characteristics and applications. Chemical Society Reviews. 2010;39(3):1153-82.

7.     Christopher GF, Anna SL. Microfluidic methods for generating continuous droplet streams. J Phys D Appl Phys. 2007;40(19):R319-R36.

8.     Teh SY, Lin R, Hung LH, Lee AP. Droplet microfluidics. Lab Chip. 2008;8(2):198-220.

9.     Demello AJ, Gulati S, Rouilly V, Niu XZ, Chappell J, Kitney RI, et al. Opportunities for microfluidic technologies in synthetic biology. Journal of the Royal Society Interface. 2009;6.

10.     Paik P, Pamula VK, Fair RB. Rapid droplet mixers for digital microfluidic systems. Lab Chip. 2003;3(4):253-9.

11.     Song H, Bringer MR, Tice JD, Gerdts CJ, Ismagilov RF. Experimental test of scaling of mixing by chaotic advection in droplets moving through microfluidic channels. Appl Phys Lett. 2003;83(22):4664-6.

12.     Baroud CN, Robert de Saint Vincent M, Delville J-P. An optical toolbox for total control of droplet microfluidics. Lab Chip. 2007;7(8):1029-33.

13.     Franke T, Abate AR, Weitz DA, Wixforth A. Surface acoustic wave (SAW) directed droplet flow in microfluidics for PDMS devices. Lab Chip. 2009;9(18):2625-7.

14.     Niu X, Gulati S, Edel JB, deMello AJ. Pillar-induced droplet merging in microfluidic circuits. Lab Chip. 2008;8(11):1837-41.

15.     Tan Y-C, Ho Y, Lee A. Microfluidic sorting of droplets by size. Microfluidics and Nanofluidics. 2008;4(4):343-8.

16.     Link DR, Anna SL, Weitz DA, Stone HA. Geometrically mediated breakup of drops in microfluidic devices. Physical Review Letters. 2004;92(5).

17.     Theberge AB, Courtois F, Schaerli Y, Fischlechner M, Abell C, Hollfelder F, et al. Microdroplets in Microfluidics: An Evolving Platform for Discoveries in Chemistry and Biology. Angewandte Chemie International Edition. 2010;49(34):5846-68.

18.     Lee AP, Teh SY, Lin R, Hung LH. Droplet microfluidics. Lab Chip. 2008;8(2):198-220.

19.     Zheng B, Gerdts CJ, Ismagilov RF. Using nanoliter plugs in microfluidics to facilitate and understand protein crystallization. Curr Opin Struc Biol. 2005;15(5):548-55.

20.     He M, Edgar JS, Jeffries GDM, Lorenz RM, Shelby JP, Chiu DT. Selective Encapsulation of Single Cells and Subcellular Organelles into Picoliter- and Femtoliter-Volume Droplets. Anal Chem. 2005;77(6):1539-44.

21.     Schaerli Y, Wootton RC, Robinson T, Stein V, Dunsby C, Neil MAA, et al. Continuous-Flow Polymerase Chain Reaction of Single-Copy DNA in Microfluidic Microdroplets. Anal Chem. 2008;81(1):302-6.

22.     Xu SQ, Nie ZH, Seo M, Lewis P, Kumacheva E, Stone HA, et al. Generation of monodisperse particles by using microfluidics: Control over size, shape, and composition. Angew Chem Int Edit. 2005;44(5):724-8.

23.     Okushima S, Nisisako T, Torii T, Higuchi T. Controlled production of monodisperse double emulsions by two-step droplet breakup in microfluidic devices. Langmuir. 2004;20(23):9905-8.

24.     Utada AS, Lorenceau E, Link DR, Kaplan PD, Stone HA, Weitz DA. Monodisperse double emulsions generated from a microcapillary device. Science. 2005;308(5721):537-41.

25.     Chang FC, Su YC. Controlled double emulsification utilizing 3D PDMS microchannels. Journal of Micromechanics and Microengineering. 2008;18(6).

26.     Bauer WAC, Fischlechner M, Abell C, Huck WTS. Hydrophilic PDMS microchannels for high-throughput formation of oil-in-water microdroplets and water-in-oil-in-water double emulsions. Lab Chip. 2010;10(14):1814-9.

27.     Chu LY, Utada AS, Shah RK, Kim JW, Weitz DA. Controllable monodisperse multiple emulsions. Angew Chem Int Edit. 2007;46(47):8970-4.

28.     Huebner A, Sharma S, Srisa-Art M, Hollfelder F, Edel JB, deMello AJ. Microdroplets: A sea of applications? Lab Chip. 2008;8(8):1244-54.

29.     Dittrich PS, Jahnz M, Schwille P. A new embedded process for compartmentalized cell-free protein expression and on-line detection in microfluidic devices. Chembiochem. 2005;6(5):811-+.

30.     Courtois F, Olguin LF, Whyte G, Bratton D, Huck WTS, Abell C, et al. An Integrated Device for Monitoring Time-Dependent in vitro Expression From Single Genes in Picolitre Droplets. Chembiochem. 2008;9(3):439-46.

31.     Renart J, Reiser J, Stark GR. Transfer of Proteins from Gels to Diazobenzyloxymethyl-Paper and Detection with Antisera - Method for Studying Antibody Specificity and Antigen Structure. Proc Natl Acad Sci U S A. 1979;76(7):3116-20.

32.     Engvall E, Perlmann P. Enzyme-Linked Immunosorbent Assay (Elisa) Quantitative Assay of Immunoglobulin-G. Immunochemistry. 1971;8(9):871-&.

33.     Joensson HN, Samuels ML, Brouzes ER, Medkova M, Uhlen M, Link DR, et al. Detection and Analysis of Low-Abundance Cell-Surface Biomarkers Using Enzymatic Amplification in Microfluidic Droplets. Angewandte Chemie-International Edition. 2009;48(14):2518-21.

34.     El-Ali J, Gaudet S, Günther A, Sorger PK, Jensen KF. Cell Stimulus and Lysis in a Microfluidic Device with Segmented Gas-Liquid Flow. Anal Chem. 2005;77(11):3629-36.

35.     Gitai Z. The new bacterial cell biology: moving parts and subcellular architecture. Cell. 2005;120(5):577-86. Epub 2005/03/16.

36.     Schwille P, Diez S. Synthetic biology of minimal systems. Critical Reviews in Biochemistry and Molecular Biology. 2009;44(4):223-42.

37.     Chang TMS. Semipermeable Microcapsules. Science. 1964;146(3643):524-5.

38.     Chang TMS. Artificial Cells with Emphasis on Cell Encapsulation of Genetically Engineered Cells. Artificial Organs. 1998;22(11):958-65.

39.     Swi Chang TM. Artificial cells with emphasis on bioencapsulation in biotechnology. In: El-Gewely MR, editor. Biotechnology Annual Review: Elsevier; 1995. p. 267-95.

40.     Tawfik DS, Griffiths AD. Man-made cell-like compartments for molecular evolution. Nat Biotech. 1998;16(7):652-6.

41.     Kelly BT, Baret J-C, Taly V, Griffiths AD. Miniaturizing chemistry and biology in microdroplets. Chemical Communications. 2007(18):1773-88.

42.     Schaerli Y, Hollfelder F. The potential of microfluidic water-in-oil droplets in experimental biology. Molecular BioSystems. 2009;5(12):1392-404.

43.     Zhu YG, Wu N, Courtois F, Surjadi R, Oakeshott J, Peat TS, et al. Enzyme synthesis and activity assay in microfluidic droplets on a chip. Engineering in Life Sciences. 2011;11(2):157-64.

44.     Zhu Y, Wu N, Oakeshott JG, Easton CJ, Peat TS, Surjadi R. A double-emulsion microfluidic platform for in vitro green fluorescent protein expression. Journal of Micromechanics and Microengineering. 2011;21(5).

45.     Libchaber A, Noireaux V. A vesicle bioreactor as a step toward an artificial cell assembly. P Natl Acad Sci USA. 2004;101(51):17669-74.

46.     Maeda YT, Nakadai T, Shin J, Uryu K, Noireaux V, Libchaber A. Assembly of MreB Filaments on Liposome Membranes: A Synthetic Biology Approach. ACS Synthetic Biology. 2011.

47.     Walde P, Cosentino K, Engel H, Stano P. Giant Vesicles: Preparations and Applications. Chembiochem. 2010;11(7):848-65.

48.     Fletcher DA, Richmond DL, Schmid EM, Martens S, Stachowiak JC, Liska N. Forming giant vesicles with controlled membrane composition, asymmetry, and contents. P Natl Acad Sci USA. 2011;108(23):9431-6.

49.     Ota S, Yoshizawa S, Takeuchi S. Microfluidic Formation of Monodisperse, Cell-Sized, and Unilamellar Vesicles. Angewandte Chemie International Edition. 2009;48(35):6533-7.

50.     Discher DE, Ahmed F. POLYMERSOMES. Annual Review of Biomedical Engineering. 2006;8(1):323-41.

51.     Weitz DA, Shum HC, Lee D, Yoon I, Kodger T. Double emulsion templated monodisperse phospholipid vesicles. Langmuir. 2008;24(15):7651-3.

52.     Luisi PL, Stano P. Synthetic biology: Minimal cell mimicry. Nat Chem. 2011;3(10):755-6.

53.     Salje J, van den Ent F, de Boer P, Löwe J. Direct Membrane Binding by Bacterial Actin MreB. Molecular Cell. 2011;43(3):478-87.

54.     van Teeffelen S, Wang S, Furchtgott L, Huang KC, Wingreen NS, Shaevitz JW, et al. The bacterial actin MreB rotates, and rotation depends on cell-wall assembly. Proc Natl Acad Sci U S A. 2011. Epub 2011/09/10.

55.     Graumann PL. Dynamics of Bacterial Cytoskeletal Elements. Cell Motil Cytoskel. 2009;66(11):909-14.

56.     Kamat NP, Katz JS, Hammer DA. Engineering Polymersome Protocells. The journal of physical chemistry letters. 2011;2(13):1612-23.

57.     Discher BM, Won Y-Y, Ege DS, Lee JC-M, Bates FS, Discher DE, et al. Polymersomes: Tough Vesicles Made from Diblock Copolymers. Science. 1999;284(5417):1143-6.

58.     Mecke A, Dittrich C, Meier W. Biomimetic membranes designed from amphiphilic block copolymers. Soft Matter. 2006;2(9):751-9.

59.     Lee JCM, Bermudez H, Discher BM, Sheehan MA, Won Y-Y, Bates FS, et al. Preparation, stability, and in vitro performance of vesicles made with diblock copolymers. Biotechnology and Bioengineering. 2001;73(2):135-45.

60.     Hammer DA, Robbins GP, Haun JB, Lin JJ, Qi W, Smith LA, et al. Leuko-polymersomes. Faraday discussions. 2008;139:129-41; discussion 213-28, 419-20. Epub 2008/12/04.

61.     Kamat NP, Robbins GP, Rawson J, Therien MJ, Dmochowski IJ, Hammer DA. A Generalized System for Photoresponsive Membrane Rupture in Polymersomes. Advanced Functional Materials. 2010;20(16):2588-96.

62.     Yu S, Azzam T, Rouiller I, Eisenberg A. "Breathing" Vesicles. Journal of the American Chemical Society. 2009;131(30):10557-66.

63.     Weitz DA, Shum HC, Kim JW. Microfluidic fabrication of monodisperse biocompatible and biodegradable polymersomes with controlled permeability. Journal of the American Chemical Society. 2008;130(29):9543-9.

64.     Kim SH, Shum HC, Kim JW, Cho JC, Weitz DA. Multiple polymersomes for programmed release of multiple components. Journal of the American Chemical Society. 2011;133(38):15165-71. Epub 2011/08/16.

65.     Whitesides GM. The origins and the future of microfluidics. Nature. 2006;442(7101):368-73.

66.     Baroud CN, Gallaire F, Dangla R. Dynamics of microfluidic droplets. Lab Chip. 2010;10(16):2032-45.

67.     R. B. Bird WESaENL. Transport Phenomena. Wiley. 1960.

68.     Liu HH, Zhang YH. Droplet formation in microfluidic cross-junctions. Phys Fluids. 2011;23(8).

69.     Thorsen T, Roberts RW, Arnold FH, Quake SR. Dynamic pattern formation in a vesicle-generating microfluidic device. Physical Review Letters. 2001;86(18):4163-6.

70.     Tan J, Xu JH, Li SW, Luo GS. Drop dispenser in a cross-junction microfluidic device: Scaling and mechanism of break-up. Chemical Engineering Journal. 2008;136(2–3):306-11.

71.     Dreyfus R, Tabeling P, Willaime H. Ordered and disordered patterns in two-phase flows in microchannels. Phys Rev Lett. 2003;90(14):144505. Epub 2003/05/07.

72.     Anna SL, Bontoux N, Stone HA. Formation of dispersions using "flow focusing" in microchannels. Appl Phys Lett. 2003;82(3):364-6.

73.     Fernando Leal-Calderon JBaVS. Emulsion Science Basic Principles. Springer. 2007. Epub Second Edition.

74.     Princen HM. Rheology of Foams and Highly Concentrated Emulsions .1. Elastic Properties and Yield Stress of a Cylindrical Model System. Journal of Colloid and Interface Science. 1983;91(1):160-75.

75.     Mason TG, Bibette J, Weitz DA. Elasticity of Compressed Emulsions. Physical Review Letters. 1995;75(10):2051-4.

76.     Taylor P. Ostwald ripening in emulsions. Adv Colloid Interfac. 1998;75(2):107-63.

77.     Pommella A. COMPORTAMENTO IN FLUSSO DI SCORRIMENTO DI VESCICOLE DI SURFATTANTE. Tesi di Laurea Specialistica, Ingegneria Chimica, Universita' degli studi di Napoli Federico II. Anno accademico 2008/2009:12.

78.     Madou MJ. Fundamentals of Microfabrication. CRC Press LLC. 2001.

79.     Franssila S. Introduction to microfabrication. Wiley. 2010.

80.     Agard D. Methods in cell biology. Elsevier. 1989;30.

81.     http://www.olympusmicro.com.

82.     Ligler TCaFS. Immobilised Biomolecules in Analysis A Pratical Approach. Oxford University Press. 1998.

83.     Lee S-W, Tai Y-C. A micro cell lysis device. Sensors and Actuators A: Physical. 1999;73(1–2):74-9.

84.     Brown RB, Audet J. Current techniques for single-cell lysis. Journal of the Royal Society, Interface / the Royal Society. 2008;5 Suppl 2:S131-8. Epub 2008/04/23.

85.     Kinosita K, Jr., Tsong TT. Hemolysis of human erythrocytes by transient electric field. Proc Natl Acad Sci U S A. 1977;74(5):1923-7. Epub 1977/05/01.

86.     Pethig R. Review Article-Dielectrophoresis: Status of the theory, technology, and applications. Biomicrofluidics. 2010;4(2).

87.     Peyker A, Rocks O, Bastiaens PIH. Imaging activation of two Ras isoforms simultaneously in a single cell. Chembiochem. 2005;6(1):78-85.

88.     Macaluso M, Russo G, Cinti C, Bazan V, Gebbia N, Russo A. Ras family genes: An interesting link between cell cycle and cancer. J Cell Physiol. 2002;192(2):125-30.

89.     Pantaloni D, Le Clainche C, Carlier MF. Cell biology - Mechanism of actin-based motility. Science. 2001;292(5521):1502-6.

90.     Zagnoni M, Le Lain G, Cooper JM. Electrocoalescence Mechanisms of Microdroplets Using Localized Electric Fields in Microfluidic Channels. Langmuir. 2010;26(18):14443-9.

91.     Bradford MM. A rapid and sensitive method for the quantification of microgram quantities of protein using principle of protein-dye binding. Analytical Biochemistry. 1976;72(1-2):248-54.

92.     Tice JD, Song H, Lyon AD, Ismagilov RF. Formation of droplets and mixing in multiphase microfluidics at low values of the Reynolds and the capillary numbers. Langmuir. 2003;19(22):9127-33.

93.     Zhu K, Kaprelyants AS, Salina EG, Markx GH. Separation by dielectrophoresis of dormant and nondormant bacterial cells of Mycobacterium smegmatis. Biomicrofluidics. 2010;4(2).

94.     Shaner NC, Steinbach PA, Tsien RY. A guide to choosing fluorescent proteins. Nat Methods. 2005;2(12):905-9.

95.     Larson DR, Ow H, Vishwasrao HD, Heikal AA, Wiesner U, Webb WW. Silica Nanoparticle Architecture Determines Radiative Properties of Encapsulated Fluorophores. Chemistry of Materials. 2008;20(8):2677-84.

96.     Huebner A, Bratton D, Whyte G, Yang M, deMello AJ, Abell C, et al. Static microdroplet arrays: a microfluidic device for droplet trapping, incubation and release for enzymatic and cell-based assays. Lab Chip. 2009;9(5):692-8.

97.     Courtois F, Olguin LF, Whyte G, Theberge AB, Huck WTS, Hollfelder F, et al. Controlling the Retention of Small Molecules in Emulsion Microdroplets for Use in Cell-Based Assays. Anal Chem. 2009;81(8):3008-16.

98.     Shim JU, Olguin LF, Whyte G, Scott D, Babtie A, Abell C, et al. Simultaneous Determination of Gene Expression and Enzymatic Activity in Individual Bacterial Cells in Microdroplet Compartments. J Am Chem Soc. 2009;131(42):15251-6.

99.     Florescu O, Wang K, Au P, Tang J, Harris E, Beatty PR, et al. On-chip magnetic separation of superparamagnetic beads for integrated molecular analysis. J Appl Phys. 2010;107(5).

100.    Zubay G. In vitro synthesis of protein in microbial systems. Annu Rev Genet. 1973;7:267-87. Epub 1973/01/01.

101.    Kim DM, Kigawa T, Choi CY, Yokoyama S. A highly efficient cell-free protein synthesis system from Escherichia coli. Eur J Biochem. 1996;239(3):881-6. Epub 1996/08/01.

102.    Abell C, Courtois F, Olguin LF, Whyte G, Bratton D, Huck WTS, et al. An integrated device for monitoring time-dependent in vitro expression from single genes in picolitre droplets. Chembiochem. 2008;9(3):439-46.

103.    Doi M, Wachi M, Ishino F, Tomioka S, Ito M, Sakagami Y, et al. Determinations of the DNA-Sequence of the Mreb-Gene and of the Gene-Products of the Mre-Region That Function in Formation of the Rod Shape of Escherichia-Coli-Cells. J Bacteriol. 1988;170(10):4619-24.

104.    Graumann PL. Cytoskeletal elements in bacteria. Annu Rev Microbiol. 2007;61:589-618.

105.    Madabhushi R, Marians KJ. Actin Homolog MreB Affects Chromosome Segregation by Regulating Topoisomerase IV in Escherichia coli. Mol Cell. 2009;33(2):171-80.

106.    Esue O, Cordero M, Wirtz D, Tseng Y. The assembly of MreB, a prokaryotic homolog of actin. J Biol Chem. 2005;280(4):2628-35.

107.    Errington J, Jones LJF, Carballido-Lopez R. Control of cell shape in bacteria: Helical, actin-like filaments in Bacillus subtilis. Cell. 2001;104(6):913-22.

108.    Bean GJ, Fllckinger ST, Westler WM, McCully ME, Sept D, Weibel DB, et al. A22 Disrupts the Bacterial Actin Cytoskeleton by Directly Binding and Inducing a Low-Affinity State in MreB. Biochemistry-Us. 2009;48(22):4852-7.

109.    Dominguez-Escobar J, Chastanet A, Crevenna AH, Fromion V, Wedlich-Soldner R, Carballido-Lopez R. Processive Movement of MreB-Associated Cell Wall Biosynthetic Complexes in Bacteria. Science. 2011;333(6039):225-8.

110.    Soufo HJD, Graumann PL. Dynamic movement of actin-like proteins within bacterial cells. Embo Rep. 2004;5(8):789-94.

111.    Lowe J, Salje J, van den Ent F, de Boer P. Direct Membrane Binding by Bacterial Actin MreB. Mol Cell. 2011;43(3):478-87.

112.    Popp D, Narita A, Maeda K, Fujisawa T, Ghoshdastider U, Iwasa M, et al. Filament Structure, Organization, and Dynamics in MreB Sheets. J Biol Chem. 2010;285(21):15858-65.

113.    Wachi M, Doi M, Tamaki S, Park W, Nakajimaiijima S, Matsuhashi M. Mutant Isolation and Molecular-Cloning of Mre-Genes, Which Determine Cell-Shape, Sensitivity to Mecillinam, and Amount of Penicillin-Binding Proteins in Escherichia-Coli. J Bacteriol. 1987;169(11):4935-40.

114.    Campbell RE, Tour O, Palmer AE, Steinbach PA, Baird GS, Zacharias DA, et al. A monomeric red fluorescent protein. P Natl Acad Sci USA. 2002;99(12):7877-82.

115.    Nie L, Wu G, Zhang W. Correlation between mRNA and protein abundance in Desulfovibrio vulgaris: a multiple regression to identify sources of variations. Biochemical and biophysical research communications. 2006;339(2):603-10.

116.    Tian Q, Stepaniants SB, Mao M, Weng L, Feetham MC, Doyle MJ, et al. Integrated genomic and proteomic analyses of gene expression in Mammalian cells. Molecular &amp; cellular proteomics : MCP. 2004;3(10):960-9.

117.    Brockmann R, Beyer A, Heinisch JJ, Wilhelm T. Posttranscriptional Expression Regulation: What Determines Translation Rates? PLoS Computational Biology. 2007;3(3):e57.

118.    Kim SY, Gitai Z, Kinkhabwala A, Shapiro L, Moerner WE. Single molecules of the bacterial actin MreB undergo directed treadmilling motion in Caulobacter crescentus. P Natl Acad Sci USA. 2006;103(29):10929-34.

119. Roodbeen R, van Hest JC. Synthetic cells and organelles: compartmentalization strategies. Bioessays. 2009;31(12):1299-308. Epub 2009/10/31.

120. Lorenceau E, Utada AS, Link DR, Cristobal G, Joanicot M, Weitz DA. Generation of Polymerosomes from Double-Emulsions. Langmuir. 2005;21(20):9183-6.

121. Shum HC, Santanach-Carreras E, Kim JW, Ehrlicher A, Bibette J, Weitz DA. Dewetting-induced membrane formation by adhesion of amphiphile-laden interfaces. J Am Chem Soc. 2011;133(12):4420-6. Epub 2011/03/09.

122. Chalmeau J, Monina N, Shin J, Vieu C, Noireaux V. alpha-Hemolysin pore formation into a supported phospholipid bilayer using cell-free expression. Biochimica Et Biophysica Acta-Biomembranes. 2011;1808(1):271-8.

123. Chanasakulniyom M, Martino C, Paterson D, Horsfall L, Rosser S, Cooper JM. Expression of membrane-associated proteins within single emulsion cell fascimiles. Analyst. 2012.

124. Sandre O, Moreaux L, Brochard-Wyart F. Dynamics of transient pores in stretched vesicles. Proc Natl Acad Sci U S A. 1999;96(19):10591-6. Epub 1999/09/15.

125. Young KD. Bacterial Shape: Two-Dimensional Questions and Possibilities. Annual Review of Microbiology, Vol 64, 2010. 2010;64:223-40.

126. Futoshi Hara KY, Naoki Nemoto, Yoshinori Ohta, Shin-ichi Yokobori, Takuo Yasunaga, Shin-ichi Hisanaga, and Akihiko Yamagishi. An Actin Homolog of the Archaeon Thermoplasma acidophilum That Retains the Ancient Characteristics of Eukaryotic Actin. J Bacteriol. 2007;189(5):2039-45.

127. Peltonen L. THE INTERFACIAL BEHAVIOUR OF SORBITAN SURFACTANT MONOLAYERS AND THE BULK PROPERTIES OF THESE SURFACTANTS AS A FUNCTION OF TEMPERATURE. Thesis, Pharmaceutical Technology Division, Department of Pharmacy, Univeristy of Helsinki. 2001:28.